



2 Pierre Friedlingstein<sup>1,2</sup>, Matthew W. Jones<sup>3</sup>, Michael O’Sullivan<sup>1</sup>, Robbie M. Andrew<sup>4</sup>, Judith  
3 Hauck<sup>5</sup>, Glen P. Peters<sup>4</sup>, Wouter Peters<sup>6,7</sup>, Julia Pongratz<sup>8,9</sup>, Stephen Sitch<sup>10</sup>, Corinne Le Quéré<sup>3</sup>,  
4 Dorothee C. E. Bakker<sup>3</sup>, Josep G. Canadell<sup>11</sup>, Philippe Ciais<sup>12</sup>, Rob Jackson<sup>13</sup>, Peter Anthoni<sup>14</sup>,  
5 Leticia Barbero<sup>15,16</sup>, Ana Bastos<sup>8</sup>, Vladislav Bastrikov<sup>12</sup>, Meike Becker<sup>17,18</sup>, Laurent Bopp<sup>2</sup>, Erik  
6 Buitenhuis<sup>3</sup>, Naveen Chandra<sup>19</sup>, Frédéric Chevallier<sup>12</sup>, Louise P. Chini<sup>20</sup>, Kim I. Currie<sup>21</sup>, Richard  
7 A. Feely<sup>22</sup>, Marion Gehlen<sup>12</sup>, Dennis Gilfillan<sup>23</sup>, Thanos Gkritzalis<sup>24</sup>, Daniel S. Goll<sup>25</sup>, Nicolas  
8 Gruber<sup>26</sup>, Sören Gutekunst<sup>27</sup>, Ian Harris<sup>28</sup>, Vanessa Haverd<sup>11</sup>, Richard A. Houghton<sup>29</sup>, George  
9 Hurtt<sup>20</sup>, Tatiana Ilyina<sup>9</sup>, Atul K. Jain<sup>30</sup>, Emilie Joetzjer<sup>31</sup>, Jed O. Kaplan<sup>32</sup>, Etsushi Kato<sup>33</sup>, Kees  
10 Klein Goldewijk<sup>34,35</sup>, Jan Ivar Korsbakken<sup>4</sup>, Peter Landschützer<sup>9</sup>, Siv K. Lauvset<sup>36,18</sup>, Nathalie  
11 Lefèvre<sup>37</sup>, Andrew Lenton<sup>38,39</sup>, Sebastian Lienert<sup>40</sup>, Danica Lombardozi<sup>41</sup>, Gregg Marland<sup>23</sup>,  
12 Patrick C. McGuire<sup>42</sup>, Joe R. Melton<sup>43</sup>, Nicolas Metzler<sup>37</sup>, David R. Munro<sup>44</sup>, Julia E. M. S. Nabel<sup>9</sup>,  
13 Shin-Ichiro Nakaoka<sup>45</sup>, Craig Neill<sup>38</sup>, Abdirahman M. Omar<sup>36,18</sup>, Tsuneo Ono<sup>46</sup>, Anna  
14 Peregón<sup>12,47</sup>, Denis Pierrot<sup>15,16</sup>, Benjamin Poulter<sup>48</sup>, Gregor Rehder<sup>49</sup>, Laure Resplandy<sup>50</sup>, Eddy  
15 Robertson<sup>51</sup>, Christian Rödenbeck<sup>52</sup>, Roland Séférian<sup>53</sup>, Jörg Schwinger<sup>36,18</sup>, Naomi Smith<sup>6,54</sup>,  
16 Pieter P. Tans<sup>55</sup>, Hanqin Tian<sup>56</sup>, Bronte Tilbrook<sup>38,57</sup>, Francesco N Tubiello<sup>58</sup>, Guido R. van der  
17 Werf<sup>59</sup>, Andrew J. Wiltshire<sup>51</sup>, Sönke Zaehle<sup>52</sup>

---

<sup>1</sup> College of Engineering, Mathematics and Physical Sciences, University of Exeter, Exeter EX4 4QF, UK

<sup>2</sup> Laboratoire de Météorologie Dynamique, Institut Pierre-Simon Laplace, CNRS-ENS-UPMC-X, Département de Géosciences, Ecole Normale Supérieure, 24 rue Lhomond, 75005 Paris, France

<sup>3</sup> Tyndall Centre for Climate Change Research, School of Environmental Sciences, University of East Anglia, Norwich Research Park, Norwich NR4 7TJ, UK

<sup>4</sup> CICERO Center for International Climate Research, Oslo 0349, Norway

<sup>5</sup> Alfred Wegener Institute Helmholtz Centre for Polar and Marine Research, Postfach 120161, 27515 Bremerhaven, Germany

<sup>6</sup> Wageningen University, Environmental Sciences Group, P.O. Box 47, 6700AA, Wageningen, The Netherlands

<sup>7</sup> University of Groningen, Centre for Isotope Research, Groningen, The Netherlands

<sup>8</sup> Ludwig-Maximilians-Universität Munich, Luisenstr. 37, 80333 München, Germany

<sup>9</sup> Max Planck Institute for Meteorology, Hamburg, Germany

<sup>10</sup> College of Life and Environmental Sciences, University of Exeter, Exeter EX4 4RJ, UK

<sup>11</sup> CSIRO Oceans and Atmosphere, GPO Box 1700, Canberra, ACT 2601, Australia

<sup>12</sup> Laboratoire des Sciences du Climat et de l’Environnement, Institut Pierre-Simon Laplace, CEA-CNRS-UVSQ, CE Orme des Merisiers, 91191 Gif sur Yvette Cedex, France

<sup>13</sup> Department of Earth System Science, Woods Institute for the Environment, and Precourt Institute for Energy, Stanford University, Stanford, CA 94305–2210, United States of America

<sup>14</sup> Karlsruhe Institute of Technology, Institute of Meteorology and Climate, Research/Atmospheric Environmental Research, 82467 Garmisch-Partenkirchen, Germany

<sup>15</sup> Cooperative Institute for Marine and Atmospheric Studies, Rosenstiel School for Marine and Atmospheric Science, University of Miami, Miami, FL 33149, USA

<sup>16</sup> National Oceanic & Atmospheric Administration/Atlantic Oceanographic & Meteorological Laboratory (NOAA/AOML), Miami, FL 33149, USA

<sup>17</sup> Geophysical Institute, University of Bergen, Bergen, Norway

<sup>18</sup> Bjerknes Centre for Climate Research, Allégaten 70, 5007 Bergen, Norway

<sup>19</sup> Earth Surface System Research Center (ESS), Japan Agency for Marine-Earth Science and Technology (JAMSTEC), Yokohama, 236-0001, Japan

<sup>20</sup> Department of Geographical Sciences, University of Maryland, College Park, Maryland 20742, USA

<sup>21</sup> NIWA / UoO Research Centre for Oceanography, PO Box 56, Dunedin 9054, New Zealand

- 
- <sup>22</sup> Pacific Marine Environmental Laboratory, National Oceanic and Atmospheric Administration, 7600 Sand Point Way NE, Seattle, WA 98115-6349, USA
- <sup>23</sup> Research Institute for Environment, Energy, and Economics, Appalachian State University, Boone, North Carolina, USA
- <sup>24</sup> Flanders Marine Institute (VLIZ), InnovOceanSite, Wandelaarkaai 7, 8400 Ostend, Belgium
- <sup>25</sup> Lehrstuhl für Physische Geographie mit Schwerpunkt Klimaforschung, Universität Augsburg, Augsburg, Germany
- <sup>26</sup> Environmental Physics Group, ETH Zürich, Institute of Biogeochemistry and Pollutant Dynamics and Center for Climate Systems Modeling (C2SM)
- <sup>27</sup> GEOMAR Helmholtz Centre for Ocean Research Kiel, Düsternbrooker Weg 20, 24105 Kiel, Germany
- <sup>28</sup> NCAS-Climate, Climatic Research Unit, School of Environmental Sciences, University of East Anglia, Norwich Research Park, Norwich, NR4 7TJ, UK
- <sup>29</sup> Woods Hole Research Center (WHRC), Falmouth, MA 02540, USA
- <sup>30</sup> Department of Atmospheric Sciences, University of Illinois, Urbana, IL 61821, USA
- <sup>31</sup> Centre National de Recherche Meteorologique, Unite mixte de recherche 3589 Météo-France/CNRS, 42 Avenue Gaspard Coriolis, 31100 Toulouse, France
- <sup>32</sup> Department of Earth Sciences, University of Hong Kong, Pokfulam Road, Hong Kong
- <sup>33</sup> Institute of Applied Energy (IAE), Minato-ku, Tokyo 105-0003, Japan
- <sup>34</sup> PBL Netherlands Environmental Assessment Agency, Bezuidenhoutseweg 30, P.O. Box 30314, 2500 GH, The Hague, the Netherlands
- <sup>35</sup> Faculty of Geosciences, Department IMEW, Copernicus Institute of Sustainable Development, Heidelberglaan 2, P.O. Box 80115, 3508 TC, Utrecht, Netherlands
- <sup>36</sup> NORCE Norwegian Research Centre, NORCE Climate, Jahnebakken 70, 5008 Bergen, Norway
- <sup>37</sup> LOCEAN/IPSL laboratory, Sorbonne Université, CNRS/IRD/MNHN, Paris, France
- <sup>38</sup> CSIRO Oceans and Atmosphere, Hobart, TAS, Australia
- <sup>39</sup> Institute for Marine and Antarctic Studies, University of Tasmania, Hobart, Tasmania
- <sup>40</sup> Climate and Environmental Physics, Physics Institute and Oeschger Centre for Climate Change Research, University of Bern, Bern, Switzerland
- <sup>41</sup> National Center for Atmospheric Research, Climate and Global Dynamics, Terrestrial Sciences Section, Boulder, CO 80305, USA
- <sup>42</sup> Department of Meteorology, Department of Geography & Environmental Science, National Centre for Atmospheric Science, University of Reading, Reading, UK,
- <sup>43</sup> Climate Research Division, Environment and Climate Change Canada, Victoria, BC, Canada
- <sup>44</sup> Cooperative Institute for Research in Environmental Sciences, University of Colorado, Boulder, CO, USA
- <sup>45</sup> Center for Global Environmental Research, National Institute for Environmental Studies (NIES), 16-2 Onogawa, Tsukuba, Ibaraki, 305-8506, Japan
- <sup>46</sup> Japan Fisheries Research and Education Agency, 2-12-4 Fukuura, Kanazawa-Ku, Yokohama 236-8648, Japan
- <sup>47</sup> Institute of Soil Science and Agrochemistry, Siberian Branch Russian Academy of Sciences (SB RAS), Pr. Akademika Lavrentyeva, 8/2, 630090, Novosibirsk, Russia
- <sup>48</sup> NASA Goddard Space Flight Center, Biospheric Sciences Laboratory, Greenbelt, Maryland 20771, USA
- <sup>49</sup> Leibniz Institute for Baltic Sea Research Warnemuende (IOW), Seestrasse 15; 18119 Rostock, Germany
- <sup>50</sup> Princeton University, Department of Geosciences and Princeton Environmental Institute, Princeton, NJ, USA

18  
19  
20  
21  
22  
23

**Correspondence:** Pierre Friedlingstein (p.friedlingstein@exeter.ac.uk)

---

<sup>51</sup> Met Office Hadley Centre, FitzRoy Road, Exeter EX1 3PB, UK

<sup>52</sup> Max Planck Institute for Biogeochemistry, P.O. Box 600164, Hans-Knöll-Str. 10, 07745 Jena, Germany

<sup>53</sup> CNRM (Météo-France/CNRS)-UMR 3589

<sup>54</sup> ICOS Carbon Portal, Lund University, Lund, Sweden

<sup>55</sup> National Oceanic & Atmospheric Administration, Earth System Research Laboratory (NOAA/ESRL), Boulder, CO 80305, USA

<sup>56</sup> International Center for Climate and Global Change Research, School of Forestry and Wildlife Sciences, Auburn University, 602 Duncan Drive, Auburn, AL 36849, USA

<sup>57</sup> Australian Antarctic Partnership Program, University of Tasmania, Hobart, Australia

<sup>58</sup> Statistics Division, Food and Agriculture Organization of the United Nations, Via Terme di Caracalla, Rome 00153, Italy

<sup>59</sup> Faculty of Science, Vrije Universiteit, Amsterdam, The Netherlands

## 24 **Abstract**

25 Accurate assessment of anthropogenic carbon dioxide (CO<sub>2</sub>) emissions and their redistribution  
26 among the atmosphere, ocean, and terrestrial biosphere – the ‘global carbon budget’ – is  
27 important to better understand the global carbon cycle, support the development of climate  
28 policies, and project future climate change. Here we describe data sets and methodology to  
29 quantify the five major components of the global carbon budget and their uncertainties. Fossil  
30 CO<sub>2</sub> emissions (E<sub>FF</sub>) are based on energy statistics and cement production data, while emissions  
31 from land-use change (E<sub>LUC</sub>), mainly deforestation, are based on land-use and land-use change  
32 data and bookkeeping models. Atmospheric CO<sub>2</sub> concentration is measured directly and its  
33 growth rate (G<sub>ATM</sub>) is computed from the annual changes in concentration. The ocean CO<sub>2</sub> sink  
34 (S<sub>OCEAN</sub>) and terrestrial CO<sub>2</sub> sink (S<sub>LAND</sub>) are estimated with global process models constrained by  
35 observations. The resulting carbon budget imbalance (B<sub>IM</sub>), the difference between the  
36 estimated total emissions and the estimated changes in the atmosphere, ocean, and terrestrial  
37 biosphere, is a measure of imperfect data and understanding of the contemporary carbon  
38 cycle. All uncertainties are reported as ±1σ. For the last decade available (2009-2018), E<sub>FF</sub> was  
39 9.5 ± 0.5 GtC yr<sup>-1</sup>, E<sub>LUC</sub> 1.5 ± 0.7 GtC yr<sup>-1</sup>, G<sub>ATM</sub> 4.9 ± 0.02 GtC yr<sup>-1</sup> (2.3 ± 0.01 ppm yr<sup>-1</sup>), S<sub>OCEAN</sub> 2.5  
40 ± 0.6 GtC yr<sup>-1</sup>, and S<sub>LAND</sub> 3.2 ± 0.6 GtC yr<sup>-1</sup>, with a budget imbalance B<sub>IM</sub> of 0.4 GtC yr<sup>-1</sup> indicating  
41 overestimated emissions and/or underestimated sinks. For year 2018 alone, the growth in E<sub>FF</sub>  
42 was about 2.1% and fossil emissions increased to 10.0 ± 0.5 GtC yr<sup>-1</sup>, reaching 10 GtC yr<sup>-1</sup> for the  
43 first time in history, E<sub>LUC</sub> was 1.5 ± 0.7 GtC yr<sup>-1</sup>, for a total anthropogenic CO<sub>2</sub> emissions of 11.5 ±  
44 0.9 GtC yr<sup>-1</sup> (42.5 ± 3.3 GtCO<sub>2</sub>). Also for 2018, G<sub>ATM</sub> was 5.1 ± 0.2 GtC yr<sup>-1</sup> (2.4 ± 0.1 ppm yr<sup>-1</sup>),  
45 S<sub>OCEAN</sub> was 2.6 ± 0.6 GtC yr<sup>-1</sup> and S<sub>LAND</sub> was 3.5 ± 0.7 GtC yr<sup>-1</sup>, with a B<sub>IM</sub> of 0.3 GtC. The global  
46 atmospheric CO<sub>2</sub> concentration reached 407.38 ± 0.1 ppm averaged over 2018. For 2019,  
47 preliminary data for the first 6-10 months indicate a reduced growth in E<sub>FF</sub> of +0.5% (range of –  
48 0.3% to 1.4%) based on national emissions projections for China, USA, the EU and India, and  
49 projections of Gross Domestic Product corrected for recent changes in the carbon intensity of  
50 the economy for the rest of the world. Overall, the mean and trend in the five components of  
51 the global carbon budget are consistently estimated over the period 1959-2018, but  
52 discrepancies of up to 1 GtC yr<sup>-1</sup> persist for the representation of semi-decadal variability in CO<sub>2</sub>  
53 fluxes. A detailed comparison among individual estimates and the introduction of a broad range  
54 of observations shows: (1) no consensus in the mean and trend in land-use change emissions  
55 over the last decade, (2) a persistent low agreement between the different methods on the

56 magnitude of the land CO<sub>2</sub> flux in the northern extra-tropics, and (3) an apparent  
57 underestimation of the CO<sub>2</sub> variability by ocean models outside the tropics. This living data  
58 update documents changes in the methods and data sets used in this new global carbon budget  
59 and the progress in understanding of the global carbon cycle compared with previous  
60 publications of this data set (Le Quéré et al., 2018b, 2018a, 2016, 2015b, 2015a, 2014, 2013).  
61 The data generated by this work are available at <https://doi.org/10.18160/gcp-2019>  
62 (Friedlingstein et al., 2019).

## 63 **1 Introduction**

64 The concentration of carbon dioxide (CO<sub>2</sub>) in the atmosphere has increased from approximately  
65 277 parts per million (ppm) in 1750 (Joos and Spahni, 2008), the beginning of the Industrial Era,  
66 to  $407.38 \pm 0.1$  ppm in 2018 (Dlugokencky and Tans, 2019); Fig. 1). The atmospheric CO<sub>2</sub>  
67 increase above pre-industrial levels was, initially, primarily caused by the release of carbon to  
68 the atmosphere from deforestation and other land-use change activities (Ciais et al., 2013).  
69 While emissions from fossil fuels started before the Industrial Era, they only became the  
70 dominant source of anthropogenic emissions to the atmosphere from around 1950 and their  
71 relative share has continued to increase until present. Anthropogenic emissions occur on top of  
72 an active natural carbon cycle that circulates carbon between the reservoirs of the atmosphere,  
73 ocean, and terrestrial biosphere on time scales from sub-daily to millennia, while exchanges  
74 with geologic reservoirs occur at longer timescales (Archer et al., 2009).

75 The global carbon budget presented here refers to the mean, variations, and trends in the  
76 perturbation of CO<sub>2</sub> in the environment, referenced to the beginning of the Industrial Era  
77 (defined here as 1750). This paper describes the components of the global carbon cycle over  
78 the historical period with a stronger focus on the recent period (since 1958, onset of  
79 atmospheric CO<sub>2</sub> measurements), the last decade (2009-2018) and the current year (2019). We  
80 quantify the input of CO<sub>2</sub> to the atmosphere by emissions from human activities, the growth  
81 rate of atmospheric CO<sub>2</sub> concentration, and the resulting changes in the storage of carbon in  
82 the land and ocean reservoirs in response to increasing atmospheric CO<sub>2</sub> levels, climate change  
83 and variability, and other anthropogenic and natural changes (Fig. 2). An understanding of this  
84 perturbation budget over time and the underlying variability and trends of the natural carbon  
85 cycle is necessary to understand the response of natural sinks to changes in climate, CO<sub>2</sub> and  
86 land-use change drivers, and the permissible emissions for a given climate stabilization target.

87 Note that this paper does not estimate the remaining future carbon emissions consistent with a  
88 given climate target (often referred to as the remaining carbon budget (Millar et al., 2017;  
89 Rogelj et al., 2016, 2019).

90 The components of the CO<sub>2</sub> budget that are reported annually in this paper include separate  
91 estimates for the CO<sub>2</sub> emissions from (1) fossil fuel combustion and oxidation from all energy  
92 and industrial processes and cement production ( $E_{FF}$ ; GtC yr<sup>-1</sup>) and (2) the emissions resulting  
93 from deliberate human activities on land, including those leading to land-use change ( $E_{LUC}$ ; GtC  
94 yr<sup>-1</sup>); and their partitioning among (3) the growth rate of atmospheric CO<sub>2</sub> concentration ( $G_{ATM}$ ;  
95 GtC yr<sup>-1</sup>), and the uptake of CO<sub>2</sub> (the ‘CO<sub>2</sub> sinks’) in (4) the ocean ( $S_{OCEAN}$ ; GtC yr<sup>-1</sup>) and (5) on  
96 land ( $S_{LAND}$ ; GtC yr<sup>-1</sup>). The CO<sub>2</sub> sinks as defined here conceptually include the response of the  
97 land (including inland waters and estuaries) and ocean (including coasts and territorial sea) to  
98 elevated CO<sub>2</sub> and changes in climate, rivers, and other environmental conditions, although in  
99 practice not all processes are fully accounted for (see Section 2.7). The global emissions and  
100 their partitioning among the atmosphere, ocean and land are in reality in balance, however due  
101 to imperfect spatial and/or temporal data coverage, errors in each estimate, and smaller terms  
102 not included in our budget estimate (discussed in Section 2.7), their sum does not necessarily  
103 add up to zero. We estimate a budget imbalance ( $B_{IM}$ ), which is a measure of the mismatch  
104 between the estimated emissions and the estimated changes in the atmosphere, land and  
105 ocean, with the full global carbon budget as follows:

$E_{FF} + E_{LUC} = G_{ATM} + S_{OCEAN} + S_{LAND} + B_{IM}$	(1)
--	-----

106  $G_{ATM}$  is usually reported in ppm yr<sup>-1</sup>, which we convert to units of carbon mass per year, GtC yr<sup>-1</sup>  
107 <sup>1</sup>, using 1 ppm = 2.124 GtC (Ballantyne et al., 2012; Table 1). We also include a quantification of  
108  $E_{FF}$  by country, computed with both territorial and consumption-based accounting (see Section  
109 2), and discuss missing terms from sources other than the combustion of fossil fuels (see  
110 Section 2.7).

111 The CO<sub>2</sub> budget has been assessed by the Intergovernmental Panel on Climate Change (IPCC) in  
112 all assessment reports (Prentice et al., 2001; Schimel et al., 1995; Watson et al., 1990; Denman  
113 et al., 2007; Ciais et al., 2013), and by others (e.g. Ballantyne et al., 2012). The IPCC  
114 methodology has been revised and used by the Global Carbon Project (GCP,  
115 [www.globalcarbonproject.org](http://www.globalcarbonproject.org), last access: 27 September 2019), which has coordinated this  
116 cooperative community effort for the annual publication of global carbon budgets for the year

117 2005 (Raupach et al., 2007; including fossil emissions only), year 2006 (Canadell et al., 2007),  
118 year 2007 (published online; GCP, 2007), year 2008 (Le Quéré et al., 2009), year 2009  
119 (Friedlingstein et al., 2010), year 2010 (Peters et al., 2012b), year 2012 (Le Quéré et al., 2013;  
120 Peters et al., 2013), year 2013 (Le Quéré et al., 2014), year 2014 (Le Quéré et al., 2015a;  
121 Friedlingstein et al., 2014), year 2015 (Jackson et al., 2016; Le Quéré et al., 2015b), year 2016  
122 (Le Quéré et al., 2016), year 2017 (Le Quéré et al., 2018a; Peters et al., 2017) and most recently  
123 year 2018 (Le Quéré et al., 2018b; Jackson et al., 2018). Each of these papers updated previous  
124 estimates with the latest available information for the entire time series.

125 We adopt a range of  $\pm 1$  standard deviation ( $\sigma$ ) to report the uncertainties in our estimates,  
126 representing a likelihood of 68% that the true value will be within the provided range if the  
127 errors have a Gaussian distribution and no bias is assumed. This choice reflects the difficulty of  
128 characterising the uncertainty in the CO<sub>2</sub> fluxes between the atmosphere and the ocean and  
129 land reservoirs individually, particularly on an annual basis, as well as the difficulty of updating  
130 the CO<sub>2</sub> emissions from land-use change. A likelihood of 68% provides an indication of our  
131 current capability to quantify each term and its uncertainty given the available information. For  
132 comparison, the Fifth Assessment Report of the IPCC (AR5) generally reported a likelihood of  
133 90% for large data sets whose uncertainty is well characterised, or for long time intervals less  
134 affected by year-to-year variability. Our 68% uncertainty value is near the 66% which the IPCC  
135 characterises as 'likely' for values falling into the  $\pm 1\sigma$  interval. The uncertainties reported here  
136 combine statistical analysis of the underlying data and expert judgement of the likelihood of  
137 results lying outside this range. The limitations of current information are discussed in the  
138 paper and have been examined in detail elsewhere (Ballantyne et al., 2015; Zscheischler et al.,  
139 2017). We also use a qualitative assessment of confidence level to characterise the annual  
140 estimates from each term based on the type, amount, quality and consistency of the evidence  
141 as defined by the IPCC (Stocker et al., 2013).

142 All quantities are presented in units of gigatonnes of carbon (GtC,  $10^{15}$  gC), which is the same as  
143 petagrams of carbon (PgC; Table 1). Units of gigatonnes of CO<sub>2</sub> (or billion tonnes of CO<sub>2</sub>) used in  
144 policy are equal to 3.664 multiplied by the value in units of GtC.

145 This paper provides a detailed description of the data sets and methodology used to compute  
146 the global carbon budget estimates for the industrial period, from 1750 to 2018, and in more  
147 detail for the period since 1959. It also provides decadal averages starting in 1960 including the

148 last decade (2009-2018), results for the year 2018, and a projection for year 2019. Finally it  
149 provides cumulative emissions from fossil fuels and land-use change since the year 1750, the  
150 pre-industrial period; and since the year 1850, the reference year for historical simulations in  
151 IPCC (AR6). This paper is updated every year using the format of ‘living data’ to keep a record of  
152 budget versions and the changes in new data, revision of data, and changes in methodology  
153 that lead to changes in estimates of the carbon budget. Additional materials associated with  
154 the release of each new version will be posted at the Global Carbon Project (GCP) website  
155 (<http://www.globalcarbonproject.org/carbonbudget>, last access: 27 September 2019), with  
156 fossil fuel emissions also available through the Global Carbon Atlas  
157 (<http://www.globalcarbonatlas.org>, last access: 4 December 2019). With this approach, we aim  
158 to provide the highest transparency and traceability in the reporting of CO<sub>2</sub>, the key driver of  
159 climate change.

## 160 **2 Methods**

161 Multiple organizations and research groups around the world generated the original  
162 measurements and data used to complete the global carbon budget. The effort presented here  
163 is thus mainly one of synthesis, where results from individual groups are collated, analysed and  
164 evaluated for consistency. We facilitate access to original data with the understanding that  
165 primary data sets will be referenced in future work (see Table 2 for how to cite the data sets).  
166 Descriptions of the measurements, models, and methodologies follow below and detailed  
167 descriptions of each component are provided elsewhere.

168 This is the 14<sup>th</sup> version of the global carbon budget and the eighth revised version in the format  
169 of a living data update in Earth System Science Data. It builds on the latest published global  
170 carbon budget of (Le Quéré et al., 2018b). The main changes are: (1) the inclusion of data to  
171 year 2018 (inclusive) and a projection for the global carbon budget for year 2019; (2) further  
172 developments to the metrics that evaluate components of the individual models used to  
173 estimate  $S_{OCEAN}$  and  $S_{LAND}$  using observations, as an effort to document, encourage and support  
174 model improvements through time; (3) a projection of the ‘rest of world’ emissions by fuel  
175 type; (4) changed method for projecting current-year global atmospheric CO<sub>2</sub> concentration  
176 increment; and (5) global emissions are calculated as the sum of countries’ emissions and  
177 bunker fuels rather than taken directly from Carbon Dioxide Information Analysis Center

178 (CDIAC). The main methodological differences between recent annual carbon budgets (2015-  
179 2018) are summarised in Table 3 and changes since 2005 are provided in Table A7.

## 180 **2.1 Fossil CO<sub>2</sub> emissions (E<sub>FF</sub>)**

### 181 **2.1.1 Emissions estimates**

182 The estimates of global and national fossil CO<sub>2</sub> emissions (E<sub>FF</sub>) include the combustion of fossil  
183 fuels through a wide range of activities (e.g. transport, heating and cooling, industry, fossil  
184 industry own use & natural gas flaring), the production of cement, and other process emissions  
185 (e.g. the production of chemicals & fertilizers). The estimates of E<sub>FF</sub> rely primarily on energy  
186 consumption data, specifically data on hydrocarbon fuels, collated and archived by several  
187 organisations (Andres et al., 2012). We use four main data sets for historical emissions (1750-  
188 2018):

- 189 1. Global and national emission estimates for coal, oil, natural gas as well as peat fuel  
190 extraction from CDIAC for the time period 1750-2016 (Gilfillan et al., 2019), as it is the only  
191 data set that extends back to 1750 by country.
- 192 2. Official UNFCCC national inventory reports annually for 1990-2017 for the 42 Annex I  
193 countries in the UNFCCC (UNFCCC, 2019). We assess these to be the most accurate  
194 estimates because they are compiled by experts within countries that have access to the  
195 most detailed data, and they are periodically reviewed.
- 196 3. The BP Statistical Review of World Energy (BP, 2019), as these are the most up-to-date  
197 estimates of national energy statistics.
- 198 4. Global and national cement emissions updated from (Andrew, 2018) following Andrew  
199 (2019) to include the latest estimates of cement production and clinker ratios.

200 In the following section we provide more details for each data set and describe the additional  
201 modifications that are required to make the data set consistent and usable.

202 *CDIAC*: The CDIAC estimates have been updated annually to the year 2016, derived primarily  
203 from energy statistics published by the United Nations (UN, 2018). Fuel masses and volumes  
204 are converted to fuel energy content using country-level coefficients provided by the UN, and  
205 then converted to CO<sub>2</sub> emissions using conversion factors that take into account the  
206 relationship between carbon content and energy (heat) content of the different fuel types

207 (coal, oil, natural gas, natural gas flaring) and the combustion efficiency (Marland and Rotty,  
208 1984).

209 *UNFCCC*: Estimates from the UNFCCC national inventory reports follow the IPCC guidelines  
210 (IPCC, 2006), but have a slightly larger system boundary than CDIAC by including emissions  
211 coming from carbonates other than in cement manufacture. We reallocate the detailed  
212 UNFCCC estimates to the CDIAC definitions of coal, oil, natural gas, cement, and other to allow  
213 more consistent comparisons over time and between countries.

214 Specific country updates: China and Saudi Arabia: The most recent version of CDIAC introduces  
215 what appear to be spurious interannual variations for these two countries (IEA, 2018),  
216 therefore we use data from the 2018 global carbon budget (Le Quéré et al., 2018b). Norway:  
217 CDIAC's method of apparent consumption results in large errors for Norway, and we therefore  
218 overwrite emissions before 1990 with estimates based on official Norwegian statistics.

219 *BP*: For the most recent period when the UNFCCC and CDIAC estimates are not available, we  
220 generate preliminary estimates using energy consumption data from the BP Statistical Review  
221 of World Energy (Andres et al., 2014; BP, 2019; Myhre et al., 2009). We apply the BP growth  
222 rates by fuel type (coal, oil, natural gas) to estimate 2018 emissions based on 2017 estimates  
223 (UNFCCC Annex I countries), and to estimate 2017-2018 emissions based on 2016 estimates  
224 (remaining countries). BP's data set explicitly covers about 70 countries (96% of global energy  
225 emissions), and for the remaining countries we use growth rates from the sub-region the  
226 country belongs to. For the most recent years, natural gas flaring is assumed constant from the  
227 most recent available year of data (2017 for Annex I countries, 2016 for the remainder).

228 *Cement*: Estimates of emissions from cement production are taken directly from Andrew  
229 (2019). Additional calcination and carbonation processes are not included explicitly here,  
230 except in national inventories provided by Annex I countries, but are discussed in Section 2.7.2.

231 *Country mappings*: The published CDIAC data set includes 257 countries and regions. This list  
232 includes countries that no longer exist, such as the USSR and Yugoslavia. We reduce the list to  
233 214 countries by reallocating emissions to currently defined territories, using mass-preserving  
234 aggregation or disaggregation. Examples of aggregation include merging East and West  
235 Germany to the currently defined Germany. Examples of disaggregation include reallocating the  
236 emissions from former USSR to the resulting independent countries. For disaggregation, we use  
237 the emission shares when the current territories first appeared (e.g. USSR in 1992), and thus

238 historical estimates of disaggregated countries should be treated with extreme care. In the case  
239 of the USSR, we were able to disaggregate 1990 and 1991 using data from the IEA. In addition,  
240 we aggregate some overseas territories (e.g. Réunion, Guadeloupe) into their governing nations  
241 (e.g. France) to align with UNFCCC reporting.

242 *Global total:* The global estimate is the sum of the individual countries' emissions and  
243 international aviation and marine bunkers. This is different to last year, where we used the  
244 independent global total estimated by CDIAC (combined with cement from Andrew (2018)). The  
245 CDIAC global total differs to the sum of the countries and bunkers since 1) the sum of imports in  
246 all countries is not equal to the sum of exports because of reporting inconsistencies, 2) changes  
247 in stocks, and 3) the share of non-oxidised carbon (e.g. as solvents, lubricants, feedstocks, etc.)  
248 at the global level is assumed to be fixed at the 1970's average while it varies in the country  
249 level data based on energy data (Andres et al., 2012). From the 2019 edition CDIAC now  
250 includes changes in stocks in the global total (pers. comm., Dennis Gilfillan), removing one  
251 contribution to this discrepancy. The discrepancy has grown over time from around zero in  
252 1990 to over 500 MtCO<sub>2</sub> in recent years, consistent with the growth in non-oxidised carbon  
253 (IEA, 2018). To remove this discrepancy we now calculate the global total as the sum of the  
254 countries and international bunkers.

### 255 **2.1.2 Uncertainty assessment for E<sub>FF</sub>**

256 We estimate the uncertainty of the global fossil CO<sub>2</sub> emissions at  $\pm 5\%$  (scaled down from the  
257 published  $\pm 10\%$  at  $\pm 2\sigma$  to the use of  $\pm 1\sigma$  bounds reported here; Andres et al., 2012). This is  
258 consistent with a more detailed analysis of uncertainty of  $\pm 8.4\%$  at  $\pm 2\sigma$  (Andres et al., 2014) and  
259 at the high-end of the range of  $\pm 5\text{-}10\%$  at  $\pm 2\sigma$  reported by (Ballantyne et al., 2015). This  
260 includes an assessment of uncertainties in the amounts of fuel consumed, the carbon and heat  
261 contents of fuels, and the combustion efficiency. While we consider a fixed uncertainty of  $\pm 5\%$   
262 for all years, the uncertainty as a percentage of the emissions is growing with time because of  
263 the larger share of global emissions from emerging economies and developing countries  
264 (Marland et al., 2009). Generally, emissions from mature economies with good statistical  
265 processes have an uncertainty of only a few per cent (Marland, 2008), while emissions from  
266 developing countries such as China have uncertainties of around  $\pm 10\%$  (for  $\pm 1\sigma$ ; Gregg et al.,  
267 2008). Uncertainties of emissions are likely to be mainly systematic errors related to underlying  
268 biases of energy statistics and to the accounting method used by each country.

269 We assign a medium confidence to the results presented here because they are based on  
270 indirect estimates of emissions using energy data (Durant et al., 2011). There is only limited and  
271 indirect evidence for emissions, although there is high agreement among the available  
272 estimates within the given uncertainty (Andres et al., 2012, 2014), and emission estimates are  
273 consistent with a range of other observations (Ciais et al., 2013), even though their regional and  
274 national partitioning is more uncertain (Francey et al., 2013).

### 275 **2.1.3 Emissions embodied in goods and services**

276 CDIAC, UNFCCC, and BP national emission statistics ‘include greenhouse gas emissions and  
277 removals taking place within national territory and offshore areas over which the country has  
278 jurisdiction’ (Rypdal et al., 2006), and are called territorial emission inventories. Consumption-  
279 based emission inventories allocate emissions to products that are consumed within a country,  
280 and are conceptually calculated as the territorial emissions minus the ‘embodied’ territorial  
281 emissions to produce exported products plus the emissions in other countries to produce  
282 imported products (Consumption = Territorial – Exports + Imports). Consumption-based  
283 emission attribution results (e.g. Davis and Caldeira, 2010) provide additional information to  
284 territorial-based emissions that can be used to understand emission drivers (Hertwich and  
285 Peters, 2009) and quantify emission transfers by the trade of products between countries  
286 (Peters et al., 2011b). The consumption-based emissions have the same global total, but reflect  
287 the trade-driven movement of emissions across the Earth's surface in response to human  
288 activities.

289 We estimate consumption-based emissions from 1990-2016 by enumerating the global supply  
290 chain using a global model of the economic relationships between economic sectors within and  
291 between every country (Andrew and Peters, 2013; Peters et al., 2011a). Our analysis is based  
292 on the economic and trade data from the Global Trade and Analysis Project (GTAP; Narayanan  
293 et al., 2015), and we make detailed estimates for the years 1997 (GTAP version 5), 2001  
294 (GTAP6), and 2004, 2007, and 2011 (GTAP9.2), covering 57 sectors and 141 countries and  
295 regions. The detailed results are then extended into an annual time-series from 1990 to the  
296 latest year of the Gross Domestic Product (GDP) data (2016 in this budget), using GDP data by  
297 expenditure in current exchange rate of US dollars (USD; from the UN National Accounts main  
298 Aggregates database; UN, 2017) and time series of trade data from GTAP (based on the  
299 methodology in (Peters et al., 2011b). We estimate the sector-level CO<sub>2</sub> emissions using the

300 GTAP data and methodology, include flaring and cement emissions from CDIAC, and then scale  
 301 the national totals (excluding bunker fuels) to match the emission estimates from the carbon  
 302 budget. We do not provide a separate uncertainty estimate for the consumption-based  
 303 emissions, but based on model comparisons and sensitivity analysis, they are unlikely to be  
 304 significantly different than for the territorial emission estimates (Peters et al., 2012a).

#### 305 **2.1.4 Growth rate in emissions**

306 We report the annual growth rate in emissions for adjacent years (in percent per year) by  
 307 calculating the difference between the two years and then normalising to the emissions in the  
 308 first year:  $(E_{FF}(t_{0+1}) - E_{FF}(t_0)) / E_{FF}(t_0) \times 100\%$ . We apply a leap-year adjustment where relevant to  
 309 ensure valid interpretations of annual growth rates. This affects the growth rate by about 0.3%  
 310  $\text{yr}^{-1}$  (1/365) and causes growth rates to go up approximately 0.3% if the first year is a leap year  
 311 and down 0.3% if the second year is a leap year.

312 The relative growth rate of  $E_{FF}$  over time periods of greater than one year can be rewritten  
 313 using its logarithm equivalent as follows:

$\frac{1}{E_{FF}} \frac{dE_{FF}}{dt} = \frac{d(\ln E_{FF})}{dt}$	(2)
--	-----

314 Here we calculate relative growth rates in emissions for multi-year periods (e.g. a decade) by  
 315 fitting a linear trend to  $\ln(E_{FF})$  in Eq. (2), reported in percent per year.

#### 316 **2.1.5 Emissions projections**

317 To gain insight on emission trends for 2019, we provide an assessment of global fossil CO<sub>2</sub>  
 318 emissions,  $E_{FF}$ , by combining individual assessments of emissions for China, USA, the EU, and  
 319 India (the four countries/regions with the largest emissions), and the rest of the world.

320 Our 2019 estimate for China uses: (1) the sum of monthly domestic production of raw coal,  
 321 crude oil, natural gas and cement from the National Bureau of Statistics (NBS, 2019c), (2)  
 322 monthly net imports of coal, coke, crude oil, refined petroleum products and natural gas from  
 323 the General Administration of Customs of the People’s Republic of China (2019a); and (3)  
 324 annual energy consumption data by fuel type and annual production data for cement from the  
 325 NBS, using final data for 2000-2017 (NBS, 2019c) and preliminary data for 2018 (NBS, 2019b).  
 326 We estimate the full-year growth rate for 2019 using a Bayesian regression for the ratio  
 327 between the annual energy consumption data (3 above) from 2014 through 2018 and monthly

328 production plus net imports through September of each year (1+2 above). The uncertainty  
329 range uses the standard deviations of the resulting posteriors. Sources of uncertainty and  
330 deviations between the monthly and annual growth rates include lack of monthly data on stock  
331 changes and energy density, variance in the trend during the last three months of the year, and  
332 partially unexplained discrepancies between supply-side and consumption data even in the  
333 final annual data. Note that in recent years, the absolute value of the annual growth rate for  
334 coal energy consumption, and hence total CO<sub>2</sub> emissions, has been consistently lower (closer to  
335 zero) than the growth suggested by the monthly, tonnage-based production and import data,  
336 and this is reflected in the projection. This pattern is only partially explained by stock changes  
337 and changes in energy content. It is therefore not possible to be certain that it will continue in  
338 the current year, but it is made plausible by a separate statement by the National Bureau of  
339 Statistics on energy consumption growth in the first half of 2019, which suggests no significant  
340 growth in energy consumption from coal for January-June (NBS, 2019a). Results and  
341 uncertainties are discussed further in Section 3.4.1.

342 For the USA, we use the forecast of the U.S. Energy Information Administration (EIA) for  
343 emissions from fossil fuels (EIA, 2019). This is based on an energy forecasting model which is  
344 updated monthly (last update with data through September 2019), and takes into account  
345 heating-degree days, household expenditures by fuel type, energy markets, policies, and other  
346 effects. We combine this with our estimate of emissions from cement production using the  
347 monthly U.S. cement data from USGS for January-July 2019, assuming changes in cement  
348 production over the first part of the year apply throughout the year. While the EIA's forecasts  
349 for current full-year emissions have on average been revised downwards, only ten such  
350 forecasts are available, so we conservatively use the full range of adjustments following  
351 revision, and additionally assume symmetrical uncertainty to give  $\pm 2.3\%$  around the central  
352 forecast.

353 For India, we use (1) monthly coal production and sales data from the (Ministry of Mines,  
354 2019), Coal India Limited (CIL, 2019) and Singareni Collieries Company Limited (SCCL, 2019),  
355 combined with import data from the Ministry of Commerce and Industry (MCI, 2019) and  
356 power station stocks data from the Central Electricity Authority (CEA, 2019a); (2) monthly oil  
357 production and consumption data from the Ministry of Petroleum and Natural Gas (PPAC,  
358 2019b); (3) monthly natural gas production and import data from the Ministry of Petroleum

359 and Natural Gas (PPAC, 2019a); and (4) monthly cement production data from the Office of the  
 360 Economic Advisor (OEA, 2019). All data were available for January to September or October  
 361 2019. We use Holt-Winters exponential smoothing with multiplicative seasonality (Chatfield,  
 362 1978) on each of these four emissions series to project to the end of India’s current financial  
 363 year (March 2020). This iterative method produces estimates of both trend and seasonality at  
 364 the end of the observation period that are a function of all prior observations, weighted most  
 365 strongly to more recent data, while maintaining some smoothing effect. The main source of  
 366 uncertainty in the projection of India’s emissions is the assumption of continued trends and  
 367 typical seasonality.

368 For the EU, we use (1) monthly coal supply data from Eurostat for the first 6-9 months of 2019  
 369 (Eurostat, 2019) cross-checked with more recent data on coal-generated electricity from  
 370 ENTSO-E for January through October 2019 (ENTSO-E, 2019); (2) monthly oil and gas demand  
 371 data for January through August from the Joint Organisations Data Initiative (JODI, 2019); and  
 372 (3) cement production is assumed stable. For oil and natural gas emissions we apply the Holt-  
 373 Winters method separately to each country and energy carrier to project to the end of the  
 374 current year, while for coal — which is much less strongly seasonal because of strong weather  
 375 variations — we assume the remaining months of the year are the same as the previous year in  
 376 each country.

377 For the rest of the world, we use the close relationship between the growth in GDP and the  
 378 growth in emissions (Raupach et al., 2007) to project emissions for the current year. This is  
 379 based on a simplified Kaya Identity, whereby  $E_{FF}$  (GtC yr<sup>-1</sup>) is decomposed by the product of GDP  
 380 (USD yr<sup>-1</sup>) and the fossil fuel carbon intensity of the economy ( $I_{FF}$ ; GtC USD<sup>-1</sup>) as follows:

$$\boxed{E_{FF} = GDP \times I_{FF}} \quad (3)$$

381 Taking a time derivative of Equation (3) and rearranging gives:

$$\boxed{\frac{1}{E_{FF}} \frac{dE_{FF}}{dt} = \frac{1}{GDP} \frac{dGDP}{dt} + \frac{1}{I_{FF}} \frac{dI_{FF}}{dt}} \quad (4)$$

382 where the left-hand term is the relative growth rate of  $E_{FF}$ , and the right-hand terms are the  
 383 relative growth rates of GDP and  $I_{FF}$ , respectively, which can simply be added linearly to give the  
 384 overall growth rate.

385 As preliminary estimates of annual change in GDP are made well before the end of a calendar  
 386 year, making assumptions on the growth rate of  $I_{FF}$  allows us to make projections of the annual

387 change in CO<sub>2</sub> emissions well before the end of a calendar year. The I<sub>FF</sub> is based on GDP in  
388 constant PPP (purchasing power parity) from the International Energy Agency (IEA) up to 2016  
389 (IEA/OECD, 2018) and extended using the International Monetary Fund (IMF) growth rates  
390 through 2018 (IMF, 2019a). Interannual variability in I<sub>FF</sub> is the largest source of uncertainty in  
391 the GDP-based emissions projections. We thus use the standard deviation of the annual I<sub>FF</sub> for  
392 the period 2009-2018 as a measure of uncertainty, reflecting a  $\pm 1\sigma$  as in the rest of the carbon  
393 budget. In this year's budget, we have extended the rest-of-the-world method to fuel type to  
394 get separate projections for coal, oil, natural gas, cement, flaring, and other components. This  
395 allows, for the first time, consistent projections of global emissions by both countries and by  
396 fuel type.

397 The 2019 projection for the world is made of the sum of the projections for China, USA, EU,  
398 India, and the rest of the world, where the sum is consistent if done by fuel type (coal, oil,  
399 natural gas) or based on total emissions. The uncertainty is added in quadrature among the five  
400 regions. The uncertainty here reflects the best of our expert opinion.

## 401 **2.2 CO<sub>2</sub> emissions from land-use, land-use change and forestry (E<sub>LUC</sub>)**

402 The net CO<sub>2</sub> flux from land-use, land-use change and forestry (E<sub>LUC</sub>, called land-use change  
403 emissions in the rest of the text) include CO<sub>2</sub> fluxes from deforestation, afforestation, logging  
404 and forest degradation (including harvest activity), shifting cultivation (cycle of cutting forest for  
405 agriculture, then abandoning), and regrowth of forests following wood harvest or  
406 abandonment of agriculture. Only some land management activities are included in our land-  
407 use change emissions estimates (Table A1). Some of these activities lead to emissions of CO<sub>2</sub> to  
408 the atmosphere, while others lead to CO<sub>2</sub> sinks. E<sub>LUC</sub> is the net sum of emissions and removals  
409 due to all anthropogenic activities considered. Our annual estimate for 1959-2018 is provided  
410 as the average of results from two bookkeeping models (Section 2.2.1): the estimate published  
411 by (Houghton and Nassikas, 2017; hereafter H&N2017) updated to 2018, and an estimate using  
412 the Bookkeeping of Land Use Emissions model (Hansis et al., 2015; hereafter BLUE). Both data  
413 sets are then extrapolated to provide a projection for 2019 (Section 2.2.4). In addition, we use  
414 results from Dynamic Global Vegetation Models (DGVMs; see Section 2.2.2 and Table 4), to help  
415 quantify the uncertainty in E<sub>LUC</sub> (Section 2.2.3), and thus better characterise our understanding.

## 416 2.2.1 Bookkeeping models

417 Land-use change CO<sub>2</sub> emissions and uptake fluxes are calculated by two bookkeeping models.  
418 Both are based on the original bookkeeping approach of Houghton (2003) that keeps track of  
419 the carbon stored in vegetation and soils before and after a land-use change (transitions  
420 between various natural vegetation types, croplands and pastures). Literature-based response  
421 curves describe decay of vegetation and soil carbon, including transfer to product pools of  
422 different lifetimes, as well as carbon uptake due to regrowth. In addition, the bookkeeping  
423 models represent long-term degradation of primary forest as lowered standing vegetation and  
424 soil carbon stocks in secondary forests, and also include forest management practices such as  
425 wood harvests.

426 The bookkeeping models do not include land ecosystems' transient response to changes in  
427 climate, atmospheric CO<sub>2</sub> and other environmental factors, and the carbon densities are based  
428 on contemporary data reflecting stable environmental conditions at that time. Since carbon  
429 densities remain fixed over time in bookkeeping models, the additional sink capacity that  
430 ecosystems provide in response to CO<sub>2</sub>-fertilization and some other environmental changes is  
431 not captured by these models (Pongratz et al., 2014; see Section 2.7.4).

432 The H&N2017 and BLUE models differ in (1) computational units (country-level vs spatially  
433 explicit treatment of land-use change), (2) processes represented (see Table A1), and (3) carbon  
434 densities assigned to vegetation and soil of each vegetation type. A notable change of  
435 H&N2017 over the original approach by Houghton (2003) used in earlier budget estimates is  
436 that no shifting cultivation or other back- and forth-transitions at a level below country are  
437 included. Only a decline in forest area in a country as indicated by the Forest Resource  
438 Assessment of the FAO that exceeds the expansion of agricultural area as indicated by FAO is  
439 assumed to represent a concurrent expansion and abandonment of cropland. In contrast, the  
440 BLUE model includes sub-grid-scale transitions at the grid level between all vegetation types as  
441 indicated by the harmonized land-use change data (LUH2) data set

442 (<https://doi.org/10.22033/ESGF/input4MIPs.1127>; Hurtt et al., 2011; Hurtt et al., in prep.).

443 Furthermore, H&N2017 assume conversion of natural grasslands to pasture, while BLUE  
444 allocates pasture proportionally on all natural vegetation that exist in a grid-cell. This is one  
445 reason for generally higher emissions in BLUE. For both H&N2017 and BLUE, we add carbon  
446 emissions from peat burning based on the Global Fire Emission Database (GFED4s; van der

447 Werf et al., 2017), and peat drainage, based on estimates by Hooijer et al. (2010) to the output  
448 of their bookkeeping model for the countries of Indonesia and Malaysia. Peat burning and  
449 emissions from the organic layers of drained peat soils, which are not captured by bookkeeping  
450 methods directly, need to be included to represent the substantially larger emissions and  
451 interannual variability due to synergies of land-use and climate variability in Southeast Asia, in  
452 particular during El-Niño events.

453 The two bookkeeping estimates used in this study differ with respect to the land-use change  
454 data used to drive the models. H&N2017 base their estimates directly on the Forest Resource  
455 Assessment of the FAO which provides statistics on forest-area change and management at  
456 intervals of five years currently updated until 2015 (FAO, 2015). The data is based on country  
457 reporting to FAO, and may include remote-sensing information in more recent assessments.  
458 Changes in land-use other than forests are based on annual, national changes in cropland and  
459 pasture areas reported by FAO (FAOSTAT, 2015). H&N2017 was extended here for 2016 to 2018  
460 by adding the annual change in total tropical emissions to the H&N2017 estimate for 2015,  
461 including estimates of peat drainage and peat burning as described above as well as emissions  
462 from tropical deforestation and degradation fires from GFED4.1s (van der Werf et al., 2017).  
463 On the other hand, BLUE uses the harmonised land-use change data LUH2 covering the entire  
464 850-2018 period (<https://doi.org/10.22033/ESGF/input4MIPs.1127>; Hurtt et al., 2011; Hurtt et  
465 al., in prep.), which describes land-use change, also based on the FAO data as well as the HYDE  
466 dataset (Goldewijk et al., 2017a, 2017b), but downscaled at a quarter-degree spatial resolution,  
467 considering sub-grid-scale transitions between primary forest, secondary forest, cropland,  
468 pasture and rangeland. The LUH2 data provides a distinction between rangelands and pasture,  
469 based on inputs from HYDE. To constrain the models' interpretation on whether rangeland  
470 implies the original natural vegetation to be transformed to grassland or not (e.g., browsing on  
471 shrubland), a forest mask was provided with LUH2; forest is assumed to be transformed, while  
472 all other natural vegetation remains. This is implemented in BLUE.

473 For  $E_{LUC}$  from 1850 onwards we average the estimates from BLUE and H&N2017. For the  
474 cumulative numbers starting 1750 an average of four earlier publications is added ( $30 \pm 20$  PgC  
475 1750-1850, rounded to nearest 5; Le Quéré et al., 2016).

## 476 **2.2.2 Dynamic Global Vegetation Models (DGVMs)**

477 Land-use change CO<sub>2</sub> emissions have also been estimated using an ensemble of 15 DGVM  
478 simulations. The DGVMs account for deforestation and regrowth, the most important  
479 components of E<sub>LUC</sub>, but they do not represent all processes resulting directly from human  
480 activities on land (Table A1). All DGVMs represent processes of vegetation growth and  
481 mortality, as well as decomposition of dead organic matter associated with natural cycles, and  
482 include the vegetation and soil carbon response to increasing atmospheric CO<sub>2</sub> concentration  
483 and to climate variability and change. Some models explicitly simulate the coupling of carbon  
484 and nitrogen cycles and account for atmospheric N deposition and N fertilisers (Table A1). The  
485 DGVMs are independent from the other budget terms except for their use of atmospheric CO<sub>2</sub>  
486 concentration to calculate the fertilization effect of CO<sub>2</sub> on plant photosynthesis.

487 Many DGVMs used the HYDE land-use change data set (Goldewijk et al., 2017a, 2017b), which  
488 provides annual (1700-2018), half-degree, fractional data on cropland and pasture. The data are  
489 based on the available annual FAO statistics of change in agricultural land area available until  
490 2015. Last year's HYDE version used FAO statistics until 2012, which are now supplemented  
491 using the annual change anomalies from FAO data for years 2013-2015 relative to year 2012.  
492 HYDE forcing was also corrected for Brazil for years 1951-2012. After the year 2015 HYDE  
493 extrapolates cropland, pasture, and urban land-use data until the year 2018. Some models also  
494 use the LUH2 data set, an update of the more comprehensive harmonised land-use data set  
495 (Hurtt et al., 2011), that further includes fractional data on primary and secondary forest  
496 vegetation, as well as all underlying transitions between land-use states (1700-2019)  
497 (<https://doi.org/10.22033/ESGF/input4MIPs.1127>; Hurtt et al., 2011; Hurtt et al., in prep.; Table  
498 A1). This new data set is of quarter degree fractional areas of land-use states and all transitions  
499 between those states, including a new wood harvest reconstruction, new representation of  
500 shifting cultivation, crop rotations, management information including irrigation and fertilizer  
501 application. The land-use states include five different crop types in addition to the pasture-  
502 rangeland split discussed before. Wood harvest patterns are constrained with Landsat-based  
503 tree cover loss data (Hansen et al. 2013). Updates of LUH2 over last year's version are using the  
504 most recent HYDE/FAO release (covering the time period up to including 2015), which also  
505 corrects an error in the version used for the 2018 budget in Brazil.

506 DGVMs implement land-use change differently (e.g. an increased cropland fraction in a grid cell  
507 can either be at the expense of grassland or shrubs, or forest, the latter resulting in  
508 deforestation; land cover fractions of the non-agricultural land differ between models).  
509 Similarly, model-specific assumptions are applied to convert deforested biomass or deforested  
510 area, and other forest product pools into carbon, and different choices are made regarding the  
511 allocation of rangelands as natural vegetation or pastures.

512 The DGVM model runs were forced by either the merged monthly CRU and 6 hourly JRA-55  
513 data set or by the monthly CRU data set, both providing observation-based temperature,  
514 precipitation, and incoming surface radiation on a  $0.5^\circ \times 0.5^\circ$  grid and updated to 2018 (Harris et  
515 al., 2014). The combination of CRU monthly data with 6 hourly forcing from JRA-55 (Kobayashi  
516 et al., 2015) is performed with methodology used in previous years (Viovy, 2016) adapted to  
517 the specifics of the JRA-55 data. The forcing data also include global atmospheric  $\text{CO}_2$ , which  
518 changes over time (Dlugokencky and Tans, 2019), and gridded, time dependent N deposition  
519 and N fertilisers (as used in some models; Table A1).

520 Two sets of simulations were performed with the DGVMs. Both applied historical changes in  
521 climate, atmospheric  $\text{CO}_2$  concentration, and N inputs. The two sets of simulations differ,  
522 however, with respect to land-use: one set applies historical changes in land-use, the other a  
523 time-invariant pre-industrial land cover distribution and pre-industrial wood harvest rates. By  
524 difference of the two simulations, the dynamic evolution of vegetation biomass and soil carbon  
525 pools in response to land-use change can be quantified in each model ( $E_{\text{LUC}}$ ). Using the  
526 difference between these two DGVM simulations to diagnose ELUC means the DGVMs account  
527 for the loss of additional sink capacity (around  $0.4 \pm 0.3 \text{ GtC yr}^{-1}$ ; see Section 2.7.4), while the  
528 bookkeeping models do not.

529 As a criterion for inclusion in this carbon budget, we only retain models that simulate a positive  
530  $E_{\text{LUC}}$  during the 1990s, as assessed in the IPCC AR4 (Denman et al., 2007) and AR5 (Ciais et al.,  
531 2013). All DGVMs met this criteria, although one model was not included in the  $E_{\text{LUC}}$  estimate  
532 from DGVMs as it exhibited a spurious response to the transient land cover change forcing after  
533 its initial spin-up.

### 534 **2.2.3 Uncertainty assessment for $E_{LUC}$**

535 Differences between the bookkeeping models and DGVM models originate from three main  
536 sources: the different methodologies; the underlying land-use/land cover data set, and the  
537 different processes represented (Table A1). We examine the results from the DGVM models  
538 and of the bookkeeping method, and use the resulting variations as a way to characterise the  
539 uncertainty in  $E_{LUC}$ .

540 The  $E_{LUC}$  estimate from the DGVMs multi-model mean is consistent with the average of the  
541 emissions from the bookkeeping models (Table 5). However there are large differences among  
542 individual DGVMs (standard deviation at around  $0.5 \text{ GtC yr}^{-1}$ ; Table 5), between the two  
543 bookkeeping models (average difference of  $0.7 \text{ GtC yr}^{-1}$ ), and between the current estimate of  
544 H&N2017 and its previous model version (Houghton et al., 2012). The uncertainty in  $E_{LUC}$  of  $\pm 0.7$   
545  $\text{GtC yr}^{-1}$  reflects our best value judgment that there is at least 68% chance ( $\pm 1\sigma$ ) that the true  
546 land-use change emission lies within the given range, for the range of processes considered  
547 here. Prior to the year 1959, the uncertainty in  $E_{LUC}$  was taken from the standard deviation of  
548 the DGVMs. We assign low confidence to the annual estimates of  $E_{LUC}$  because of the  
549 inconsistencies among estimates and of the difficulties to quantify some of the processes in  
550 DGVMs.

### 551 **2.2.4 Emissions projections**

552 We project the 2019 land-use emissions for both H&N2017 and BLUE, starting from their  
553 estimates for 2018 and adding observed changes in emissions from peat drainage (update on  
554 (Hooijer et al., 2010) as well as emissions from peat fires, tropical deforestation and  
555 degradation as estimated using active fire data (MCD14ML; Giglio et al., 2016). Those latter  
556 scale almost linearly with GFED over large areas (van der Werf et al., 2017), and thus allows for  
557 tracking fire emissions in deforestation and tropical peat zones in near-real time. During most  
558 years, emissions during January-September cover most of the fire season in the Amazon and  
559 Southeast Asia, where a large part of the global deforestation takes place. While the degree to  
560 which the fires in 2019 in the Amazon are related to land-use change requires more scrutiny,  
561 initial analyses based on fire radiative power (FRP) of the fires detected indicate that many fires  
562 were associated with deforestation (<http://www.globalfiredata.org/forecast.html>, accessed  
563 September 23, 2019). Most fires burning in Indonesia were on peatlands, which also represent  
564 a net source of  $\text{CO}_2$ .

## 565 **2.3 Growth rate in atmospheric CO<sub>2</sub> concentration (G<sub>ATM</sub>)**

### 566 **2.3.1 Global growth rate in atmospheric CO<sub>2</sub> concentration**

567 The rate of growth of the atmospheric CO<sub>2</sub> concentration is provided by the US National  
568 Oceanic and Atmospheric Administration Earth System Research Laboratory (NOAA/ESRL;  
569 Dlugokencky and Tans, 2019), which is updated from Ballantyne et al. (2012). For the 1959-  
570 1979 period, the global growth rate is based on measurements of atmospheric CO<sub>2</sub>  
571 concentration averaged from the Mauna Loa and South Pole stations, as observed by the CO<sub>2</sub>  
572 Program at Scripps Institution of Oceanography (Keeling et al., 1976). For the 1980-2018 time  
573 period, the global growth rate is based on the average of multiple stations selected from the  
574 marine boundary layer sites with well-mixed background air (Ballantyne et al., 2012), after  
575 fitting each station with a smoothed curve as a function of time, and averaging by latitude band  
576 (Masarie and Tans, 1995). The annual growth rate is estimated by Dlugokencky and Tans (2019)  
577 from atmospheric CO<sub>2</sub> concentration by taking the average of the most recent December-  
578 January months corrected for the average seasonal cycle and subtracting this same average one  
579 year earlier. The growth rate in units of ppm yr<sup>-1</sup> is converted to units of GtC yr<sup>-1</sup> by multiplying  
580 by a factor of 2.124 GtC per ppm (Ballantyne et al., 2012).

581 The uncertainty around the atmospheric growth rate is due to three main factors. First, the  
582 long-term reproducibility of reference gas standards (around 0.03 ppm for 1σ from the 1980s;  
583 Dlugokencky and Tans, 2019). Second, small unexplained systematic analytical errors that may  
584 have a duration of several months to two years come and go. They have been simulated by  
585 randomizing both the duration and the magnitude (determined from the existing evidence) in a  
586 Monte Carlo procedure. Third, the network composition of the marine boundary layer with  
587 some sites coming or going, gaps in the time series at each site, etc (Dlugokencky and Tans,  
588 2019). The latter uncertainty was estimated by NOAA/ESRL with a Monte Carlo method by  
589 constructing 100 "alternative" networks (Masarie and Tans, 1995; NOAA/ESRL, 2019). The  
590 second and third uncertainties, summed in quadrature, add up to 0.085 ppm on average  
591 (Dlugokencky and Tans, 2019). Fourth, the uncertainty associated with using the average CO<sub>2</sub>  
592 concentration from a surface network to approximate the true atmospheric average CO<sub>2</sub>  
593 concentration (mass-weighted, in 3 dimensions) as needed to assess the total atmospheric CO<sub>2</sub>  
594 burden. In reality, CO<sub>2</sub> variations measured at the stations will not exactly track changes in total  
595 atmospheric burden, with offsets in magnitude and phasing due to vertical and horizontal

596 mixing. This effect must be very small on decadal and longer time scales, when the atmosphere  
597 can be considered well mixed. Preliminary estimates suggest this effect would increase the  
598 annual uncertainty, but a full analysis is not yet available. We therefore maintain an uncertainty  
599 around the annual growth rate based on the multiple stations data set ranges between 0.11  
600 and 0.72 GtC yr<sup>-1</sup>, with a mean of 0.61 GtC yr<sup>-1</sup> for 1959-1979 and 0.17 GtC yr<sup>-1</sup> for 1980-2018,  
601 when a larger set of stations were available as provided by Dlugokencky and Tans (2019), but  
602 recognise further exploration of this uncertainty is required. At this time, we estimate the  
603 uncertainty of the decadal averaged growth rate after 1980 at 0.02 GtC yr<sup>-1</sup> based on the  
604 calibration and the annual growth rate uncertainty, but stretched over a 10-year interval. For  
605 years prior to 1980, we estimate the decadal averaged uncertainty to be 0.07 GtC yr<sup>-1</sup> based on  
606 a factor proportional to the annual uncertainty prior and after 1980 (0.02 \* [0.61/0.17] GtC yr<sup>-1</sup>).  
607

608 We assign a high confidence to the annual estimates of G<sub>ATM</sub> because they are based on direct  
609 measurements from multiple and consistent instruments and stations distributed around the  
610 world (Ballantyne et al., 2012).

611 In order to estimate the total carbon accumulated in the atmosphere since 1750 or 1850, we  
612 use an atmospheric CO<sub>2</sub> concentration of 277 ± 3 ppm or 286 ± 3 ppm, respectively, based on a  
613 cubic spline fit to ice core data (Joos and Spahni, 2008). The uncertainty of ±3 ppm (converted  
614 to ±1σ) is taken directly from the IPCC's assessment (Ciais et al., 2013). Typical uncertainties in  
615 the growth rate in atmospheric CO<sub>2</sub> concentration from ice core data are equivalent to ±0.1-  
616 0.15 GtC yr<sup>-1</sup> as evaluated from the Law Dome data (Etheridge et al., 1996) for individual 20-  
617 year intervals over the period from 1850 to 1960 (Bruno and Joos, 1997).

### 618 **2.3.2 Atmospheric growth rate projection**

619 We provide an assessment of G<sub>ATM</sub> for 2019 based on the monthly calculated global  
620 atmospheric CO<sub>2</sub> concentration (GLO) through July (Dlugokencky and Tans, 2019), and bias-  
621 adjusted Holt–Winters exponential smoothing with additive seasonality (Chatfield, 1978) to  
622 project to January 2020. The assessment method used this year differs from the forecast  
623 method used last year (Le Quéré et al., 2018b), which was based on the observed  
624 concentrations at Mauna Loa (MLO) only, using the historical relationship between the MLO  
625 and GLO series. Additional analysis suggests that the first half of the year shows more  
626 interannual variability than the second half of the year, so that the exact projection method

627 applied to the second half of the year has a relatively smaller impact on the projection of the  
628 full year. Uncertainty is estimated from past variability using the standard deviation of the last 5  
629 years' monthly growth rates.

## 630 **2.4 Ocean CO<sub>2</sub> sink**

631 Estimates of the global ocean CO<sub>2</sub> sink  $S_{\text{OCEAN}}$  are from an ensemble of global ocean  
632 biogeochemistry models (GOBMs, Table A2) that meet observational constraints over the 1990s  
633 (see below). We use observation-based estimates of  $S_{\text{OCEAN}}$  to provide a qualitative assessment  
634 of confidence in the reported results, and two diagnostic ocean models to estimate  $S_{\text{OCEAN}}$  over  
635 the industrial era (see below).

### 636 **2.4.1 Observation-based estimates**

637 We use the observational constraints assessed by IPCC of a mean ocean CO<sub>2</sub> sink of  $2.2 \pm 0.4$   
638 GtC yr<sup>-1</sup> for the 1990s (Denman et al., 2007) to verify that the GOBMs provide a realistic  
639 assessment of  $S_{\text{OCEAN}}$ . This is based on indirect observations with seven different methodologies  
640 and their uncertainties, using the methods that are deemed most reliable for the assessment of  
641 this quantity (Denman et al., 2007). The IPCC confirmed this assessment in 2013 (Ciais et al.,  
642 2013). The observational-based estimates use the ocean/land CO<sub>2</sub> sink partitioning from  
643 observed atmospheric O<sub>2</sub>/N<sub>2</sub> concentration trends (Manning and Keeling, 2006; updated in  
644 Keeling and Manning, 2014), an oceanic inversion method constrained by ocean  
645 biogeochemistry data (Mikaloff Fletcher et al., 2006), and a method based on penetration time  
646 scale for chlorofluorocarbons (McNeil et al., 2003). The IPCC estimate of 2.2 GtC yr<sup>-1</sup> for the  
647 1990s is consistent with a range of methods (Wanninkhof et al., 2013).

648 We also use three estimates of the ocean CO<sub>2</sub> sink and its variability based on interpolations of  
649 measurements of surface ocean fugacity of CO<sub>2</sub> (pCO<sub>2</sub> corrected for the non-ideal behaviour of  
650 the gas; Pfeil et al., 2013). We refer to these as pCO<sub>2</sub>-based flux estimates. The measurements  
651 are from the Surface Ocean CO<sub>2</sub> Atlas version 2019, which is an update of version 3 (Bakker et  
652 al., 2016) and contains quality-controlled data to 2018 (see data attribution Table A4). The  
653 SOCAT v2019 data were mapped using a data-driven diagnostic method (Rödenbeck et al.,  
654 2013; referred to here as Jena-MLS), a combined self-organising map and feed-forward neural  
655 network (Landschützer et al., 2014; MPI-SOMFFN), and an artificial neural network model  
656 (Denvil-Sommer et al., 2019; Copernicus Marine Environment Monitoring Service (CMEMS)).

657 The global pCO<sub>2</sub>-based flux estimates were adjusted to remove the pre-industrial ocean source  
658 of CO<sub>2</sub> to the atmosphere of 0.78 GtC yr<sup>-1</sup> from river input to the ocean (Resplandy et al., 2018),  
659 per our definition of S<sub>OCEAN</sub>. Several other ocean sink products based on observations are also  
660 available but they continue to show large unresolved discrepancies with observed variability.  
661 Here we used, as in our previous annual budgets, the two pCO<sub>2</sub>-based flux products that had  
662 the best fit to observations for their representation of tropical and global variability (Rödenbeck  
663 et al., 2015), plus CMEMS which has a similarly good fit with observations. The CO<sub>2</sub> flux from  
664 each pCO<sub>2</sub>-based product is scaled by the ratio of the total ocean area covered by the  
665 respective product to the total ocean area (361.9e6 km<sup>2</sup>) from ETOPO1 (Amante and Eakins,  
666 2009; Eakins and Sharman, 2010). In products where the covered area varies with time (MPI-  
667 SOMFFN, CMEMS) we use the maximum area coverage. The data-products cover 88% (MPI-  
668 SOMFFN, CMEMS) to 101% of the observed total ocean area, so two products are effectively  
669 corrected upwards by a factor of 1.126.

670 We further use results from two diagnostic ocean models of Khatiwala et al. (2013) and DeVries  
671 (2014) to estimate the anthropogenic carbon accumulated in the ocean prior to 1959. The two  
672 approaches assume constant ocean circulation and biological fluxes, with S<sub>OCEAN</sub> estimated as a  
673 response in the change in atmospheric CO<sub>2</sub> concentration calibrated to observations. The  
674 uncertainty in cumulative uptake of ±20 GtC (converted to ±1σ) is taken directly from the IPCC's  
675 review of the literature (Rhein et al., 2013), or about ±30% for the annual values (Khatiwala et  
676 al., 2009).

#### 677 **2.4.2 Global Ocean Biogeochemistry Models (GOBMs)**

678 The ocean CO<sub>2</sub> sink for 1959-2018 is estimated using nine GOBMs (Table A2). The GOBMs  
679 represent the physical, chemical and biological processes that influence the surface ocean  
680 concentration of CO<sub>2</sub> and thus the air-sea CO<sub>2</sub> flux. The GOBMs are forced by meteorological  
681 reanalysis and atmospheric CO<sub>2</sub> concentration data available for the entire time period. They  
682 mostly differ in the source of the atmospheric forcing data (meteorological reanalysis), spin up  
683 strategies, and in their horizontal and vertical resolutions (Table A2). GOBMs do not include the  
684 effects of anthropogenic changes in nutrient supply, which could lead to an increase of the  
685 ocean sink of up to about 0.3 GtC yr<sup>-1</sup> over the industrial period (Duce et al., 2008). They also do  
686 not include the perturbation associated with changes in riverine organic carbon (see Section  
687 2.7.3).

688 The annual mean air-sea CO<sub>2</sub> flux from the GOBMs is corrected for any model bias or drift by  
689 subtracting the time-dependent model bias. The time-dependent model bias is calculated as a  
690 linear fit to the annual CO<sub>2</sub> flux from a control simulation with no climate variability and change  
691 and constant pre-industrial CO<sub>2</sub> concentration. The absolute biases per model in the 1990s vary  
692 between 0.005 GtC yr<sup>-1</sup> and 0.362 GtC yr<sup>-1</sup>, with some models having positive and some having  
693 negative biases. The bias-correction reduces the model mean ocean carbon sink by 0.06 GtC yr<sup>-1</sup>  
694 in the 1990s. The CO<sub>2</sub> flux from each model is scaled by the ratio of the total ocean area  
695 covered by the respective GOBM to the total ocean area (361.9e6 km<sup>2</sup>) from ETOPO1 (Amante  
696 and Eakins, 2009; Eakins and Sharman, 2010). The ocean models cover 97% to 101% of the total  
697 ocean area, so the effect of this correction is small. All models fell within the observational  
698 constraint for the 1990s before and after applying the corrections.

#### 699 **2.4.3 GOBM evaluation and uncertainty assessment for S<sub>OCEAN</sub>**

700 The mean ocean CO<sub>2</sub> sink for all GOBMs falls within 90% confidence of the observed range, or  
701 1.6 to 2.8 GtC yr<sup>-1</sup> for the 1990s. Here we have adjusted the confidence interval to the IPCC  
702 confidence interval of 90% to avoid rejecting models that may be outliers but are still plausible.

703 The GOBMs and flux products have been further evaluated using air-sea CO<sub>2</sub> flux (fCO<sub>2</sub>) from  
704 the SOCAT v2019 database (Bakker et al., 2016; updated). We focused this evaluation on the  
705 root mean squared error (RMSE) between observed fCO<sub>2</sub> and modelled pCO<sub>2</sub> and on a measure  
706 of the amplitude of the interannual variability of the flux (Rödenbeck et al., 2015). The  
707 amplitude of the S<sub>OCEAN</sub> interannual variability (A-IAV) is calculated as the temporal standard  
708 deviation of a 12-months running mean over the CO<sub>2</sub> flux time-series (Rödenbeck et al., 2015).

709 The RMSE is only calculated for open ocean (water depth > 400 m) grid points on a 1 degree x 1  
710 degree x monthly grid where actual observations exist. These metrics are chosen because RMSE  
711 is the most direct measure of data-model mismatch and the A-IAV is a direct measure of the  
712 variability of S<sub>OCEAN</sub> on interannual timescales. We apply these metrics globally and by latitude  
713 bands (Fig. B1). Results are shown in Fig. B1 and discussed in Section 3.1.3.

714 The uncertainty around the mean ocean sink of anthropogenic CO<sub>2</sub> was quantified by Denman  
715 et al. (2007) for the 1990s (see Section 2.4.1). To quantify the uncertainty around annual values,  
716 we examine the standard deviation of the GOBM ensemble, which averages 0.3 GtC yr<sup>-1</sup> during  
717 1959-2018. We estimate that the uncertainty in the annual ocean CO<sub>2</sub> sink is about ± 0.5 GtC yr<sup>-1</sup>

718 <sup>1</sup> from the combined uncertainty of the mean flux based on observations of  $\pm 0.4 \text{ GtC yr}^{-1}$   
719 (Denman et al., 2007) and the standard deviation across GOBMs of up to  $\pm 0.4 \text{ GtC yr}^{-1}$ ,  
720 reflecting both the uncertainty in the mean sink from observations during the 1990's (Denman  
721 et al., 2007; Section 2.4.1) and in the interannual variability as assessed by GOBMs.  
722 We examine the consistency between the variability of the model-based and the pCO<sub>2</sub>-based  
723 flux products to assess confidence in S<sub>OCEAN</sub>. The interannual variability of the ocean fluxes  
724 (quantified as the standard deviation) of the three pCO<sub>2</sub>-based flux products for 1985-2018  
725 (where they overlap) is  $\pm 0.37 \text{ GtC yr}^{-1}$  (Jena-MLS),  $\pm 0.46 \text{ GtC yr}^{-1}$  (MPI-SOMFFN) and  $\pm 0.51 \text{ GtC}$   
726  $\text{yr}^{-1}$  (CMEMS). The inter-annual variability in the mean of the pCO<sub>2</sub>-based flux estimates is  $\pm$   
727  $0.41 \text{ GtC yr}^{-1}$  for the 1985-2018 period, compared to  $\pm 0.31 \text{ GtC yr}^{-1}$  for the GOBM ensemble.  
728 The standard deviation includes a component of trend and decadal variability in addition to  
729 interannual variability, and their relative influence differs across estimates. Individual estimates  
730 (both GOBM and flux products) generally produce a higher ocean CO<sub>2</sub> sink during strong El Niño  
731 events. The annual pCO<sub>2</sub>-based flux products correlate with the ocean CO<sub>2</sub> sink estimated here  
732 with a correlation of  $r = 0.75$  (0.55 to 0.79 for individual GOBMs),  $r = 0.86$  (0.70 to 0.87) and  
733  $0.93$  (0.83 to 0.93) for the pCO<sub>2</sub>-based flux products of Jena-MLS, MPI-SOMFFN and CMEMS,  
734 respectively (simple linear regression). The average of the GOBM estimates and of the data-  
735 based estimates have a mutual correlation of 0.91. The agreement between the models and the  
736 flux products reflects some consistency in their representation of underlying variability since  
737 there is little overlap in their methodology or use of observations. We assess a medium  
738 confidence level to the annual ocean CO<sub>2</sub> sink and its uncertainty because it is based on  
739 multiple lines of evidence, and the results are consistent in that the interannual variability in  
740 the GOBMs and data-based estimates are all generally small compared to the variability in the  
741 growth rate of atmospheric CO<sub>2</sub> concentration.

## 742 **2.5 Terrestrial CO<sub>2</sub> sink**

### 743 **2.5.1 DGVM simulations**

744 The terrestrial land sink (S<sub>LAND</sub>) is thought to be due to the combined effects of fertilisation by  
745 rising atmospheric CO<sub>2</sub> and N inputs on plant growth, as well as the effects of climate change  
746 such as the lengthening of the growing season in northern temperate and boreal areas. S<sub>LAND</sub>  
747 does not include land sinks directly resulting from land-use and land-use change (e.g. regrowth

748 of vegetation) as these are part of the land-use flux ( $E_{LUC}$ ), although system boundaries make it  
749 difficult to attribute exactly  $CO_2$  fluxes on land between  $S_{LAND}$  and  $E_{LUC}$  (Erb et al., 2013).

750  $S_{LAND}$  is estimated from the multi-model mean of 16 DGVMs (Table 4). As described in section  
751 2.2.2, DGVM simulations include all climate variability and  $CO_2$  effects over land, with some  
752 DGVMs also including the effect of N inputs. The DGVMs do not include the export of carbon to  
753 aquatic systems or its historical perturbation, which is discussed in section 2.7.3.

## 754 **2.5.2 DGVM evaluation and uncertainty assessment for $S_{LAND}$**

755 We apply three criteria for minimum DGVM realism by including only those DGVMs with (1)  
756 steady state after spin up, (2) net land fluxes ( $S_{LAND} - E_{LUC}$ ) that is an atmosphere-to-land carbon  
757 flux over the 1990s ranging between  $-0.3$  and  $2.3 \text{ GtC yr}^{-1}$ , within 90% confidence of constraints  
758 by global atmospheric and oceanic observations (Keeling and Manning, 2014; Wanninkhof et  
759 al., 2013), and (3) global  $E_{LUC}$  that is a carbon source to the atmosphere over the 1990s, as  
760 mentioned in section 2.2.2. All 16 DGVMs meet these three criteria.

761 In addition, the DGVM results are also evaluated using the International Land Model  
762 Benchmarking system (ILAMB; Collier et al., 2018). This evaluation is provided here to  
763 document, encourage and support model improvements through time. ILAMB variables cover  
764 key processes that are relevant for the quantification of  $S_{LAND}$  and resulting aggregated  
765 outcomes. The selected variables are vegetation biomass, gross primary productivity, leaf area  
766 index, net ecosystem exchange, ecosystem respiration, evapotranspiration, soil carbon, and  
767 runoff (see Fig. B2 for the results and for the list of observed databases). Results are shown in  
768 Fig. B2 and discussed in Section 3.1.3.

769 For the uncertainty for  $S_{LAND}$ , we use the standard deviation of the annual  $CO_2$  sink across the  
770 DGVMs, averaging to about  $\pm 0.6 \text{ GtC yr}^{-1}$  for the period 1959 to 2018. We attach a medium  
771 confidence level to the annual land  $CO_2$  sink and its uncertainty because the estimates from the  
772 residual budget and averaged DGVMs match well within their respective uncertainties (Table  
773 5).

## 774 **2.6 The atmospheric perspective**

775 The world-wide network of atmospheric measurements can be used with atmospheric  
776 inversion methods to constrain the location of the combined total surface  $CO_2$  fluxes from all  
777 sources, including fossil and land-use change emissions and land and ocean  $CO_2$  fluxes. The

778 inversions assume  $E_{FF}$  to be well known, and they solve for the spatial and temporal distribution  
779 of land and ocean fluxes from the residual gradients of  $CO_2$  between stations that are not  
780 explained by fossil fuel emissions.

781 Three atmospheric inversions (Table A3) used atmospheric  $CO_2$  data to the end of 2018  
782 (including preliminary values in some cases) to infer the spatio-temporal distribution of the  $CO_2$   
783 flux exchanged between the atmosphere and the land or oceans. We focus here on the largest  
784 and most consistent sources of information, namely the total land and ocean  $CO_2$  flux and their  
785 partitioning among the mid-high latitude region of the Northern Hemisphere ( $30^\circ N$ - $90^\circ N$ ), the  
786 tropics ( $30^\circ S$ - $30^\circ N$ ) and the mid-high latitude region of the Southern Hemisphere ( $30^\circ S$ - $90^\circ S$ ).  
787 We also break down those estimates for the land and ocean regions separately, to further  
788 scrutinise the constraints from atmospheric observations. We use these estimates to comment  
789 on the consistency across various data streams and process-based estimates.

### 790 **2.6.1 Atmospheric inversions**

791 The three inversion systems used in this release are the CarbonTracker Europe (CTE; Van Der  
792 Laan-Luijkx et al., 2017), the Jena CarboScope (Rödenbeck, 2005, with updates from Rödenbeck  
793 et al., 2018) and the Copernicus Atmosphere Monitoring Service (CAMS; Chevallier et al., 2005).  
794 See Table A3 for version numbers. The inversions are based on Bayesian inversion principles  
795 with prior information on fluxes and their uncertainty that interpret the same, for the most  
796 part, observed time series (or subsets thereof), but use different methodologies (Table A3).  
797 These differences mainly concern the selection of atmospheric  $CO_2$  data, the used prior fluxes,  
798 spatial breakdown (i.e. grid size), assumed correlation structures, and mathematical approach.  
799 The details of these approaches are documented extensively in the references provided above.  
800 Each system uses a different transport model, which was demonstrated to be a driving factor  
801 behind differences in atmospheric-based flux estimates, and specifically their distribution  
802 across latitudinal bands (e.g., Gaubert et al., 2018).

803 The inversions use atmospheric  $CO_2$  observations from various flask and in situ networks, as  
804 detailed in Table A3. They prescribe global fossil fuel emissions, which is already scaled to the  
805 present estimate of  $E_{FF}$  for CAMS, while CTE and CarboScope used slightly different  $E_{FF}$  values  
806 ( $<0.39 \text{ GtC yr}^{-1}$ ) based on alternative emissions compilations. Since this is known to result in  
807 different total  $CO_2$  uptake in atmospheric inversions (Peylin et al., 2013; Gaubert et al., 2018)  
808 we adjusted the land sink of each inversion estimate (where most of the fossil fuel emissions

809 occur) by its fossil fuel difference to the CAMS model. These differences amount to up to 0.5  
810 GtC for certain years in the region NH and are thus an important consideration in an inverse  
811 flux comparison.

812 The land/ocean CO<sub>2</sub> fluxes from atmospheric inversions contain anthropogenic perturbation  
813 and natural pre-industrial CO<sub>2</sub> fluxes. Natural pre-industrial fluxes are primarily land CO<sub>2</sub> sinks  
814 and ocean CO<sub>2</sub> sources corresponding to carbon taken up on land, transported by rivers from  
815 land to ocean, and outgassed by the ocean. These pre-industrial land CO<sub>2</sub> sinks are thus  
816 compensated over the globe by ocean CO<sub>2</sub> sources corresponding to the outgassing of riverine  
817 carbon inputs to the ocean. We apply the distribution of land-to-ocean C fluxes from rivers in  
818 three latitude bands using estimates from Resplandy et al. (2018), which are constrained by  
819 ocean heat transport to a total land-to-ocean carbon transfer of 0.78 GtC yr<sup>-1</sup>. The latitude  
820 distribution of river-induced ocean CO<sub>2</sub> sources (North: 0.20 GtC yr<sup>-1</sup>, Tropics: 0.19 GtC yr<sup>-1</sup>,  
821 South: 0.38 GtC yr<sup>-1</sup>) are derived from a simulation of the IPSL GOBM using as an input the river  
822 flux constrained by heat transport of Resplandy et al. (2018). To facilitate the comparison, we  
823 adjusted the inversions estimates of the land and ocean fluxes per latitude band with these  
824 numbers based on these results to produce historical perturbation CO<sub>2</sub> fluxes from inversions.

825 The atmospheric inversions are also evaluated using vertical profiles of atmospheric CO<sub>2</sub>  
826 concentrations (Fig. B3). More than 30 aircraft programs over the globe, either regular  
827 programs or repeated surveys over at least 9 months, have been used in order to draw a robust  
828 picture of the model performance (with space-time data coverage irregular and denser in the 0-  
829 45°N latitude band). The three models are compared to the independent aircraft CO<sub>2</sub>  
830 measurements between 2 and 7 km above sea level between 2001 and 2017. Results are shown  
831 in Fig. B3 and discussed in Section 3.1.3.

## 832 **2.7 Processes not included in the global carbon budget**

833 The contribution of anthropogenic CO and CH<sub>4</sub> to the global carbon budget is not fully  
834 accounted for in Eq. (1) and is described in Section 2.7.1. The contributions of other carbonates  
835 to CO<sub>2</sub> emissions is described in Section 2.7.2. The contribution of anthropogenic changes in  
836 river fluxes is conceptually included in Eq. (1) in S<sub>OCEAN</sub> and in S<sub>LAND</sub>, but it is not represented in  
837 the process models used to quantify these fluxes. This effect is discussed in Section 2.7.3 .  
838 Similarly, the loss of additional sink capacity from reduced forest cover is missing in the

839 combination of approaches used here to estimate both land fluxes ( $E_{LUC}$  and  $S_{LAND}$ ) and its  
840 potential effect is discussed and quantified in Section 2.7.4.

### 841 **2.7.1 Contribution of anthropogenic CO and CH<sub>4</sub> to the global carbon budget**

842 Equation (1) includes only partly the net input of CO<sub>2</sub> to the atmosphere from the chemical  
843 oxidation of reactive carbon-containing gases from sources other than the combustion of fossil  
844 fuels, such as: (1) cement process emissions, since these do not come from combustion of fossil  
845 fuels, (2) the oxidation of fossil fuels, (3) the assumption of immediate oxidation of vented  
846 methane in oil production. It omits however any other anthropogenic carbon-containing gases  
847 that are eventually oxidised in the atmosphere, such as anthropogenic emissions of CO and CH<sub>4</sub>.  
848 An attempt is made in this section to estimate their magnitude, and identify the sources of  
849 uncertainty. Anthropogenic CO emissions are from incomplete fossil fuel and biofuel burning  
850 and deforestation fires. The main anthropogenic emissions of fossil CH<sub>4</sub> that matter for the  
851 global carbon budget are the fugitive emissions of coal, oil and gas upstream sectors (see  
852 below). These emissions of CO and CH<sub>4</sub> contribute a net addition of fossil carbon to the  
853 atmosphere.

854 In our estimate of  $E_{FF}$  we assumed (Section 2.1.1) that all the fuel burned is emitted as CO<sub>2</sub>, thus  
855 CO anthropogenic emissions associated with incomplete combustion and their atmospheric  
856 oxidation into CO<sub>2</sub> within a few months are already counted implicitly in  $E_{FF}$  and should not be  
857 counted twice (same for  $E_{LUC}$  and anthropogenic CO emissions by deforestation fires).  
858 Anthropogenic emissions of fossil CH<sub>4</sub> are not included in  $E_{FF}$ , because these fugitive emissions  
859 are not included in the fuel inventories. Yet they contribute to the annual CO<sub>2</sub> growth rate after  
860 CH<sub>4</sub> gets oxidized into CO<sub>2</sub>. Anthropogenic emissions of fossil CH<sub>4</sub> represent 15% of total CH<sub>4</sub>  
861 emissions (Kirschke et al., 2013), that is 0.072 GtC yr<sup>-1</sup> for the past decade. Assuming steady  
862 state, these emissions are all converted to CO<sub>2</sub> by OH oxidation, and thus explain 0.06 GtC yr<sup>-1</sup>  
863 of the global CO<sub>2</sub> growth rate in the past decade, or 0.07-0.1 GtC yr<sup>-1</sup> using the higher CH<sub>4</sub>  
864 emissions reported recently (Schwietzke et al., 2016).

865 Other anthropogenic changes in the sources of CO and CH<sub>4</sub> from wildfires, vegetation biomass,  
866 wetlands, ruminants or permafrost changes are similarly assumed to have a small effect on the  
867 CO<sub>2</sub> growth rate. The CH<sub>4</sub> and CO emissions and sinks are published and analysed separately in  
868 the Global Methane Budget and Global Carbon Monoxide Budget publications, which follow a  
869 similar approach to that presented here (Saunio et al., 2016; Zheng et al., 2019).

## 870 **2.7.2 Contribution of other carbonates to CO<sub>2</sub> emissions**

871 The contribution of fossil carbonates other than cement production is not systematically  
872 included in estimates of  $E_{FF}$ , except at the national level where they are accounted in the  
873 UNFCCC national inventories. The missing processes include CO<sub>2</sub> emissions associated with the  
874 calcination of lime and limestone outside cement production, and the reabsorption of CO<sub>2</sub> by  
875 the rocks and concrete from carbonation through their lifetime (Xi et al., 2016). Carbonates are  
876 used in various industries, including in iron and steel manufacture and in agriculture. They are  
877 found naturally in some coals. Carbonation from cement life-cycle, including demolition and  
878 crushing, was estimated by one study to be around 0.25 GtC yr<sup>-1</sup> for year 2013 (Xi et al., 2016).  
879 Carbonation emissions from cement life-cycle would offset calcination emissions from lime and  
880 limestone production. The balance of these two processes is not clear.

## 881 **2.7.3 Anthropogenic carbon fluxes in the land-to-ocean aquatic continuum**

882 The approach used to determine the global carbon budget refers to the mean, variations, and  
883 trends in the perturbation of CO<sub>2</sub> in the atmosphere, referenced to the pre-industrial era.  
884 Carbon is continuously displaced from the land to the ocean through the land-ocean aquatic  
885 continuum (LOAC) comprising freshwaters, estuaries and coastal areas (Bauer et al., 2013;  
886 Regnier et al., 2013). A significant fraction of this lateral carbon flux is entirely 'natural' and is  
887 thus a steady state component of the pre-industrial carbon cycle. We account for this pre-  
888 industrial flux where appropriate in our study. However, changes in environmental conditions  
889 and land-use change have caused an increase in the lateral transport of carbon into the LOAC –  
890 a perturbation that is relevant for the global carbon budget presented here.

891 The results of the analysis of Regnier et al. (2013) can be summarized in two points of relevance  
892 for the anthropogenic CO<sub>2</sub> budget. First, the anthropogenic perturbation has increased the  
893 organic carbon export from terrestrial ecosystems to the hydrosphere by as much as  $1.0 \pm 0.5$   
894 GtC yr<sup>-1</sup> since pre-industrial, mainly owing to enhanced carbon export from soils. Second, this  
895 exported anthropogenic carbon is partly respired through the LOAC, partly sequestered in  
896 sediments along the LOAC and to a lesser extent, transferred to the open ocean where it may  
897 accumulate. The increase in storage of land-derived organic carbon in the LOAC and open  
898 ocean combined is estimated by Regnier et al. (2013) at  $0.65 \pm 0.35$  GtC yr<sup>-1</sup>. We do not attempt  
899 to incorporate the changes in LOAC in our study.

900 The inclusion of freshwater fluxes of anthropogenic CO<sub>2</sub> affects the estimates of, and  
901 partitioning between, S<sub>LAND</sub> and S<sub>OCEAN</sub> in Eq. (1), but does not affect the other terms. This effect  
902 is not included in the GOBMs and DGVMs used in our global carbon budget analysis presented  
903 here.

#### 904 **2.7.4 Loss of additional sink capacity**

905 Historical land-cover change was dominated by transitions from vegetation types that can  
906 provide a large carbon sink per area unit (typically, forests) to others less efficient in removing  
907 CO<sub>2</sub> from the atmosphere (typically, croplands). The resultant decrease in land sink, called the  
908 ‘loss of sink capacity’, is calculated as the difference between the actual land sink under  
909 changing land-cover and the counter-factual land sink under pre-industrial land-cover. An  
910 efficient protocol has yet to be designed to estimate the magnitude of the loss of additional  
911 sink capacity in DGVMs. Here, we provide a quantitative estimate of this term to be used in the  
912 discussion. Our estimate uses the compact Earth system model OSCAR whose land carbon cycle  
913 component is designed to emulate the behaviour of DGVMs (Gasser et al., 2017). We use  
914 OSCAR v2.2.1 (an update of v2.2 with minor changes) in a probabilistic setup identical to the  
915 one of (Arneeth et al., 2017) but with a Monte Carlo ensemble of 2000 simulations. For each, we  
916 calculate separately S<sub>LAND</sub> and the loss of additional sink capacity. We then constrain the  
917 ensemble by weighting each member to obtain a distribution of cumulative S<sub>LAND</sub> over 1850-  
918 2005 close to the DGVMs used here. From this ensemble, we estimate a loss of additional sink  
919 capacity of  $0.4 \pm 0.3$  GtC yr<sup>-1</sup> on average over 2005-2014, and of about  $20 \pm 15$  GtC when  
920 accumulated between 1850 and 2018 (using a linear extrapolation of the trend to estimate the  
921 last few years).

### 922 **3 Results**

#### 923 **3.1 Global carbon budget mean and variability for 1959 – 2018**

924 The global carbon budget averaged over the last half-century is shown in Fig. 3. For this time  
925 period, 82% of the total emissions (E<sub>FF</sub> + E<sub>LUC</sub>) were caused by fossil CO<sub>2</sub> emissions, and 18% by  
926 land-use change. The total emissions were partitioned among the atmosphere (45%), ocean  
927 (24%) and land (29%), with an unattributed budget imbalance (2%). All components except  
928 land-use change emissions have significantly grown since 1959, with important interannual  
929 variability in the growth rate in atmospheric CO<sub>2</sub> concentration and in the land CO<sub>2</sub> sink (Fig. 4),

930 and some decadal variability in all terms (Table 6). Differences with previous budget releases is  
931 documented in Fig. B4.

### 932 **3.1.1 CO<sub>2</sub> emissions**

933 Global fossil CO<sub>2</sub> emissions have increased every decade from an average of  $3.0 \pm 0.2$  GtC yr<sup>-1</sup> in  
934 the 1960s to an average of  $9.5 \pm 0.5$  GtC yr<sup>-1</sup> during 2009-2018 (Table 6, Fig. 2 and Fig. 5). The  
935 growth rate in these emissions decreased between the 1960s and the 1990s, from 4.4% yr<sup>-1</sup> in  
936 the 1960s (1960-1969), 2.8% yr<sup>-1</sup> in the 1970s (1970-1979), 1.9% yr<sup>-1</sup> in the 1980s (1980-1989),  
937 to 0.9% yr<sup>-1</sup> in the 1990s (1990-1999). After this period, the growth rate began increasing again  
938 in the 2000s at an average growth rate of 3.0% yr<sup>-1</sup>, decreasing to 1.3% yr<sup>-1</sup> for the last decade  
939 (2009-2018).

940 In contrast, CO<sub>2</sub> emissions from land-use, land-use change and forestry have remained  
941 relatively constant, at around  $1.3 \pm 0.7$  GtC yr<sup>-1</sup> over the past half-century (Table 6) but with  
942 large spread across estimates (Table 5, Fig. 6). These emissions are also relatively constant in  
943 the DGVM ensemble of models, except during the last decade when they increase to  $2.0 \pm 0.5$   
944 GtC yr<sup>-1</sup>. However, there is no agreement on this recent increase between the two bookkeeping  
945 models, each suggesting an opposite trend (Fig. 6).

### 946 **3.1.2 Partitioning among the atmosphere, ocean and land**

947 The growth rate in atmospheric CO<sub>2</sub> level increased from  $1.8 \pm 0.07$  GtC yr<sup>-1</sup> in the 1960s to  $4.9$   
948  $\pm 0.02$  GtC yr<sup>-1</sup> during 2009-2018 with important decadal variations (Table 6 and Fig. 2). Both  
949 ocean and land CO<sub>2</sub> sinks have increased roughly in line with the atmospheric increase, but with  
950 significant decadal variability on land (Table 6 and Fig. 6), and possibly in the ocean (Fig. 7). The  
951 ocean CO<sub>2</sub> sink increased from  $1.0 \pm 0.6$  GtC yr<sup>-1</sup> in the 1960s to  $2.5 \pm 0.6$  GtC yr<sup>-1</sup> during 2009-  
952 2018, with interannual variations of the order of a few tenths of GtC yr<sup>-1</sup> generally showing an  
953 increased ocean sink during large El Niño events (i.e. 1997-1998) (Fig. 7; Rödenbeck et al.,  
954 2014). There is coherence among the GOBMs and pCO<sub>2</sub>-based flux products regarding the  
955 mean, and the patterns of temporal variability, however, the ocean models underestimate the  
956 magnitude of decadal variability (Section 2.4.3 and Fig. 7; DeVries et al., 2019).

957 The terrestrial CO<sub>2</sub> sink increased from  $1.3 \pm 0.4$  GtC yr<sup>-1</sup> in the 1960s to  $3.2 \pm 0.7$  GtC yr<sup>-1</sup> during  
958 2009-2018, with important interannual variations of up to 2 GtC yr<sup>-1</sup> generally showing a  
959 decreased land sink during El Niño events (Fig. 6), responsible for the corresponding enhanced

960 growth rate in atmospheric CO<sub>2</sub> concentration. The larger land CO<sub>2</sub> sink during 2009-2018  
961 compared to the 1960s is reproduced by all the DGVMs in response to the combined  
962 atmospheric CO<sub>2</sub> increase and the changes in climate, and consistent with constraints from the  
963 other budget terms (Table 5).

964 The total atmosphere-to-land fluxes ( $S_{\text{LAND}} - E_{\text{LUC}}$ ), calculated here as the difference between  
965  $S_{\text{LAND}}$  from the DGVMs and  $E_{\text{LUC}}$  from the bookkeeping models, increased from a  $0.2 \pm 0.8$  GtC yr<sup>-1</sup>  
966 source in the 1960s to a  $1.7 \pm 0.9$  GtC yr<sup>-1</sup> sink during 2009-2018 (Table 5). Estimates of total  
967 atmosphere-to-land fluxes ( $S_{\text{LAND}} - E_{\text{LUC}}$ ) from the DGVMs alone are consistent with our  
968 estimate and also with the global carbon budget constraint ( $E_{\text{FF}} - G_{\text{ATM}} - S_{\text{OCEAN}}$ , Table 5), except  
969 during 2009-2018, where the DGVM ensemble estimates a total atmosphere-to-land flux of  $1.0$   
970  $\pm 0.8$  GtC yr<sup>-1</sup>, likely below both our estimate of  $1.7 \pm 0.9$  GtC yr<sup>-1</sup> and the carbon budget  
971 constraint of  $2.1 \pm 0.7$  GtC yr<sup>-1</sup> but still within the range of the inversions ( $1.1$ - $2.2$  GtC yr<sup>-1</sup>)  
972 (Table 5). Over the last decade, the land use emission estimate from the DGVMs is significantly  
973 larger than the bookkeeping estimate, mainly explaining why the DGVMs total atmosphere-to-  
974 land flux estimate is lower than the other estimates.

### 975 **3.1.3 Model evaluation**

976 The evaluation of the ocean estimates (Fig. B1) shows a RMSE of 15 to 17  $\mu\text{atm}$  for the three  
977 pCO<sub>2</sub>-based flux products over the globe, relative to the pCO<sub>2</sub> observations from the SOCAT  
978 v2019 database for the period 1985-2018. The GOBM RMSEs are a factor of two to three larger  
979 and range between 29 to 49  $\mu\text{atm}$ . The RMSEs are generally larger at high latitudes compared  
980 to the tropics, for both the flux products and the GOBMs. The three flux products have similar  
981 RMSEs of around 12 to 14  $\mu\text{atm}$  in the tropics, around 17 to 18  $\mu\text{atm}$  in the north, and 17 to 24  
982  $\mu\text{atm}$  in the south. Note that the flux products are based on the SOCAT v2019 database, hence  
983 these are no independent data set for the evaluation of the flux products. The GOBM RMSEs  
984 are more spread across regions, ranging from 21 to 34  $\mu\text{atm}$  in the tropics, 32 to 48  $\mu\text{atm}$  in the  
985 North, and 31 to 77  $\mu\text{atm}$  in the South. The higher RMSEs occur in regions with stronger climate  
986 variability, such as the northern and southern high latitudes (poleward of the subtropical  
987 gyres).

988 The evaluation of the DGVMs (Fig. B2) shows generally high skill scores across models for  
989 runoff, and to a lesser extent for vegetation biomass, GPP, and ecosystem respiration (Fig. B2,  
990 left panel). Skill score was lowest for leaf area index and net ecosystem exchange, with a widest

991 disparity among models for soil carbon. Further analysis of the results will be provided  
992 separately, focusing on the strengths and weaknesses in the DGVM ensemble and its validity for  
993 use in the global carbon budget.

994 The evaluation of the atmospheric inversions (Fig. B3) shows long-term mean biases in the free  
995 troposphere better than 0.4 ppm in absolute values for each product. These biases show some  
996 dependency on latitude and are different for each inverse model, which may reveal biases in  
997 the surface fluxes (e.g., Houweling et al., 2015). Such model- and campaign-specific  
998 performance will be analysed separately.

### 999 **3.1.4 Budget imbalance**

1000 The carbon budget imbalance ( $B_{IM}$ ; Eq. 1) quantifies the mismatch between the estimated total  
1001 emissions and the estimated changes in the atmosphere, land and ocean reservoirs. The mean  
1002 budget imbalance from 1959 to 2018 is small (average of  $0.17 \text{ GtC yr}^{-1}$ ) and shows no trend  
1003 over the full time series. The process models (GOBMs and DGVMs) have been selected to  
1004 match observational constraints in the 1990s but no further constraints have been applied to  
1005 their representation of trend and variability. Therefore, the near-zero mean and trend in the  
1006 budget imbalance is an indirect evidence of a coherent community understanding of the  
1007 emissions and their partitioning on those time scales (Fig. 4). However, the budget imbalance  
1008 shows substantial variability of the order of  $\pm 1 \text{ GtC yr}^{-1}$ , particularly over semi-decadal time  
1009 scales, although most of the variability is within the uncertainty of the estimates. The positive  
1010 carbon imbalance during the 1960s, early 1990s, and in the last decade, suggest that either the  
1011 emissions were overestimated or the sinks were underestimated during these periods. The  
1012 reverse is true for the 1970s and around 1995-2000 (Fig. 4).

1013 We cannot attribute the cause of the variability in the budget imbalance with our analysis, only  
1014 to note that the budget imbalance is unlikely to be explained by errors or biases in the  
1015 emissions alone because of its large semi-decadal variability component, a variability that is  
1016 untypical of emissions and has not changed in the past 50 years in spite of a near tripling in  
1017 emissions (Fig. 4). Errors in  $S_{LAND}$  and  $S_{OCEAN}$  are more likely to be the main cause for the budget  
1018 imbalance. For example, underestimation of the  $S_{LAND}$  by DGVMs has been reported following  
1019 the eruption of Mount Pinatubo in 1991 possibly due to missing responses to changes in diffuse  
1020 radiation (Mercado et al., 2009) or other yet unknown factors, and DGVMs are suspected to  
1021 overestimate the land sink in response to the wet decade of the 1970s (Sitch et al., 2008).

1022 Decadal and semi-decadal variability in the ocean sink has also been reported recently (DeVries  
1023 et al., 2019, 2017; Landschützer et al., 2015), with the pCO<sub>2</sub>-based ocean flux products and a  
1024 decadal ocean inverse model suggesting a smaller than expected ocean CO<sub>2</sub> sink in the 1990s  
1025 and a larger than expected sink in the 2000s (Fig. 7; DeVries et al., 2019). The decadal variability  
1026 is possibly caused by changes in ocean circulation (DeVries et al., 2017) not captured in coarse  
1027 resolution GOBMs used here (Dufour et al., 2013), or by internal variability, which is not  
1028 captured by single realizations of coarse resolution model simulations (Li and Ilyina, 2018) The  
1029 decadal variability is thought to be largest in regions with strong seasonal and interannual  
1030 climate variability, i.e. the high latitude ocean regions (poleward of the subtropical gyres) and  
1031 the equatorial Pacific (Li and Ilyina, 2018; McKinley et al., 2016). Some of these errors could be  
1032 driven by errors in the climatic forcing data, particularly precipitation (for S<sub>LAND</sub>) and wind (for  
1033 S<sub>OCEAN</sub>) rather than in the models.

## 1034 **3.2 Global carbon budget for the last decade (2009 – 2018)**

1035 The global carbon budget averaged over the last decade (2009-2018) is shown in Fig. 2 and Fig.  
1036 9. For this time period, 86% of the total emissions (E<sub>FF</sub> + E<sub>LUC</sub>) were from fossil CO<sub>2</sub> emissions  
1037 (E<sub>FF</sub>), and 14% from land-use change (E<sub>LUC</sub>). The total emissions were partitioned among the  
1038 atmosphere (44%), ocean (23%) and land (29%), with a unattributed budget imbalance (4%).

### 1039 **3.2.1 CO<sub>2</sub> emissions**

1040 Global fossil CO<sub>2</sub> emissions grew at a rate of 1.3% yr<sup>-1</sup> for the last decade (2009-2018). China's  
1041 emissions increased by +2.2% yr<sup>-1</sup> on average (increasing by +0.063 GtC yr<sup>-1</sup> during the 10-year  
1042 period) dominating the global trend, followed by India's emissions increase by +5.1% yr<sup>-1</sup>  
1043 (increasing by +0.025 GtC yr<sup>-1</sup>), while emissions decreased in EU28 by -1.4% yr<sup>-1</sup> (decreasing by  
1044 -0.010 GtC yr<sup>-1</sup>), and in the USA by -0.5% yr<sup>-1</sup> (decreasing by -0.002 GtC yr<sup>-1</sup>). In the past  
1045 decade, fossil CO<sub>2</sub> emissions decreased significantly (at the 95% level) in 19 growing economies:  
1046 Belgium, Croatia, Czech Republic, Denmark, Finland, France, Italy, Latvia, Luxembourg, Republic  
1047 of Macedonia, Malta, the Netherlands, Romania, Slovenia, Sweden, Switzerland, United  
1048 Kingdom, USA and Uzbekistan. The drivers of recent decarbonisation are examined in Le Quéré  
1049 et al. (2019).

1050 In contrast, there is no clear trend in CO<sub>2</sub> emissions from land-use change over the last decade  
1051 (Fig. 6), though the data are very uncertain, with only one of the two bookkeeping estimates

1052 showing a positive trend over the last decade. Larger emissions are expected increasingly over  
1053 time for DGVM-based estimates as they include the loss of additional sink capacity, while the  
1054 bookkeeping estimates do not. The LUH2 data set also features large dynamics in land-use in  
1055 particular in the tropics in recent years, causing higher emissions in DGVMs and BLUE than in  
1056 H&N.

### 1057 **3.2.2 Partitioning among the atmosphere, ocean and land**

1058 The growth rate in atmospheric CO<sub>2</sub> concentration increased during 2009-2018, in contrast to  
1059 more constant levels in the previous decade and reflecting a similar decrease in the land sink  
1060 compared to an increase in the previous decade, albeit with large interannual variability (Fig. 4).  
1061 During the same period, the ocean CO<sub>2</sub> sink appears to have intensified, an effect which is  
1062 particularly apparent in the pCO<sub>2</sub>-based flux products (Fig. 7) and a decadal ocean inverse  
1063 model (DeVries et al., 2019). The GOBMs show the same patterns of decadal variability as the  
1064 mean of the pCO<sub>2</sub>-based flux products, but of weaker magnitude (Fig. 7). The pCO<sub>2</sub>-based flux  
1065 products and the ocean inverse model highlight different regions as the main origin of this  
1066 decadal variability, with the pCO<sub>2</sub>-based flux products placing more of the weakening trend in  
1067 the Southern Ocean and the ocean inverse model suggesting that more of the weakening trend  
1068 occurred in the North Atlantic and North Pacific (DeVries et al., 2019). Both approaches show  
1069 also decadal trends in the low-latitude oceans (DeVries et al., 2019).

1070 The budget imbalance (Table 6) and the residual sink from global budget (Table 5) include an  
1071 error term due to the inconsistency that arises from using  $E_{LUC}$  from bookkeeping models, and  
1072  $S_{LAND}$  from DGVMs. This error term includes the fundamental differences between bookkeeping  
1073 models and DGVMs, most notably the loss of additional sink capacity. Other differences  
1074 include: an incomplete accounting of LUC practices and processes in DGVMs, while they are all  
1075 accounted for in bookkeeping models by using observed carbon densities, and bookkeeping  
1076 error of keeping present-day carbon densities fixed in the past. That the budget imbalance  
1077 shows no clear trend towards larger values over time is an indication that the loss of additional  
1078 sink capacity plays a minor role compared to other errors in  $S_{LAND}$  or  $S_{OCEAN}$  (discussed in Section  
1079 3.1.4).

### 1080 3.2.3 Regional distribution

1081 Fig. 8 shows the partitioning of the total atmosphere-to-surface fluxes excluding fossil CO<sub>2</sub>  
1082 emissions ( $S_{\text{LAND}} + S_{\text{OCEAN}} - E_{\text{LUC}}$ ) according to the multi-model average of the process models in  
1083 the ocean and on land (GOBMs and DGVMs), and to the atmospheric inversions. Fig. 8 provides  
1084 information on the regional distribution of those fluxes by latitude bands. The global mean total  
1085 atmosphere-to-surface CO<sub>2</sub> fluxes from process models for 2009-2018 is  $3.5 \pm 0.9$  GtC yr<sup>-1</sup>. This  
1086 is below but still within the uncertainty range of a global mean atmosphere-to-surface flux of  
1087  $4.6 \pm 0.5$  GtC yr<sup>-1</sup> inferred from the carbon budget ( $E_{\text{FF}} - G_{\text{ATM}}$  in Equation 1; Table 6). The total  
1088 atmosphere-to-surface CO<sub>2</sub> fluxes from the three inversions are very similar, ranging from 4.6  
1089 to 4.9 GtC yr<sup>-1</sup>, consistent with the carbon budget as expected from the constraints on the  
1090 inversions and the adjustments to the same  $E_{\text{FF}}$  distribution (See Section 2.6).

1091 In the south (south of 30°S), the atmospheric inversions suggest an atmosphere-to-surface flux  
1092 for 2009-2018 around 1.7-2.0 GtC yr<sup>-1</sup>, slightly above the process models' estimate of  $1.4 \pm 0.3$   
1093 GtC yr<sup>-1</sup> (Fig. 8). The higher flux in the pCO<sub>2</sub>-based flux products than in the ocean models might  
1094 be explained by a known lack of surface ocean pCO<sub>2</sub> observations in winter, when CO<sub>2</sub>  
1095 outgassing occurs south of the Polar Front (Gray et al., 2018).

1096 The interannual variability in the south is low because of the dominance of ocean area with low  
1097 variability compared to land areas. The split between land ( $S_{\text{LAND}} - E_{\text{LUC}}$ ) and ocean ( $S_{\text{OCEAN}}$ ) shows  
1098 a small contribution to variability in the south coming from the land, with no consistency  
1099 between the DGVMs and the inversions or among inversions. This is expected due to the  
1100 difficulty of separating exactly the land and oceanic fluxes when viewed from atmospheric  
1101 observations alone. The oceanic variability in the south is estimated to be significant in the  
1102 three pCO<sub>2</sub>-based flux products, with decadal variability of 0.18 to 0.22 GtC yr<sup>-1</sup> (Fig. B1). The  
1103 GOBMs show slightly lower interannual variability (0.11 to 0.18 GtC yr<sup>-1</sup>, Fig. B1).

1104 In the tropics (30°S-30°N), both the atmospheric inversions and process models suggest the  
1105 total carbon balance in this region is close to neutral on average over the past decade. The  
1106 three inversion models suggest an atmosphere-to-surface flux between  $-0.5$  and  $+0.3$  GtC yr<sup>-1</sup>  
1107 for the 2009-2018 period, which is within the range of the process models' estimates of  $0.1 \pm$   
1108  $0.4$  GtC yr<sup>-1</sup>. The agreement between inversions and models is significantly better for the last  
1109 decade than for any previous decade, although the reasons for this better agreement are still

1110 unclear. Both the process models and the inversions consistently allocate more year-to-year  
1111 variability of CO<sub>2</sub> fluxes to the tropics compared to the north (north of 30°N; Fig. 8). The split  
1112 between the land and ocean indicates the land is the origin of most of the tropical variability,  
1113 consistently among models (both for the land and for the ocean) and inversions. The oceanic  
1114 variability in the tropics is similar among the three ocean flux products (A-IAV 0.12 to 0.14 GtC  
1115 yr<sup>-1</sup>) and the models, although the model spread is larger (A-IAV 0.08 to 0.19 GtC yr<sup>-1</sup>, Section  
1116 3.1.3, Fig. B1). While the inversions indicate that atmosphere-to-land CO<sub>2</sub> fluxes are more  
1117 variable than atmosphere-to-ocean CO<sub>2</sub> fluxes in the tropics, the correspondence between the  
1118 inversions and the ocean flux products or GOBMs is much poorer, partly caused by a substantial  
1119 tropical ocean carbon sink produced by one of the three inversions.

1120 In the north (north of 30°N), models, inversions and pCO<sub>2</sub>-based flux products consistently  
1121 suggest that most of the variability stems from the land (Fig. 8). Inversions, GOBMs and pCO<sub>2</sub>-  
1122 based flux products agree on the mean of S<sub>OCEAN</sub>, but with a higher variability in the pCO<sub>2</sub>-based  
1123 flux products (A-IAV: 0.12 to 0.13 GtC yr<sup>-1</sup>) than in the models (A-IAV: 0.03 to 0.08 GtC yr<sup>-1</sup>, Fig.  
1124 B1). Atmospheric inversions and process models show less agreement on the magnitude of the  
1125 atmosphere-to-land flux, with the ensemble mean of the process models suggesting a total  
1126 Northern Hemisphere sink for 2009-2018 of 2.1 ± 0.5 GtC yr<sup>-1</sup>, below the estimates from the  
1127 inversions ranging from 2.5 to 3.4 GtC yr<sup>-1</sup> (Fig. 8). The discrepancy in the north-tropics  
1128 distribution of CO<sub>2</sub> fluxes between the inversions and models arises from the differences in  
1129 mean fluxes over the northern land. This discrepancy is also evidenced over the previous  
1130 decade and highlights not only persistent issues with the quantification of the drivers of the net  
1131 land CO<sub>2</sub> flux (Arneeth et al., 2017; Huntzinger et al., 2017) but also the distribution of  
1132 atmosphere-to-land fluxes between the tropics and higher latitudes that is particularly marked  
1133 in previous decades, as highlighted previously (Baccini et al., 2017; Schimel et al., 2015;  
1134 Stephens et al., 2007).

1135 Differences between inversions may be related for example to differences in their  
1136 interhemispheric transport, and other inversion settings (Table A3). Separate analysis has  
1137 shown that the influence of the chosen prior land and ocean fluxes is minor compared to other  
1138 aspects of each inversion, while fossil fuel inputs were adjusted to match that of E<sub>FF</sub> used in this  
1139 analysis (see Section 2.6), therefore removing differences due to fossil emissions prior.  
1140 Differences between inversions and the ensemble of process models in the north cannot be

1141 simply explained. They could either reflect a bias in the inversions or missing processes or  
1142 biases in the process models, such as the lack of adequate parameterizations for land  
1143 management for the DGVMs. The estimated contribution of the north and its uncertainty from  
1144 process models is sensitive both to the ensemble of process models used and to the specifics of  
1145 each inversion.

1146 Resolving the differences in the Northern Hemisphere land sink will require the consideration  
1147 and inclusion of larger volumes of semi-continuous observations of concentrations, fluxes as  
1148 well as auxiliary variables collected from (tall) towers close to the surface CO<sub>2</sub> exchange.  
1149 Moreover, effective use of such information would demand a more process-based approach to  
1150 land-surface exchange of CO<sub>2</sub> than currently employed in inverse models. Such process-based  
1151 approach would represent constraints on carbon exchange derived from local observations and  
1152 biogeochemical relations on multiple time-scales, which in turn would be constrained by the  
1153 regional-to-continental scale mass-balance of atmospheric CO<sub>2</sub>. Some of these near-surface  
1154 data are now becoming available, but not used in the current inverse models sometimes due to  
1155 the short records, and sometimes because the coarse transport models cannot adequately  
1156 represent these time series. Improvements in model resolution and atmospheric transport  
1157 realism together with expansion of the observational record (also in the data sparse Boreal  
1158 Eurasian area) will help anchor the mid-latitude fluxes per continent. In addition, new metrics  
1159 could potentially differentiate between the more- and less realistic realisations of the Northern  
1160 Hemisphere land sink shown in Fig. 8.

### 1161 **3.2.4 Budget imbalance**

1162 The budget imbalance was +0.4 GtC yr<sup>-1</sup> on average over 2009-2018. Although the uncertainties  
1163 are large in each term, the sustained imbalance over this last decade suggests an  
1164 overestimation of the emissions and/or an underestimation of the sinks. An origin in the land  
1165 and/or ocean sink may be more likely, given the large variability of the land sink and the  
1166 suspected underestimation of decadal variability in the ocean sink. An underestimate of S<sub>LAND</sub>  
1167 would also reconcile model results with inversions estimates for fluxes in the total land during  
1168 the past decade (Fig. 8; Table 5). An underestimation of S<sub>OCEAN</sub> is also possible given slightly  
1169 higher estimates for S<sub>OCEAN</sub> from ocean interior carbon observations over the period 1994 to  
1170 2007 ( $2.6 \pm 0.3$  GtC yr<sup>-1</sup>; Gruber et al., 2019) compared to the estimate from GOBMs of  $2.1 \pm 0.5$   
1171 GtC yr<sup>-1</sup> over the same period, although uncertainties overlap. However, we cannot exclude

1172 that the budget imbalance over the last decade could partly be due to an overestimation of CO<sub>2</sub>  
1173 emissions, in particular from land-use change, given their large uncertainty, as has been  
1174 suggested elsewhere (Piao et al., 2018). More integrated use of observations in the Global  
1175 Carbon Budget, either on their own or for further constraining model results, should help  
1176 resolve some of the budget imbalance (Peters et al., 2017; Section 4).

### 1177 **3.3 Global carbon budget for year 2018**

#### 1178 **3.3.1 CO<sub>2</sub> emissions**

1179 Preliminary estimates of global fossil CO<sub>2</sub> emissions are for growth of 2.1% between 2017 and  
1180 2018 to reach  $10.0 \pm 0.5$  GtC in 2018 (Fig. 5), distributed among coal (40%), oil (34%), natural  
1181 gas (20%), cement (4%) and others (1.3%). Compared to the previous year, emissions from coal  
1182 increased by 1.4%, while emissions from oil, natural gas, and cement increased by 1.2%, 5.4%,  
1183 and 2.1%, respectively. All growth rates presented are adjusted for the leap year, unless stated  
1184 otherwise.

1185 In 2018, the largest absolute contributions to global CO<sub>2</sub> emissions were from China (28%), the  
1186 USA (15%), the EU (28-member states; 9%), and India (7%). These four regions account for 59%  
1187 of global CO<sub>2</sub> emissions, while the rest of the world contributed 41% which includes aviation  
1188 and marine bunker fuels (3.4% of the total). Growth rates for these countries from 2017 to  
1189 2018 were +2.3% (China), 2.8% (USA), -2.1% (EU28), and 8.0% (India), with +1.8% for the rest of  
1190 the world. The per-capita CO<sub>2</sub> emissions in 2018 were 1.3 tC person<sup>-1</sup> yr<sup>-1</sup> for the globe, and  
1191 were 4.5 (USA), 1.9 (China), 1.8 (EU28) and 0.5 (India) tC person<sup>-1</sup> yr<sup>-1</sup> for the four highest  
1192 emitting countries (Fig. 5).

1193 The growth in emissions of 2.1% in 2018 is within the range of the projected growth of 2.7%  
1194 (range of 1.8 to 3.7%) published in Le Quéré et al. (2018b) based on national emissions  
1195 projections for China, the USA, and India and projections of gross domestic product corrected  
1196 for I<sub>FF</sub> trends for the rest of the world. The growth in emissions in 2018 for China, the USA,  
1197 EU28, India, and the rest of the world were all within their previously projected range (Table 7).

1198 In 2016 (the last year available), the largest absolute contributions to global CO<sub>2</sub> emissions from  
1199 a consumption perspective were China (25%), USA (16%), the EU (12%), and India (6%). The  
1200 difference between territorial and consumption emissions (the net emission transfer via

1201 international trade) has generally increased from 1990 to around 2005 and remained relatively  
1202 stable afterwards until the last year available (2016; Fig. 5).

1203 The global CO<sub>2</sub> emissions from land-use change are estimated as  $1.5 \pm 0.7$  GtC in 2018, close to  
1204 the previous decade but with low confidence in the annual change. This brings the total CO<sub>2</sub>  
1205 emissions from fossil plus land-use change ( $E_{FF}+E_{LUC}$ ) to  $11.5 \pm 0.9$  GtC ( $42.5 \pm 3.3$  GtCO<sub>2</sub>).

### 1206 **3.3.2 Partitioning among the atmosphere, ocean and land**

1207 The growth rate in atmospheric CO<sub>2</sub> concentration was  $5.1 \pm 0.2$  GtC in 2018 ( $2.42 \pm 0.08$  ppm;  
1208 Fig. 4; Dlugokencky and Tans, 2019). This is near the 2009-2018 average of  $4.9 \pm 0.02$  GtC yr<sup>-1</sup>.

1209 The estimated ocean CO<sub>2</sub> sink was  $2.6 \pm 0.6$  GtC in 2018. The multi-model mean agrees with the  
1210 mean of the pCO<sub>2</sub>-based flux products on an average increase of 0.11 GtC in 2018. Six models  
1211 and two flux products show an increase of SOCEAN (up to +0.38 GtC), while three models and  
1212 one flux product show no change or a decrease of SOCEAN (down to -0.15 GtC) (Fig. 7).

1213 The terrestrial CO<sub>2</sub> sink from the DGVM model ensemble was  $3.5 \pm 0.7$  GtC in 2018, slightly  
1214 above the decadal average (Fig. 4) and consistent with constraints from the rest of the budget  
1215 (Table 5). The budget imbalance was +0.3 GtC in 2018, consistent with its average over the last  
1216 decade (Table 6). This imbalance is indicative only, given the large uncertainties in the  
1217 estimation of the  $B_{IM}$ .

## 1218 **3.4 Global carbon budget projection for year 2019**

### 1219 **3.4.1 CO<sub>2</sub> emissions**

1220 Based on the available data as of 5 November 2019 (see Section 2.1.5), fossil CO<sub>2</sub> emissions ( $E_{FF}$ )  
1221 for 2019 are projected to increase by +0.5% (range of -0.3% to +1.4%; Table 7). Our method  
1222 contains several assumptions that could influence the estimate beyond the given range, and as  
1223 such, it has an indicative value only. Within the given assumptions, global emissions would be  
1224  $10.0 \pm 0.5$  GtC ( $36.7 \pm 1.8$  GtCO<sub>2</sub>) in 2019.

1225 For China, the expected change is for an increase in emissions of +2.6% (range of +0.7% to  
1226 +4.4%) in 2019 compared to 2018. This is based on estimated growth in coal (+0.8%; the main  
1227 fuel source in China), oil (+6.9%), natural gas (+9.1%) consumption, and cement production  
1228 (+6.3%). The uncertainty range considers the variations in the difference between preliminary  
1229 January–September data and final full-year data, lack of monthly data on stock changes,

1230 variances in the discrepancies between supply-side and demand data, the uncertainty in the  
1231 preliminary data used for the 2018 base, and uncertainty in the evolution of the average energy  
1232 density of each of the fossil fuels.

1233 For the USA, the EIA emissions projection for 2019 combined with cement data from USGS  
1234 gives a decrease of  $-2.4\%$  (range of  $-5.0$  to  $+0.0\%$ ) compared to 2018. This is based on separate  
1235 projections for coal  $-12.8\%$ , oil  $-0.8\%$ , natural gas  $+3.2\%$ , and cement  $+0.7\%$ .

1236 For the European Union, our projection for 2019 is for a decrease of  $-1.7\%$  (range of  $-3.4\%$  to  
1237  $+0.1\%$ ) over 2018. This is based on separate projections for coal of  $-10.0\%$ , oil of  $+0.5\%$ , natural  
1238 gas of  $+3.0\%$ , and stable cement emissions. Uncertainty is largest in coal, where two alternative  
1239 methods give divergent estimates.

1240 For India, our projection for 2019 is for an increase of  $+1.8\%$  (range of  $-0.7\%$  to  $+3.7\%$ ) over  
1241 2018. This is based on separate projections for coal ( $+2.0\%$ ), oil ( $+1.5\%$ ), natural gas ( $+2.5\%$ ) and  
1242 cement ( $+0.0\%$ ). The wide uncertainty range reflects an anomalous year: the 2019 monsoon  
1243 year produced above average rainfall, particularly in September, with 52% higher rainfall than  
1244 the long-term average (IMD, 2019). This heavier rainfall led both to flooded coal mines  
1245 (Varadhan, 2019) and high hydropower generation (CEA, 2019b). In addition, the Indian  
1246 economy has slowed rapidly during the year (IMF, 2019b). Furthermore, our forecast for India  
1247 covers its financial year, April 2019 to March 2020, reflecting the underlying emissions data,  
1248 adding to uncertainty.

1249 For the rest of the world, the expected growth for 2019 is  $+0.5\%$  (range of  $-0.8\%$  to  $+1.8\%$ ). This  
1250 is computed using the GDP projection for the world excluding China, USA, EU, and India, of  
1251  $1.9\%$  made by the IMF (IMF, 2019a) and a decrease in  $I_{FF}$  of  $-1.4\% \text{ yr}^{-1}$  which is the average from  
1252 2009-2018. The uncertainty range is based on the standard deviation of the interannual  
1253 variability in  $I_{FF}$  during 2009-2018 of  $\pm 0.8\% \text{ yr}^{-1}$  and our estimate of uncertainty in the IMF's GDP  
1254 forecast of  $\pm 0.5\%$ . The methodology allows independent projections for coal, oil, natural gas,  
1255 cement, and other components, which add to the total emissions in the rest of the world. The  
1256 2019 growth rates for coal were  $+0.1\%$  (range  $-2.9\%$  to  $+3.2\%$ ), oil  $+0.1\%$  (range  $-0.9\%$  to  
1257  $+1.2\%$ ), natural gas  $+1.4\%$  (range  $-0.7\%$  to  $+3.4\%$ ), and cement  $+1.3\%$  (range  $-1.2\%$  to  $+3.9\%$ ).

1258 Each of our regional projections contains separate projections for coal, oil, natural gas, cement,  
1259 and other smaller components. This allows us, for the first time, to supplement our global fossil  
1260  $\text{CO}_2$  emission projection of  $+0.5\%$  (range of  $-0.4\%$  to  $+1.4\%$ ) with separate global projections of

1261 the CO<sub>2</sub> emissions from coal -1.1% (range -2.3% to +0.2%), oil +0.9% (range 0.1% to +1.7%),  
1262 natural gas +2.5% (range +1.2% to +3.9%), and cement +3.7% (range +0.4% to +7.3%).

1263 Preliminary estimate of fire emissions in deforestation zones indicate that emissions from land-  
1264 use change ( $E_{LUC}$ ) for 2019 were above the 2009-2018 average, amounting to 427 TgC by  
1265 October 31st, and are expected to remain at this level for the remainder of the year. We  
1266 therefore expect  $E_{LUC}$  emissions of around 1.7 GtC in 2019, for a total anthropogenic CO<sub>2</sub>  
1267 emissions of  $11.7 \pm 0.9$  GtC ( $42.9 \pm 3.2$  GtCO<sub>2</sub>) in 2019.

### 1268 **3.4.2 Partitioning among the atmosphere, ocean and land**

1269 The 2019 growth in atmospheric CO<sub>2</sub> concentration ( $G_{ATM}$ ) is projected to be  $4.6 \pm 0.9$  GtC ( $2.2 \pm$   
1270  $0.4$  ppm) based on GLO observations until the end of July 2019, bringing the atmospheric CO<sub>2</sub>  
1271 concentration to an expected level of 410 ppm averaged over the year. Combining projected  
1272  $E_{FF}$ ,  $E_{LUC}$  and  $G_{ATM}$  suggests a combined land and ocean sink ( $S_{LAND} + S_{OCEAN}$ ) of about 7.1 GtC for  
1273 2019. Although each term has large uncertainty, the oceanic sink  $S_{OCEAN}$  has generally low  
1274 interannual variability and is likely to remain close to its 2018 value of around 2.6 GtC, leaving a  
1275 rough estimated land sink  $S_{LAND}$  (including any budget imbalance) of around 4.5 GtC,  
1276 substantially above the 2018 estimate.

### 1277 **3.5 Cumulative sources and sinks**

1278 Cumulative historical sources and sinks are estimated as in Eq. (1) with semi-independent  
1279 estimates for each term and a global carbon budget imbalance. Cumulative fossil CO<sub>2</sub> emissions  
1280 for 1850-2018 were  $440 \pm 20$  GtC for  $E_{FF}$  and  $205 \pm 60$  GtC for  $E_{LUC}$  (Table 8; Fig. 9), for a total of  
1281  $645 \pm 65$  GtC. The cumulative emissions from  $E_{LUC}$  are particularly uncertain, with large spread  
1282 among individual estimates of 150 GtC (H&N) and 260 GtC (BLUE) for the two bookkeeping  
1283 models and a similar wide estimate of  $185 \pm 60$  GtC for the DGVMs. These estimates are  
1284 consistent with indirect constraints from vegetation biomass observations (Li et al., 2017), but  
1285 given the large spread a best estimate is difficult to ascertain.

1286 Emissions during the period 1850-2018 were partitioned among the atmosphere ( $255 \pm 5$  GtC;  
1287 40%), ocean ( $160 \pm 20$  GtC; 25%), and the land ( $195 \pm 40$  GtC; 31%). This cumulative land sink is  
1288 broadly equal to the cumulative land-use emissions, making the global land near neutral over  
1289 the 1850-2018 period. The use of nearly independent estimates for the individual terms shows  
1290 a cumulative budget imbalance of 30 GtC (4%) during 1850-2018 (Fig. 2), which, if correct,

1291 suggests emissions are too high by the same proportion or the land or ocean sinks are  
1292 underestimated. The bulk of the imbalance could originate from the estimation of large  $E_{LUC}$   
1293 between the mid 1920s and the mid 1960s which is unmatched by a growth in atmospheric  $CO_2$   
1294 concentration as recorded in ice cores (Fig. 3). The known loss of additional sink capacity of  
1295 about  $20 \pm 15$  GtC due to reduced forest cover has not been accounted in our method and  
1296 would further exacerbate the budget imbalance (Section 2.7.4).

1297 Cumulative emissions through to year 2019 increase to  $655 \pm 65$  GtC ( $2340 \pm 240$  Gt $CO_2$ ), with  
1298 about 70% contribution from  $E_{FF}$  and about 30% contribution from  $E_{LUC}$ . Cumulative emissions  
1299 and their partitioning for different periods are provided in Table 8.

1300 Given the large and persistent uncertainties in historical cumulative emissions, we suggest  
1301 extreme caution is needed if using this estimate to determine the remaining cumulative  $CO_2$   
1302 emissions consistent with an ambition to stay below a given temperature limit (Millar et al.,  
1303 2017; Rogelj et al., 2016, 2019).

#### 1304 **4 Discussion**

1305 Each year when the global carbon budget is published, each flux component is updated for all  
1306 previous years to consider corrections that are the result of further scrutiny and verification of  
1307 the underlying data in the primary input data sets. Annual estimates may improve with  
1308 improvements in data quality and timeliness (e.g. to eliminate the need for extrapolation of  
1309 forcing data such as land-use). Of the various terms in the global budget, only the fossil  $CO_2$   
1310 emissions and the growth rate in atmospheric  $CO_2$  concentration are based primarily on  
1311 empirical inputs supporting annual estimates in this carbon budget. Although it is an imperfect  
1312 measure, the carbon budget imbalance provides a strong indication of the limitations in  
1313 observations, in understanding or full representation of processes in models, and/or in the  
1314 integration of the carbon budget components.

1315 The persistent unexplained variability in the carbon budget imbalance limits our ability to verify  
1316 reported emissions (Peters et al., 2017) and suggests we do not yet have a complete  
1317 understanding of the underlying carbon cycle processes. Resolving most of this unexplained  
1318 variability should be possible through different and complementary approaches. First, as  
1319 intended with our annual updates, the imbalance as an error term is reduced by improvements  
1320 of individual components of the global carbon budget that follow from improving the

1321 underlying data and statistics and by improving the models through the resolution of some of  
1322 the key uncertainties detailed in Table 9. Second, additional clues to the origin and processes  
1323 responsible for the current imbalance could be obtained through a closer scrutiny of carbon  
1324 variability in light of other Earth system data (e.g. heat balance, water balance), and the use of  
1325 a wider range of biogeochemical observations to better understand the land-ocean partitioning  
1326 of the carbon imbalance (e.g. oxygen, carbon isotopes). Finally, additional information could  
1327 also be obtained through higher resolution and process knowledge at the regional level, and  
1328 through the introduction of inferred fluxes such as those based on satellite CO<sub>2</sub> retrievals. The  
1329 limit of the resolution of the carbon budget imbalance is yet unclear, but most certainly not yet  
1330 reached given the possibilities for improvements that lie ahead.

1331 The assessment of the GOBMs used for  $S_{\text{OCEAN}}$  with flux products based on observations  
1332 highlights substantial discrepancy at mid and high latitudes. Given the good data coverage of  
1333 pCO<sub>2</sub> observations in the Northern Hemisphere (Bakker et al., 2016), this discrepancy points at  
1334 an underestimation of variability in the GOBMs globally and consequently, the variability in  
1335  $S_{\text{OCEAN}}$  appears to be underestimated. The size of the underestimation of the amplitude of  
1336 interannual variability (order of 0.1 GtC yr<sup>-1</sup>, A-IAV, see Fig. B1) could account for some of the  
1337 budget imbalance, but not all. Increasing model resolution or using model ensembles (Li and  
1338 Ilyina, 2018) have been suggested as ways to increase model variability (Section 3.1.4).

1339 The assessment of the net land-atmosphere exchange derived from land sink and net land-use  
1340 change flux with atmospheric inversions also shows substantial discrepancy, particularly for the  
1341 estimate of the total land flux over the northern extra-tropics in the past decade. This  
1342 discrepancy highlights the difficulty to quantify complex processes (CO<sub>2</sub> fertilisation, nitrogen  
1343 deposition, N fertilisers, climate change and variability, land management, etc.) that collectively  
1344 determine the net land CO<sub>2</sub> flux. Resolving the differences in the Northern Hemisphere land  
1345 sink will require the consideration and inclusion of larger volumes of observations (Section  
1346 3.2.3).

1347 Estimates of  $E_{\text{LUC}}$  suffer from a range of intertwined issues, including the poor quality of  
1348 historical land-cover and land-use change maps, the rudimentary representation of  
1349 management processes in most models, and the confusion in methodologies and boundary  
1350 conditions used across methods (e.g. Arneeth et al., 2017; Pongratz et al., 2014), and Section  
1351 2.7.4 on the loss of sink capacity). Uncertainties in current and historical carbon stocks in soils

1352 and vegetation also add uncertainty in the LUC flux estimates. Unless a major effort to resolve  
1353 these issues is made, little progress is expected in the resolution of  $E_{LUC}$ . This is particularly  
1354 concerning given the growing importance of  $E_{LUC}$  for climate mitigation strategies, and the large  
1355 issues in the quantification of the cumulative emissions over the historical period that arise  
1356 from large uncertainties in  $E_{LUC}$ .

1357 As introduced last year, we provide metrics for the evaluation of the ocean and land models  
1358 and atmospheric inversions. These metrics expand the use of observations in the global carbon  
1359 budget, helping 1) to support improvements in the ocean and land carbon models that produce  
1360 the sink estimates, and 2) to constrain the representation of key underlying processes in the  
1361 models and to allocate the regional partitioning of the  $CO_2$  fluxes. This is an initial step towards  
1362 the introduction of a broader range of observations that we hope will support continued  
1363 improvements in the annual estimates of the global carbon budget.

1364 We assessed before (Peters et al., 2017) that a sustained decrease of  $-1\%$  in global emissions  
1365 could be detected at the 66% likelihood level after a decade only. Similarly, a change in  
1366 behaviour of the land and/or ocean carbon sink would take as long to detect, and much longer  
1367 if it emerges more slowly. Reducing the carbon imbalance, regionalising the carbon budget, and  
1368 integrating multiple variables are powerful ways to shorten the detection limit and ensure the  
1369 research community can rapidly identify growing issues of concern in the evolution of the  
1370 global carbon cycle under the current rapid and unprecedented changing environmental  
1371 conditions.

## 1372 **5 Conclusions**

1373 The estimation of global  $CO_2$  emissions and sinks is a major effort by the carbon cycle research  
1374 community that requires a careful compilation and synthesis of measurements, statistical  
1375 estimates and model results. The delivery of an annual carbon budget serves two purposes.  
1376 First, there is a large demand for up-to-date information on the state of the anthropogenic  
1377 perturbation of the climate system and its underpinning causes. A broad stakeholder  
1378 community relies on the data sets associated with the annual carbon budget including  
1379 scientists, policy makers, businesses, journalists, and non-governmental organizations engaged

1380 in adapting to and mitigating human-driven climate change. Second, over the last decade we  
1381 have seen unprecedented changes in the human and biophysical environments (e.g. changes in  
1382 the growth of fossil fuel emissions, Earth's temperatures, and strength of the carbon sinks),  
1383 which call for frequent assessments of the state of the planet, a better quantification of the  
1384 causes of changes in the contemporary global carbon cycle, and an improved capacity to  
1385 anticipate its evolution in the future. Building this scientific understanding to meet the  
1386 extraordinary climate mitigation challenge requires frequent, robust, transparent and traceable  
1387 data sets and methods that can be scrutinized and replicated. This paper via 'living data' helps  
1388 to keep track of new budget updates.

## 1389 **6 Data availability**

1390 The data presented here are made available in the belief that their wide dissemination will lead  
1391 to greater understanding and new scientific insights of how the carbon cycle works, how  
1392 humans are altering it, and how we can mitigate the resulting human-driven climate change.  
1393 The free availability of these data does not constitute permission for publication of the data.  
1394 For research projects, if the data are essential to the work, or if an important result or  
1395 conclusion depends on the data, co-authorship may need to be considered for the relevant  
1396 data providers. Full contact details and information on how to cite the data shown here are  
1397 given at the top of each page in the accompanying database and summarised in Table 2.

1398 The accompanying database includes two Excel files organised in the following spreadsheets:

1399 File Global\_Carbon\_Budget\_2019v1.0.xlsx includes the following:

- 1400 1. Summary
- 1401 2. The global carbon budget (1959-2018);
- 1402 3. Global CO<sub>2</sub> emissions from fossil fuels and cement production by fuel type, and the per-  
1403 capita emissions (1959-2018);
- 1404 4. CO<sub>2</sub> emissions from land-use change from the individual methods and models (1959-2018);
- 1405 5. Ocean CO<sub>2</sub> sink from the individual ocean models and pCO<sub>2</sub>-based products (1959-2018);
- 1406 6. Terrestrial CO<sub>2</sub> sink from the DGVMs (1959-2018);

1407 7. Additional information on the historical global carbon budget prior to 1959 (1750-2018).

1408 File National\_Carbon\_Emissions\_2019v1.0.xlsx includes the following:

1409 1. Summary

1410 2. Territorial country CO<sub>2</sub> emissions from fossil CO<sub>2</sub> emissions (1959-2018) from CDIAC with  
1411 UNFCCC data overwritten where available, extended to 2018 using BP data;

1412 3. Consumption country CO<sub>2</sub> emissions from fossil CO<sub>2</sub> emissions and emissions transfer from  
1413 the international trade of goods and services (1990-2016) using CDIAC/UNFCCC data  
1414 (worksheet 3 above) as reference;

1415 4. Emissions transfers (Consumption minus territorial emissions; 1990-2016);

1416 5. Country definitions;

1417 6. Details of disaggregated countries;

1418 7. Details of aggregated countries.

1419 Both spreadsheets are published by the Integrated Carbon Observation System (ICOS) Carbon  
1420 Portal and are available at <https://doi.org/10.18160/gcp-2019> (Friedlingstein et al., 2019).

1421 National emissions data are also available from the Global Carbon Atlas  
1422 (<http://www.globalcarbonatlas.org/>, last access: 4 December 2019).

1423

1424 **Author contributions.** PF, MWJ, MOS, CLQ, RMA, JH, GPP, WP, JP, SS, DCEB, JGC, PC and RBJ

1425 designed the study, conducted the analysis, and wrote the paper. RMA, GPP and JIK produced

1426 the emissions and their uncertainties, 2019 emission projections, and analysed the emissions

1427 data. DG and GM provided emission data. PPT provided key atmospheric CO<sub>2</sub> data. WP, PC, FC,

1428 CR, NN and NS provided an updated atmospheric inversion, developed the protocol and

1429 produced the evaluation. JP, AB and RAH provided updated bookkeeping land-use change

1430 emissions. LPC, GH, KKG, FNT, and GRvdW provided forcing data for land-use change. PA, VB,

1431 DSG, VH, AKJ, EJ, EK, SL, DL, PCM, JRM, JEMSN, BP, HT, APW, AJW and SZ provided an update of

1432 a DGVM. IH and JOK provided forcing data for the DGVMs. ER provided the evaluation of the

1433 DGVMs. JH, LBo, EB, NG, TI, AL, JS and RS provided an update of a GOBM. MG, PL and CR

1434 provided an update of an ocean flux product. LBa, MB, KIC, RAF, TG, SG, NL, NM, DRM, SIN, CN,

1435 AMO, TO, DP, GR and BT provided ocean pCO<sub>2</sub> measurements for the year 2018, with synthesis  
1436 by DCEB and SKL. LR provided an updated river flux estimate. AP contributed to setting up the  
1437 GCB dataset at globalcarbonatlas.org. PF, MWJ and MOS revised all figures, tables, text and/or  
1438 numbers to ensure the update is clear from the 2018 edition and in phase with the  
1439 globalcarbonatlas.org.

1440

1441 **Competing interests.** The authors declare that they have no conflict of interest.

1442

1443 **Acknowledgements.** We thank all people and institutions who provided the data used in this  
1444 carbon budget; Vivek Arora, Jinfeng Chang, Eunkyong Choi, Julie Deshayes, Christian Ethé, M.  
1445 Fortier, Tristan Quaife, Shijie Shu, Anthony Walker and Ulrich Weber for their involvement in  
1446 the development, use and analysis of the models and data-products used here. We thank Ed  
1447 Dlugokencky for providing atmospheric CO<sub>2</sub> measurements; Benjamin Pfeil, and Steve Jones of  
1448 the Bjerknes Climate Data Centre and the ICOS Ocean Thematic Centre of the EU Integrated  
1449 Carbon Observation System (ICOS) at the University of Bergen, as well as Karl Smith and Kevin  
1450 O'Brien of NOAA's Pacific Marine Environmental Laboratory , who helped with SOCAT data  
1451 management; and Alice Benoit-Cattin-Breton; Sólveig Ólafsdóttir, Frank Millero and Geun-Ha  
1452 Park, who contributed to the provision of ocean pCO<sub>2</sub> observations (see Table A4). This is  
1453 NOAA-PMEL contribution number 4847. We thank the institutions and funding agencies  
1454 responsible for the collection and quality control of the data in SOCAT, and the International  
1455 Ocean Carbon Coordination Project (IOCCP) for its support. We thank FAO and its member  
1456 countries for the collection and free dissemination of data relevant to this work. We thank data  
1457 providers to ObsPack GLOBALVIEWplus v4.2 and NRT v4.40 for atmospheric CO<sub>2</sub> observations.  
1458 We thank Trang Chau who produced the CMEMS pCO<sub>2</sub>-based ocean flux data and designed the

1459 system together with MG, Anna Denvil-Sommer, and FC. We thank the individuals and  
1460 institutions that provided the databases used for the model evaluations introduced here, and  
1461 Nigel Hawtin for producing Figure 2 and Figure 9. We thank Fortunat Joos, Samar Khatiwala and  
1462 Timothy DeVries for providing historical data. We thank all people and institutions who  
1463 provided the data used in this carbon budget and the Global Carbon Project members for their  
1464 input throughout the development of this update. Finally, we thank all funders who have  
1465 supported the individual and joint contributions to this work (see Table A5), as well as the  
1466 reviewers of this manuscript and previous versions, and the many researchers who have  
1467 provided feedback.

1468

1469 **References**

- 1470 Adcroft, A., Anderson, W., Balaji, V., Blanton, C., Bushuk, M., Dufour, C. O., Dunne, J. P., Griffies,  
1471 S. M., Hallberg, R., Harrison, M. J., Held, I. M., Jansen, M. F., John, J. G., Krasting, J. P.,  
1472 Langenhorst, A. R., Legg, S., Liang, Z., McHugh, C., Radhakrishnan, A., Reichl, B. G., Rosati,  
1473 T., Samuels, B. L., Shao, A., Stouffer, R., Winton, M., Wittenberg, A. T., Xiang, B., Zadeh, N.  
1474 and Zhang, R.: The GFDL Global Ocean and Sea Ice Model OM4.0: Model Description and  
1475 Simulation Features, *J. Adv. Model. Earth Syst.*, 2019MS001726,  
1476 doi:10.1029/2019MS001726, 2019.
- 1477 Alton, P. B.: Retrieval of seasonal Rubisco-limited photosynthetic capacity at global FLUXNET  
1478 sites from hyperspectral satellite remote sensing: Impact on carbon modelling, *Agric. For.*  
1479 *Meteorol.*, 232, 74–88, doi:10.1016/j.agrformet.2016.08.001, 2017.
- 1480 Amante, C. and Eakins, B. W.: ETOPO1 1 Arc-Minute Global Relief Model: Procedures, Data  
1481 Sources and Analysis. NOAA Technical Memorandum NESDIS NGDC-24. National  
1482 Geophysical Data Center, NOAA. doi:10.7289/V5C8276M, 2009.
- 1483 Andres, R. J., Boden, T. A., Bréon, F. M., Ciais, P., Davis, S., Erickson, D., Gregg, J. S., Jacobson, A.,  
1484 Marland, G., Miller, J., Oda, T., Olivier, J. G. J., Raupach, M. R., Rayner, P. and Treanton, K.:  
1485 A synthesis of carbon dioxide emissions from fossil-fuel combustion, *Biogeosciences*,  
1486 doi:10.5194/bg-9-1845-2012, 2012.
- 1487 Andres, R. J., Boden, T. A. and Higdon, D.: A new evaluation of the uncertainty associated with  
1488 CDIAC estimates of fossil fuel carbon dioxide emission, *Tellus Ser. B-Chemical Phys.*  
1489 *Meteorol.*, 66, 23616, doi:ARTN 2361610.3402/tellusb.v66.23616, 2014.
- 1490 Andrew, R. M.: Global CO<sub>2</sub> emissions from cement production, 1928–2017, *Earth Syst. Sci. Data*,  
1491 10(4), 2213–2239, doi:10.5194/essd-10-2213-2018, 2018.
- 1492 Andrew, R. M.: Global CO<sub>2</sub> emissions from cement production, 1928–2018, *Earth Syst. Sci. Data*,

1493 doi:10.5194/essd-2019-152, 2019.

1494 Andrew, R. M. and Peters, G. P.: A Multi-Region Input-Output Table Based on the Global Trade  
1495 Analysis Project Database (Gtap-Mrio), *Econ. Syst. Res.*, 25(1), 99–121,  
1496 doi:10.1080/09535314.2012.761953, 2013.

1497 Archer, D., Eby, M., Brovkin, V., Ridgwell, A., Cao, L., Mikolajewicz, U., Caldeira, K., Matsumoto,  
1498 K., Munhoven, G., Montenegro, A. and Tokos, K.: Atmospheric Lifetime of Fossil Fuel  
1499 Carbon Dioxide, *Annu. Rev. Earth Planet. Sci.*, 37, 117–134,  
1500 doi:10.1146/annurev.earth.031208.100206, 2009.

1501 Arneeth, A., Sitch, S., Pongratz, J., Stocker, B. D., Ciais, P., Poulter, B., Bayer, A. D., Bondeau, A.,  
1502 Calle, L., Chini, L. P., Gasser, T., Fader, M., Friedlingstein, P., Kato, E., Li, W., Lindeskog, M.,  
1503 Nabel, J. E. M. S., Pugh, T. A. M., Robertson, E., Viovy, N., Yue, C. and Zaehle, S.: Historical  
1504 carbon dioxide emissions caused by land-use changes are possibly larger than assumed,  
1505 *Nat. Geosci.*, 10(2), 79–84, doi:10.1038/ngeo2882, 2017.

1506 Arora, V. K., Boer, G. J., Christian, J. R., Curry, C. L., Denman, K. L., Zahariev, K., Flato, G. M.,  
1507 Scinocca, J. F., Merryfield, W. J. and Lee, W. G.: The Effect of Terrestrial Photosynthesis  
1508 Down Regulation on the Twentieth-Century Carbon Budget Simulated with the CCCma  
1509 Earth System Model, *J. Clim.*, 22(22), 6066–6088, doi:10.1175/2009jcli3037.1, 2009.

1510 Aumont, O., Ethé, C., Tagliabue, A., Bopp, L. and Gehlen, M.: PISCES-v2: an ocean  
1511 biogeochemical model for carbon and ecosystem studies, *Geosci. Model Dev.*, 8(8), 2465–  
1512 2513, doi:10.5194/gmd-8-2465-2015, 2015.

1513 Avitabile, V., Herold, M., Heuvelink, G. B. M., Lewis, S. L., Phillips, O. L., Asner, G. P., Armston, J.,  
1514 Ashton, P. S., Banin, L., Bayol, N., Berry, N. J., Boeckx, P., de Jong, B. H. J., DeVries, B.,  
1515 Girardin, C. A. J., Kearsley, E., Lindsell, J. A., Lopez-Gonzalez, G., Lucas, R., Malhi, Y., Morel,  
1516 A., Mitchard, E. T. A., Nagy, L., Qie, L., Quinones, M. J., Ryan, C. M., Ferry, S. J. W.,

1517 Sunderland, T., Laurin, G. V., Gatti, R. C., Valentini, R., Verbeeck, H., Wijaya, A. and  
1518 Willcock, S.: An integrated pan-tropical biomass map using multiple reference datasets,  
1519 Glob. Chang. Biol., 22(4), 1406–1420, doi:10.1111/gcb.13139, 2016.

1520 Baccini, A., Walker, W., Carvalho, L., Farina, M., Sulla-Menashe, D. and Houghton, R. A.: Tropical  
1521 forests are a net carbon source based on aboveground measurements of gain and loss,  
1522 Science (80-. ), 358(6360), 230–234, doi:10.1126/science.aam5962, 2017.

1523 Bakker, D. C. E., Pfeil, B., Landa, C. S., Metzl, N., O’Brien, K. M., Olsen, A., Smith, K., Cosca, C.,  
1524 Harasawa, S., Jones, S. D., Nakaoka, S., Nojiri, Y., Schuster, U., Steinhoff, T., Sweeney, C.,  
1525 Takahashi, T., Tilbrook, B., Wada, C., Wanninkhof, R., Alin, S. R., Balestrini, C. F., Barbero,  
1526 L., Bates, N. R., Bianchi, A. A., Bonou, F., Boutin, J., Bozec, Y., Burger, E. F., Cai, W. J., Castle,  
1527 R. D., Chen, L. Q., Chierici, M., Currie, K., Evans, W., Featherstone, C., Feely, R. A., Fransson,  
1528 A., Goyet, C., Greenwood, N., Gregor, L., Hankin, S., Hardman-Mountford, N. J., Harlay, J.,  
1529 Hauck, J., Hoppema, M., Humphreys, M. P., Hunt, C., Huss, B., Ibanez, J. S. P.,  
1530 Johannessen, T., Keeling, R., Kitidis, V., Kortzinger, A., Kozyr, A., Krasakopoulou, E., Kuwata,  
1531 A., Landschutzer, P., Lauvset, S. K., Lefevre, N., Lo Monaco, C., Manke, A., Mathis, J. T.,  
1532 Merlivat, L., Millero, F. J., Monteiro, P. M. S., Munro, D. R., Murata, A., Newberger, T.,  
1533 Omar, A. M., Ono, T., Paterson, K., Pearce, D., Pierrot, D., Robbins, L. L., Saito, S., Salisbury,  
1534 J., Schlitzer, R., Schneider, B., Schweitzer, R., Sieger, R., Skjelvan, I., Sullivan, K. F.,  
1535 Sutherland, S. C., Sutton, A. J., Tadokoro, K., Telszewski, M., Tuma, M., van Heuven, S. M.  
1536 A. C., Vandemark, D., Ward, B., Watson, A. J. and Xu, S. Q.: A multi-decade record of high-  
1537 quality fCO<sub>2</sub> data in version 3 of the Surface Ocean CO<sub>2</sub> Atlas (SOCAT), Earth Syst. Sci.  
1538 Data, 8(2), 383–413, doi:10.5194/essd-8-383-2016, 2016.

1539 Ballantyne, A. P., Alden, C. B., Miller, J. B., Tans, P. P. and White, J. W. C.: Increase in observed  
1540 net carbon dioxide uptake by land and oceans during the past 50 years, Nature, 488(7409),

1541 70–72, doi:10.1038/nature11299, 2012.

1542 Ballantyne, A. P., Andres, R., Houghton, R., Stocker, B. D., Wanninkhof, R., Anderegg, W.,  
1543 Cooper, L. A., DeGrandpre, M., Tans, P. P., Miller, J. B., Alden, C. and White, J. W. C.: Audit  
1544 of the global carbon budget: Estimate errors and their impact on uptake uncertainty,  
1545 Biogeosciences, 12(8), 2565–2584, doi:10.5194/bg-12-2565-2015, 2015.

1546 Bauer, J. E., Cai, W.-J., Raymond, P. a, Bianchi, T. S., Hopkinson, C. S. and Regnier, P. a G.: The  
1547 changing carbon cycle of the coastal ocean, Nature, 504(7478), 61–70,  
1548 doi:10.1038/nature12857, 2013.

1549 Berthet, S., Séférian, R., Bricaud, C., Chevallier, M., Voldoire, A. and Ethé, C.: Evaluation of an  
1550 Online Grid-Coarsening Algorithm in a Global Eddy-Admitting Ocean Biogeochemical  
1551 Model, J. Adv. Model. Earth Syst., 11(6), 1759–1783, doi:10.1029/2019MS001644, 2019.

1552 Best, M. J., Pryor, M., Clark, D. B., Rooney, G. G., Essery, R. . L. H., Ménard, C. B., Edwards, J. M.,  
1553 Hendry, M. A., Porson, A., Gedney, N., Mercado, L. M., Sitch, S., Blyth, E., Boucher, O., Cox,  
1554 P. M., Grimmond, C. S. B. and Harding, R. J.: The Joint UK Land Environment Simulator  
1555 (JULES), model description – Part 1: Energy and water fluxes, Geosci. Model Dev., 4(3),  
1556 677–699, doi:10.5194/gmd-4-677-2011, 2011.

1557 BP: BP Statistical Review of World Energy June 2019, available at:  
1558 [https://www.bp.com/en/global/corporate/energy-economics/statistical-review-of-world-](https://www.bp.com/en/global/corporate/energy-economics/statistical-review-of-world-energy.html)  
1559 [energy.html](https://www.bp.com/en/global/corporate/energy-economics/statistical-review-of-world-energy.html), last access: June 2019., 2019.

1560 Bruno, M. and Joos, F.: Terrestrial carbon storage during the past 200 years: A Monte Carlo  
1561 Analysis of CO<sub>2</sub> data from ice core and atmospheric measurements, Global Biogeochem.  
1562 Cycles, 11(1), 111–124, doi:10.1029/96GB03611, 1997.

1563 Buitenhuis, E. T., Hashioka, T. and Le Quéré, C.: Combined constraints on global ocean primary  
1564 production using observations and models, Global Biogeochem. Cycles, 27(3), 847–858,

1565 doi:10.1002/gbc.20074, 2013.

1566 Canadell, J. G., Le Quéré, C., Raupach, M. R., Field, C. B., Buitenhuis, E. T., Ciais, P., Conway, T. J.,  
1567 Gillett, N. P., Houghton, R. A. and Marland, G.: Contributions to accelerating atmospheric  
1568 CO<sub>2</sub> growth from economic activity, carbon intensity, and efficiency of natural sinks, Proc.  
1569 Natl. Acad. Sci., 104(47), 18866–18870, doi:10.1073/pnas.0702737104, 2007.

1570 Carbontracker Team: Compilation of near real time atmospheric carbon dioxide data provided  
1571 by NOAA and EC; obspack\_co2\_1\_NRT\_v4.4.2\_2019-06-10; NOAA Earth System Research  
1572 Laboratory, Global Monitoring Division. doi:10.25925/20190610., 2019.

1573 CEA: Central Electricity Authority (CEA): Daily Coal – Archive. Central Electricity Authority,  
1574 available at: <http://www.cea.nic.in/dailyarchive.html>, last access: 3 November 2019.,  
1575 2019a.

1576 CEA: Generation Overview Report September 2019: Summary All India. Available at  
1577 <http://cea.nic.in/reports/monthly/generation/2019/September/actual/actual.html>. Last  
1578 accessed 6 November 2019., 2019b.

1579 CGADIP: Cooperative Global Atmospheric Data Integration Project: Multi-laboratory  
1580 compilation of atmospheric carbon dioxide data for the period 1957-2017;  
1581 obspack\_co2\_1\_GLOBALVIEWplus\_v4.2.2\_2019-06-05, Earth System Research Laboratory,  
1582 Global Monitoring Division., 2019.

1583 Chatfield, C.: The Holt-Winters Forecasting Procedure, Appl. Stat., 27(3), 264–279,  
1584 doi:10.2307/2347162, 1978.

1585 Chevallier, F., Fisher, M., Peylin, P., Serrar, S., Bousquet, P., Bréon, F.-M., Chédin, A. and Ciais,  
1586 P.: Inferring CO<sub>2</sub> sources and sinks from satellite observations: Method and application to  
1587 TOVS data, J. Geophys. Res., 110(D24), D24309, doi:10.1029/2005JD006390, 2005.

1588 Ciais, P., Sabine, C., Govindasamy, B., Bopp, L., Brovkin, V., Canadell, J., Chhabra, A., DeFries, R.,

1589 Galloway, J., Heimann, M., Jones, C., Le Quéré, C., Myneni, R., Piao, S. and Thornton, P.:  
1590 Chapter 6: Carbon and Other Biogeochemical Cycles, in *Climate Change 2013 The Physical*  
1591 *Science Basis*, edited by T. Stocker, D. Qin, and G.-K. Plattner, Cambridge University Press,  
1592 Cambridge., 2013.

1593 CIL: Coal India Limited: Production and Offtake Performance of CIL and Subsidiary Companies,  
1594 available at: <https://www.coalindia.in/en-us/performance/physical.aspx>, last access: 1  
1595 November 2019., 2019.

1596 Clark, D. B., Mercado, L. M., Sitch, S., Jones, C. D., Gedney, N., Best, M. J., Pryor, M., Rooney, G.  
1597 G., Essery, R. L. H., Blyth, E., Boucher, O., Harding, R. J., Huntingford, C. and Cox, P. M.: The  
1598 Joint UK Land Environment Simulator (JULES), model description – Part 2: Carbon fluxes  
1599 and vegetation dynamics, *Geosci. Model Dev.*, 4(3), 701–722, doi:10.5194/gmd-4-701-  
1600 2011, 2011.

1601 Collier, N., Hoffman, F. M., Lawrence, D. M., Keppel-Aleks, G., Koven, C. D., Riley, W. J., Mu, M.  
1602 Q. and Randerson, J. T.: The International Land Model Benchmarking (ILAMB) System:  
1603 Design, Theory, and Implementation, *J. Adv. Model. Earth Syst.*, 10(11), 2731–2754,  
1604 doi:10.1029/2018ms001354, 2018.

1605 Cox, P. M., Pearson, D., Booth, B. B., Friedlingstein, P., Huntingford, C., Jones, C. D. and Luke, C.  
1606 M.: Sensitivity of tropical carbon to climate change constrained by carbon dioxide  
1607 variability, *Nature*, 494(7437), 341–344, doi:10.1038/nature11882, 2013.

1608 Dai, A. and Trenberth, K. E.: Estimates of Freshwater Discharge from Continents: Latitudinal and  
1609 Seasonal Variations, *J. Hydrometeorol.*, 3(6), 660–687, doi:10.1175/1525-  
1610 7541(2002)003<0660:EOFDFC>2.0.CO;2, 2002.

1611 Davis, S. J. and Caldeira, K.: Consumption-based accounting of CO<sub>2</sub> emissions, *Proc. Natl. Acad.*  
1612 *Sci.*, 107(12), 5687–5692, doi:10.1073/pnas.0906974107, 2010.

1613 De Kauwe, M. G., Disney, M. I., Quaife, T., Lewis, P. and Williams, M.: An assessment of the  
1614 MODIS collection 5 leaf area index product for a region of mixed coniferous forest, *Remote*  
1615 *Sens. Environ.*, 115(2), 767–780, doi:10.1016/j.rse.2010.11.004, 2011.

1616 Decharme, B., Delire, C., Minvielle, M., Colin, J., Vergnes, J., Alias, A., Saint-Martin, D., Séférian,  
1617 R., Sénési, S. and Voldoire, A.: Recent Changes in the ISBA-CTRIP Land Surface System for  
1618 Use in the CNRM-CM6 Climate Model and in Global Off-Line Hydrological Applications, *J.*  
1619 *Adv. Model. Earth Syst.*, 11(5), 1207–1252, doi:10.1029/2018MS001545, 2019.

1620 Delire, C., Séférian, R., Decharme, B., Alkama, R., Carrer, D., Joetzjer, E., Morel, X. and Rocher,  
1621 M.: The global land carbon cycle simulated with ISBA (in review), *J. Adv. Model. Earth Syst.*,  
1622 2019.

1623 Denman, K. L., Brasseur, G., Chidthaisong, A., Ciais, P., Cox, P. M., Dickinson, R. E., Hauglustaine,  
1624 D., Heinze, C., Holland, E., Jacob, D., Lohmann, U., Ramachandran, S., Leite da Silva Dias, P.,  
1625 Wofsy, S. C. and Zhang, X.: Couplings Between Changes in the Climate System and  
1626 Biogeochemistry, in *Climate Change 2007: The Physical Science Basis. Contribution of*  
1627 *Working Group I to the Fourth Assessment Report of the Intergovernmental Panel on*  
1628 *Climate Change*, edited by S. Solomon, Qin D., Manning M., Marquis M., Averyt K., Tignor  
1629 M. M. B., H. L. Miller, and Chen Z. L., pp. 499–587, Cambridge University Press, Cambridge,  
1630 UK and New York, USA., 2007.

1631 Denvil-Sommer, A., Gehlen, M., Vrac, M. and Mejia, C.: LSCE-FFNN-v1: LSCE-FFNN-v1: a two-  
1632 step neural network model for the reconstruction of surface ocean pCO<sub>2</sub> over the global  
1633 ocean, *Geosci. Model Dev.*, 12(5), 2091–2105, doi:10.5194/gmd-12-2091-2019, 2019.

1634 DeVries, T.: The oceanic anthropogenic CO<sub>2</sub> sink: Storage, air-sea fluxes, and transports over the  
1635 industrial era, *Global Biogeochem. Cycles*, 28(7), 631–647, doi:10.1002/2013gb004739,  
1636 2014.

1637 DeVries, T., Holzer, M. and Primeau, F.: Recent increase in oceanic carbon uptake driven by  
1638 weaker upper-ocean overturning, *Nature*, 542(7640), 215–218, doi:10.1038/nature21068,  
1639 2017.

1640 DeVries, T., Le Quéré, C., Andrews, O., Berthet, S., Hauck, J., Ilyina, T., Landschützer, P., Lenton,  
1641 A., Lima, I. D., Nowicki, M., Schwinger, J. and Séférian, R.: Decadal trends in the ocean  
1642 carbon sink, *Proc. Natl. Acad. Sci.*, doi:10.1073/pnas.1900371116, 2019.

1643 Dlugokencky, E. and Tans, P.: Trends in atmospheric carbon dioxide, National Oceanic &  
1644 Atmospheric Administration, Earth System Research Laboratory (NOAA/ESRL), available at:  
1645 <http://www.esrl.noaa.gov/gmd/ccgg/trends/global.html>, last access: 3 November 2019.,  
1646 2019.

1647 Doney, S. C., Lima, I., Feely, R. A., Glover, D. M., Lindsay, K., Mahowald, N., Moore, J. K. and  
1648 Wanninkhof, R.: Mechanisms governing interannual variability in upper-ocean inorganic  
1649 carbon system and air-sea CO<sub>2</sub> fluxes: Physical climate and atmospheric dust, *Deep. Res.*  
1650 *Part II-Topical Stud. Oceanogr.*, 56(8–10), 640–655, doi:10.1016/j.dsr2.2008.12.006, 2009.

1651 Duce, R. A., LaRoche, J., Altieri, K., Arrigo, K. R., Baker, A. R., Capone, D. G., Cornell, S.,  
1652 Dentener, F., Galloway, J., Ganeshram, R. S., Geider, R. J., Jickells, T., Kuypers, M. M.,  
1653 Langlois, R., Liss, P. S., Liu, S. M., Middelburg, J. J., Moore, C. M., Nickovic, S., Oschlies, A.,  
1654 Pedersen, T., Prospero, J., Schlitzer, R., Seitzinger, S., Sorensen, L. L., Uematsu, M., Ulloa,  
1655 O., Voss, M., Ward, B. and Zamora, L.: Impacts of Atmospheric Anthropogenic Nitrogen on  
1656 the Open Ocean, *Science (80-. )*, 320(5878), 893–897, doi:10.1126/science.1150369, 2008.

1657 Dufour, C. O., Le Sommer, J., Gehlen, M., Orr, J. C., Molines, J. M., Simeon, J. and Barnier, B.:  
1658 Eddy compensation and controls of the enhanced sea-to-air CO<sub>2</sub> flux during positive  
1659 phases of the Southern Annular Mode, *Global Biogeochem. Cycles*, 27(3), 950–961,  
1660 doi:10.1002/gbc.20090, 2013.

1661 Durant, A. J., Le Quéré, C., Hope, C. and Friend, A. D.: Economic value of improved  
1662 quantification in global sources and sinks of carbon dioxide, *Philos Trans A Math Phys Eng*  
1663 *Sci*, 369(1943), 1967–1979, doi:10.1098/rsta.2011.0002, 2011.

1664 Eakins, B. W. and Sharman, G. F.: Volumes of the World’s Oceans from ETOPO1; NOAA National  
1665 Geophysical Data Center, available at:  
1666 [http://www.ngdc.noaa.gov/mgg/global/etopo1\\_ocean\\_volumes.html](http://www.ngdc.noaa.gov/mgg/global/etopo1_ocean_volumes.html), last accessed: 27  
1667 September 2019., 2010.

1668 EIA: U.S. Energy Information Administration, Short-Term Energy Outlook, available at:  
1669 <http://www.eia.gov/forecasts/steo/outlook.cfm>, last access: 27 September 2019., 2019.

1670 ENTSO-E: The European Network of Transmission System Operators Electricity Transparency  
1671 Platform, available at: <https://transparency.entsoe.eu/>, last access: 3 November 2019.,  
1672 2019.

1673 Erb, K. H., Kastner, T., Luyssaert, S., Houghton, R. A., Kuemmerle, T., Olofsson, P. and Haberl, H.:  
1674 COMMENTARY: Bias in the attribution of forest carbon sinks, *Nat. Clim. Chang.*, 3(10), 854–  
1675 856, doi:10.1038/nclimate2004, 2013.

1676 Etheridge, D. M., Steele, L. P., Langenfelds, R. L., Francey, R. J., Barnola, J. M. and Morgan, V. I.:  
1677 Natural and anthropogenic changes in atmospheric CO<sub>2</sub> over the last 1000 years from air in  
1678 Antarctic ice and firn, *J. Geophys. Res.*, 101(D2), 4115–4128, doi:Doi 10.1029/95jd03410,  
1679 1996.

1680 Eurostat: Supply and transformation of solid fuels - monthly data (nrg\_101m), available at:  
1681 <https://ec.europa.eu/eurostat/data/database>, last access: 5 November 2019., 2019.

1682 FAO: Food and Agriculture Organization of the United Nations: Global Forest Resources  
1683 Assessment 2015, available at: [http://www.fao.org/forest-resources-assessment/past-](http://www.fao.org/forest-resources-assessment/past-assessments/fra-2015/en/)  
1684 [assessments/fra-2015/en/](http://www.fao.org/forest-resources-assessment/past-assessments/fra-2015/en/), last access: 27 September 2019, Rome, Italy., 2015.

1685 FAO/STAT: Food and Agriculture Organization Statistics Division, available at:  
1686 <http://faostat.fao.org/>, last access: 27 September 2019., 2015.

1687 Francey, R. J., Trudinger, C. M., van der Schoot, M., Law, R. M., Krummel, P. B., Langenfelds, R.  
1688 L., Steele, L. P., Allison, C. E., Stavert, A. R., Andres, R. J. and Rödenbeck, C.: Reply to  
1689 “Anthropogenic CO<sub>2</sub> emissions,” *Nat. Clim. Chang.*, 3(7), 604, doi:10.1038/nclimate1925,  
1690 2013.

1691 Friedlingstein, P., Houghton, R. A., Marland, G., Hackler, J., Boden, T. A., Conway, T. J., Canadell,  
1692 J. G., Raupach, M. R., Ciais, P. and Le Quéré, C.: Update on CO<sub>2</sub> emissions, *Nat. Geosci.*,  
1693 3(12), 811–812, doi:10.1038/ngeo1022, 2010.

1694 Friedlingstein, P., Andrew, R. M., Rogelj, J., Peters, G. P., Canadell, J. G., Knutti, R., Luderer, G.,  
1695 Raupach, M. R., Schaeffer, M., van Vuuren, D. P. and Le Quéré, C.: Persistent growth of CO<sub>2</sub>  
1696 emissions and implications for reaching climate targets, *Nat. Geosci.*, 7(10), 709–715,  
1697 doi:10.1038/Ngeo2248, 2014.

1698 Friedlingstein, P., Jones, M. W., O’Sullivan, M., Andrew, R. M., Hauck, J., Peters, G. P., Peters,  
1699 W., Pongratz, J., Sitch, S., Le Quéré, C., Bakker, D. C. E., Canadell, J. G., Ciais, P., Jackson, R.,  
1700 Anthoni, P., Barbero, L., Bastos, A., Bastrikov, V., Becker, M., Bopp, L., Buitenhuis, E.,  
1701 Chandra, N., Chevallier, F., Chini, L. P., Currie, K. I., Feely, R. A., Gehlen, M., Gilfillan, D.,  
1702 Gkritzalis, T., Goll, D. S., Gruber, N., Gutekunst, S., Harris, I., Haverd, V., Houghton, R. A.,  
1703 Hurtt, G., Ilyina, T., Jain, A. K., Joetzjer, E., Kaplan, J. O., Kato, E., Goldewijk, K. K.,  
1704 Korsbakken, J. I., Landschützer, P., Lauvset, S. K., Lefèvre, N., Lenton, A., Lienert, S.,  
1705 Lombardozzi, D., Marland, G., McGuire, P. C., Melton, J. R., Metzl, N., Munro, D. R., Nabel,  
1706 J. E. M. S., Nakaoka, S.-I., Neill, C., Omar, A. M., Ono, T., Peregon, A., Pierrot, D., Poulter, B.,  
1707 Rehder, G., Resplandy, L., Robertson, E., Rödenbeck, C., Séférian, R., Schwinger, J., Smith,  
1708 N., Tans, P. P., Tian, H., Tilbrook, B., Tubiello, F. N., van der Werf, G. R., Wiltshire, A. J. and

1709 Zaehle, S.: Supplemental data of the Global Carbon Budget 2019, available at:  
1710 <https://doi.org/10.18160/gcp-2019>, ICOS-ERIC Carbon Portal, last accessed: 2 October  
1711 2019, 2019.

1712 Gasser, T., Ciais, P., Boucher, O., Quilcaille, Y., Tortora, M., Bopp, L. and Hauglustaine, D.: The  
1713 compact Earth system model OSCAR v2.2: description and first results, *Geosci. Model Dev.*,  
1714 10(1), 271–319, doi:10.5194/gmd-10-271-2017, 2017.

1715 Gaubert, B., Stephens, B. B., Basu, S., Chevallier, F., Deng, F., Kort, E. A., Patra, P. K., Peters, W.,  
1716 Rödenbeck, C., Saeki, T., Schimel, D., Van der Laan-Luijkx, I., Wofsy, S. and Yin, Y.: Global  
1717 atmospheric CO<sub>2</sub> inverse models converging on neutral tropical  
1718 land exchange but diverging on fossil fuel and atmospheric growth rate, *Biogeosciences*  
1719 *Discuss.*, 2018, 1–25, doi:10.5194/bg-2018-384, 2018.

1720 GCP: The Global Carbon Budget 2007, available at:  
1721 <http://www.globalcarbonproject.org/carbonbudget/archive.htm>, last access: 7 November  
1722 2016., 2007.

1723 General Administration of Customs of the People’s Republic of China: Monthly statistics reports  
1724 (统计月报), <http://www.customs.gov.cn/customs/302249/302274/302277/index.html>.  
1725 Last access: 1 November 2019., 2019.

1726 Giglio, L., Schroeder, W. and Justice, C. O.: The collection 6 MODIS active fire detection  
1727 algorithm and fire products, *Remote Sens. Environ.*, 178, 31–41,  
1728 doi:10.1016/j.rse.2016.02.054, 2016.

1729 Gilfillan, D., Marland, G., Boden, T. and Andres, R.: Global, Regional, and National Fossil-Fuel  
1730 CO<sub>2</sub> Emissions, available at: <https://energy.appstate.edu/CDIAC>, last access: 27 September  
1731 2019, 2019.

1732 Gitz, V. and Ciais, P.: Amplifying effects of land-use change on future atmospheric CO<sub>2</sub> levels,

1733 Global Biogeochem. Cycles, 17(1), 1024, doi:10.1029/2002GB001963, 2003.

1734 Goldewijk, K. K., Beusen, A., Doelman, J. and Stehfest, E.: Anthropogenic land use estimates for  
1735 the Holocene - HYDE 3.2, Earth Syst. Sci. Data, 9(2), 927–953, doi:10.5194/essd-9-927-  
1736 2017, 2017a.

1737 Goldewijk, K. K., Dekker, S. C. and van Zanden, J. L.: Per-capita estimations of long-term  
1738 historical land use and the consequences for global change research, J. Land Use Sci.,  
1739 12(5), 313–337, doi:10.1080/1747423x.2017.1354938, 2017b.

1740 Goll, D. S., Winkler, A. J., Raddatz, T., Dong, N., Colin Prentice, I., Ciais, P. and Brovkin, V.:  
1741 Carbon-nitrogen interactions in idealized simulations with JSBACH (version 3.10), Geosci.  
1742 Model Dev., 10(5), 2009–2030, doi:10.5194/gmd-10-2009-2017, 2017.

1743 Goll, D. S., Joetzjer, E., Huang, M. and Ciais, P.: Low Phosphorus Availability Decreases  
1744 Susceptibility of Tropical Primary Productivity to Droughts, Geophys. Res. Lett., 45(16),  
1745 8231–8240, doi:10.1029/2018GL077736, 2018.

1746 Gray, A. R., Johnson, K. S., Bushinsky, S. M., Riser, S. C., Russell, J. L., Talley, L. D., Wanninkhof,  
1747 R., Williams, N. L. and Sarmiento, J. L.: Autonomous Biogeochemical Floats Detect  
1748 Significant Carbon Dioxide Outgassing in the High-Latitude Southern Ocean, Geophys. Res.  
1749 Lett., 45(17), 9049–9057, doi:10.1029/2018GL078013, 2018.

1750 Gregg, J. S., Andres, R. J. and Marland, G.: China: Emissions pattern of the world leader in CO<sub>2</sub>  
1751 emissions from fossil fuel consumption and cement production, Geophys. Res. Lett., 35(8),  
1752 L08806, doi:Artn L0880610.1029/2007gl032887, 2008.

1753 Gruber, N., Clement, D., Carter, B. R., Feely, R. A., van Heuven, S., Hoppema, M., Ishii, M., Key,  
1754 R. M., Kozyr, A., Lauvset, S. K., Lo Monaco, C., Mathis, J. T., Murata, A., Olsen, A., Perez, F.  
1755 F., Sabine, C. L., Tanhua, T. and Wanninkhof, R.: The oceanic sink for anthropogenic CO<sub>2</sub>  
1756 from 1994 to 2007, Science (80-. ), 363(6432), 1193–1199, doi:10.1126/science.aau5153,

1757 2019.

1758 Hansis, E., Davis, S. J. and Pongratz, J.: Relevance of methodological choices for accounting of  
1759 land use change carbon fluxes, *Global Biogeochem. Cycles*, 29(8), 1230–1246,  
1760 doi:10.1002/2014GB004997, 2015.

1761 Harris, I., Jones, P. D., Osborn, T. J. and Lister, D. H.: Updated high-resolution grids of monthly  
1762 climatic observations - the CRU TS3.10 Dataset, *Int. J. Climatol.*, 34(3), 623–642,  
1763 doi:10.1002/joc.3711, 2014.

1764 Haverd, V., Smith, B., Nieradzick, L., Briggs, P. R., Woodgate, W., Trudinger, C. M., Canadell, J. G.  
1765 and Cuntz, M.: A new version of the CABLE land surface model (Subversion revision r4601)  
1766 incorporating land use and land cover change, woody vegetation demography, and a novel  
1767 optimisation-based approach to plant coordination of photosynthesis, *Geosci. Model Dev.*,  
1768 11(7), 2995–3026, doi:10.5194/gmd-11-2995-2018, 2018.

1769 Hertwich, E. G. and Peters, G. P.: Carbon footprint of nations: a global, trade-linked analysis,  
1770 *Env. Sci Technol*, 43(16), 6414–6420, doi:10.1021/es803496a, 2009.

1771 Hooijer, A., Page, S., Canadell, J. G., Silvius, M., Kwadijk, J., Wosten, H. and Jauhiainen, J.:  
1772 Current and future CO<sub>2</sub> emissions from drained peatlands in Southeast Asia,  
1773 *Biogeosciences*, 7(5), 1505–1514, doi:10.5194/bg-7-1505-2010, 2010.

1774 Houghton, R. A.: Revised estimates of the annual net flux of carbon to the atmosphere from  
1775 changes in land use and land management 1850-2000, *Tellus Ser. B-Chemical Phys.*  
1776 *Meteorol.*, 55(2), 378–390, doi:DOI 10.1034/j.1600-0889.2003.01450.x, 2003.

1777 Houghton, R. A. and Nassikas, A. A.: Global and regional fluxes of carbon from land use and land  
1778 cover change 1850-2015, *Global Biogeochem. Cycles*, 31(3), 456–472,  
1779 doi:10.1002/2016gb005546, 2017.

1780 Houghton, R. A., House, J. I., Pongratz, J., Van Der Werf, G. R., Defries, R. S., Hansen, M. C., Le

1781 Quéré, C. and Ramankutty, N.: Carbon emissions from land use and land-cover change,  
1782 Biogeosciences, 9(12), 5125–5142, doi:10.5194/bg-9-5125-2012, 2012.

1783 Houweling, S., Baker, D., Basu, S., Boesch, H., Butz, A., Chevallier, F., Deng, F., Dlugokencky, E. J.,  
1784 Feng, L., Ganshin, A., Hasekamp, O., Jones, D., Maksyutov, S., Marshall, J., Oda, T., O’Dell,  
1785 C. W., Oshchepkov, S., Palmer, P. I., Peylin, P., Poussi, Z., Reum, F., Takagi, H., Yoshida, Y.  
1786 and Zhuravlev, R.: An intercomparison of inverse models for estimating sources and sinks  
1787 of CO<sub>2</sub> using GOSAT measurements, J. Geophys. Res., 120(10), 5253–5266,  
1788 doi:10.1002/2014jd022962, 2015.

1789 Hugelius, G., Bockheim, J. G., Camill, P., Elberling, B., Grosse, G., Harden, J. W., Johnson, K.,  
1790 Jorgenson, T., Koven, C. D., Kuhry, P., Michaelson, G., Mishra, U., Palmtag, J., Ping, C. L.,  
1791 O’Donnell, J., Schirmer, L., Schuur, E. A. G., Sheng, Y., Smith, L. C., Strauss, J. and Yu, Z.:  
1792 A new data set for estimating organic carbon storage to 3m depth in soils of the northern  
1793 circumpolar permafrost region, Earth Syst. Sci. Data, 5(2), 393–402, doi:10.5194/essd-5-  
1794 393-2013, 2013.

1795 Huntzinger, D. N., Michalak, A. M., Schwalm, C., Ciais, P., King, A. W., Fang, Y., Schaefer, K., Wei,  
1796 Y., Cook, R. B., Fisher, J. B., Hayes, D., Huang, M., Ito, A., Jain, A. K., Lei, H., Lu, C., Maignan,  
1797 F., Mao, J., Parazoo, N., Peng, S., Poulter, B., Ricciuto, D., Shi, X., Tian, H., Wang, W., Zeng,  
1798 N. and Zhao, F.: Uncertainty in the response of terrestrial carbon sink to environmental  
1799 drivers undermines carbon-climate feedback predictions, Sci. Rep., 7(1), 4765,  
1800 doi:10.1038/s41598-017-03818-2, 2017.

1801 Hurtt, G., Chini, L., Sahajpal, R., Frohking, S., Calvin, K., Fujimori, S., Klein Goldewijk, K.,  
1802 Hasegawa, T., Havlik, P. and Heinemann, A.: Harmonization of global land-use change and  
1803 management for the period 850–2100, in preparation, Geosci. Model Dev., 2019.

1804 Hurtt, G. C., Chini, L. P., Frohking, S., Betts, R. A., Feddema, J., Fischer, G., Fisk, J. P., Hibbard, K.,

1805 Houghton, R. A., Janetos, A., Jones, C. D., Kindermann, G., Kinoshita, T., Goldewijk, K. K.,  
1806 Riahi, K., Shevliakova, E., Smith, S., Stehfest, E., Thomson, A., Thornton, P., van Vuuren, D.  
1807 P. and Wang, Y. P.: Harmonization of land-use scenarios for the period 1500-2100: 600  
1808 years of global gridded annual land-use transitions, wood harvest, and resulting secondary  
1809 lands, *Clim. Change*, 109(1–2), 117–161, doi:10.1007/s10584-011-0153-2, 2011.

1810 IEA/OECD: International Energy Agency/Organisation for Economic Cooperation and  
1811 Development: CO<sub>2</sub> emissions from fuel combustion, available at:  
1812 <https://webstore.iea.org/co2-emissions-from-fuel-combustion-2018-highlights>, Paris.,  
1813 2018.

1814 IEA: World Energy Statistics (2018 Edition), available at: [www.iea.org](http://www.iea.org), 2018.

1815 IMD: India Meteorological Department, Ministry of Earth Sciences (IMD): 2019 Southwest  
1816 Monsoon Season Rainfall and IMD’s Long Range Forecasts. Available at:  
1817 [http://www.imd.gov.in/pages/press\\_release.php](http://www.imd.gov.in/pages/press_release.php). Last accessed 6 November 2019., 2019.

1818 IMF: IMF: World Economic Outlook Update, July 2019: Still Sluggish Global Growth, available at:  
1819 <http://www.imf.org>, last access: 16 October 2019., 2019a.

1820 IMF: World Economic Outlook: Global Manufacturing Downturn, Rising Trade Barriers.  
1821 International Monetary Fund. Available at: [www.imf.org](http://www.imf.org). Last accessed 30 October 2019.,  
1822 2019b.

1823 IPCC: 2006 IPCC Guidelines for National Greenhouse Gas Inventories, Prepared by the National  
1824 Greenhouse Gas Inventories Programme, edited by S. Eggleston, L. Buendia, K. Miwa, T.  
1825 Ngara, and K. Tanabe, Intergovernmental Panel on Climate Change, Institute for Global  
1826 Environmental Strategies, Japan., 2006.

1827 Ito, A. and Inatomi, M.: Use of a process-based model for assessing the methane budgets of  
1828 global terrestrial ecosystems and evaluation of uncertainty, *Biogeosciences*, 9(2), 759–773,

1829 doi:10.5194/bg-9-759-2012, 2012.

1830 Jackson, R. B., Canadell, J. G., Le Quéré, C., Andrew, R. M., Korsbakken, J. I., Peters, G. P. and  
1831 Nakicenovic, N.: Reaching peak emissions, *Nat. Clim. Chang.*, 6(1), 7–10,  
1832 doi:10.1038/nclimate2892, 2016.

1833 Jackson, R. B., Le Quéré, C., Andrew, R. M., Canadell, J. G., Korsbakken, J. I., Liu, Z., Peters, G. P.  
1834 and Zheng, B.: Global energy growth is outpacing decarbonization, *Environ. Res. Lett.*,  
1835 13(12), 120401, doi:10.1088/1748-9326/aaf303, 2018.

1836 Jacobson, A. R., Mikaloff Fletcher, S. E., Gruber, N., Sarmiento, J. L. and Gloor, M.: A joint  
1837 atmosphere-ocean inversion for surface fluxes of carbon dioxide: 2. Regional results,  
1838 *Global Biogeochem. Cycles*, 21(1), doi:10.1029/2006GB002703, 2007.

1839 JODI: Joint Organisations Data Initiative, available at: <https://www.jodidata.org>, last access: 3  
1840 November 2019., 2019.

1841 Joetzjer, E., Delire, C., Douville, H., Ciais, P., Decharme, B., Carrer, D., Verbeeck, H., De Weirdt,  
1842 M. and Bonal, D.: Improving the ISBA<sub>cc</sub> land surface model simulation of water and carbon  
1843 fluxes and stocks over the Amazon forest, *Geosci. Model Dev.*, 8(6), 1709–1727,  
1844 doi:10.5194/gmd-8-1709-2015, 2015.

1845 Jones, M. W., Le Quéré, C., Andrew, R., Peters, G., Chevallier, F., Ciais, P., Janssens-Maenhout,  
1846 G., van der Laan-Luijkx, I., Patra, P. Peters, W. and Rödenbeck, C.: Gridded fossil CO<sub>2</sub>  
1847 emissions and related O<sub>2</sub> combustion consistent with national inventories 1959-2018, in  
1848 preparation, 2019.

1849 Joos, F. and Spahni, R.: Rates of change in natural and anthropogenic radiative forcing over the  
1850 past 20,000 years, *Proc. Natl. Acad. Sci.*, doi:10.1073/pnas.0707386105, 2008.

1851 Jung, M., Reichstein, M., Ciais, P., Seneviratne, S. I., Sheffield, J., Goulden, M. L., Bonan, G.,  
1852 Cescatti, A., Chen, J., de Jeu, R., Dolman, A. J., Eugster, W., Gerten, D., Gianelle, D., Gobron,

1853 N., Heinke, J., Kimball, J., Law, B. E., Montagnani, L., Mu, Q., Mueller, B., Oleson, K., Papale,  
1854 D., Richardson, A. D., Rouspard, O., Running, S., Tomelleri, E., Viovy, N., Weber, U.,  
1855 Williams, C., Wood, E., Zaehle, S. and Zhang, K.: Recent decline in the global land  
1856 evapotranspiration trend due to limited moisture supply, *Nature*, 467(7318), 951–954,  
1857 doi:10.1038/nature09396, 2010.

1858 Kato, E., Kinoshita, T., Ito, A., Kawamiya, M. and Yamagata, Y.: Evaluation of spatially explicit  
1859 emission scenario of land-use change and biomass burning using a process-based  
1860 biogeochemical model, *J. Land Use Sci.*, 8(1), 104–122,  
1861 doi:10.1080/1747423x.2011.628705, 2013.

1862 Keeling, C. D., Bacastow, R. B., Bainbridge, A. E., Ekdahl, C. A., Guenther, P. R., Waterman, L. S.  
1863 and Chin, J. F. S.: Atmospheric Carbon-Dioxide Variations at Mauna-Loa Observatory,  
1864 Hawaii, *Tellus*, 28(6), 538–551, doi:10.1111/j.2153-3490.1976.tb00701.x, 1976.

1865 Keeling, R. F. and Manning, A. C.: Studies of Recent Changes in Atmospheric O<sub>2</sub> Content, in  
1866 *Treatise on Geochemistry*, vol. 5, edited by H. D. Holland and K. K. Turekian, pp. 385–404,  
1867 Elsevier, Oxford., 2014.

1868 Khatiwala, S., Primeau, F. and Hall, T.: Reconstruction of the history of anthropogenic CO<sub>2</sub>  
1869 concentrations in the ocean, *Nature*, 462(7271), 346-U110, doi:10.1038/nature08526,  
1870 2009.

1871 Khatiwala, S., Tanhua, T., Fletcher, S. M., Gerber, M., Doney, S. C., Graven, H. D., Gruber, N.,  
1872 McKinley, G. A., Murata, A., Rios, A. F. and Sabine, C. L.: Global ocean storage of  
1873 anthropogenic carbon, *Biogeosciences*, 10(4), 2169–2191, doi:10.5194/bg-10-2169-2013,  
1874 2013.

1875 Kirschke, S., Bousquet, P., Ciais, P., Saunois, M., Canadell, J. G., Dlugokencky, E. J., Bergamaschi,  
1876 P., Bergmann, D., Blake, D. R., Bruhwiler, L., Cameron-Smith, P., Castaldi, S., Chevallier, F.,

1877 Feng, L., Fraser, A., Heimann, M., Hodson, E. L., Houweling, S., Josse, B., Fraser, P. J.,  
1878 Krummel, P. B., Lamarque, J. F., Langenfelds, R. L., Le Quéré, C., Naik, V., O'Doherty, S.,  
1879 Palmer, P. I., Pison, I., Plummer, D., Poulter, B., Prinn, R. G., Rigby, M., Ringeval, B., Santini,  
1880 M., Schmidt, M., Shindell, D. T., Simpson, I. J., Spahni, R., Steele, L. P., Strode, S. A., Sudo,  
1881 K., Szopa, S., van der Werf, G. R., Voulgarakis, A., van Weele, M., Weiss, R. F., Williams, J. E.  
1882 and Zeng, G.: Three decades of global methane sources and sinks, *Nat. Geosci.*, 6(10), 813–  
1883 823, doi:10.1038/Ngeo1955, 2013.

1884 Kobayashi, S., Ota, Y., Harada, Y., Ebita, A., Moriya, M., Onoda, H., Onogi, K., Kamahori, H.,  
1885 Kobayashi, C., Endo, H., Miyaoka, K. and Takahashi, K.: The JRA-55 Reanalysis: General  
1886 Specifications and Basic Characteristics, *J. Meteorol. Soc. Japan*, 93(1), 5–48,  
1887 doi:10.2151/jmsj.2015-001, 2015.

1888 Korsbakken, J. I., Peters, G. P. and Andrew, R. M.: Uncertainties around reductions in China's  
1889 coal use and CO<sub>2</sub> emissions, *Nat. Clim. Chang.*, 6(7), 687–690, doi:10.1038/nclimate2963,  
1890 2016.

1891 Krinner, G., Viovy, N., de Noblet-Ducoudré, N., Ogée, J., Polcher, J., Friedlingstein, P., Ciais, P.,  
1892 Sitch, S. and Prentice, I. C.: A dynamic global vegetation model for studies of the coupled  
1893 atmosphere-biosphere system, *Global Biogeochem. Cycles*, 19(1), 1–33,  
1894 doi:10.1029/2003GB002199, 2005.

1895 Landschützer, P., Gruber, N., Bakker, D. C. E. and Schuster, U.: Recent variability of the global  
1896 ocean carbon sink, *Global Biogeochem. Cycles*, 28(9), 927–949,  
1897 doi:10.1002/2014GB004853, 2014.

1898 Landschützer, P., Gruber, N., Haumann, F. A., Rödenbeck, C., Bakker, D. C. E., van Heuven, S.,  
1899 Hoppema, M., Metzl, N., Sweeney, C., Takahashi, T., Tilbrook, B. and Wanninkhof, R.: The  
1900 reinvigoration of the Southern Ocean carbon sink, *Science* (80-. ), 349(6253), 1221–1224,

1901 doi:10.1126/science.aab2620, 2015.

1902 Landschützer, P., Gruber, N. and Bakker, D. C. E.: Decadal variations and trends of the global  
1903 ocean carbon sink, *Global Biogeochem. Cycles*, 30(10), 1396–1417,  
1904 doi:10.1002/2015gb005359, 2016.

1905 Landschützer, P., Gruber, N., Bakker, D. C. E., Stemmler, I. and Six, K. D.: Strengthening seasonal  
1906 marine CO<sub>2</sub> variations due to increasing atmospheric CO<sub>2</sub>, *Nat. Clim. Chang.*, 8(2), 146–150,  
1907 doi:10.1038/s41558-017-0057-x, 2018.

1908 Lasslop, G., Reichstein, M., Papale, D., Richardson, A. D., Arneth, A., Barr, A., Stoy, P. and  
1909 Wohlfahrt, G.: Separation of net ecosystem exchange into assimilation and respiration  
1910 using a light response curve approach: critical issues and global evaluation, *Glob. Chang.*  
1911 *Biol.*, 16(1), 187–208, doi:10.1111/j.1365-2486.2009.02041.x, 2010.

1912 Lawrence, D. M., Fisher, R. A., Koven, C. D., Oleson, K. W., Swenson, S. C., Bonan, G., Collier, N.,  
1913 Ghimire, B., Kampenhout, L., Kennedy, D., Kluzek, E., Lawrence, P. J., Li, F., Li, H.,  
1914 Lombardozzi, D., Riley, W. J., Sacks, W. J., Shi, M., Vertenstein, M., Wieder, W. R., Xu, C.,  
1915 Ali, A. A., Badger, A. M., Bisht, G., Broeke, M., Brunke, M. A., Burns, S. P., Buzan, J., Clark,  
1916 M., Craig, A., Dahlin, K., Drewniak, B., Fisher, J. B., Flanner, M., Fox, A. M., Gentine, P.,  
1917 Hoffman, F., Keppel-Aleks, G., Knox, R., Kumar, S., Lenaerts, J., Leung, L. R., Lipscomb, W.  
1918 H., Lu, Y., Pandey, A., Pelletier, J. D., Perket, J., Randerson, J. T., Ricciuto, D. M., Sanderson,  
1919 B. M., Slater, A., Subin, Z. M., Tang, J., Thomas, R. Q., Val Martin, M. and Zeng, X.: The  
1920 Community Land Model version 5: Description of new features, benchmarking, and impact  
1921 of forcing uncertainty, *J. Adv. Model. Earth Syst.*, 2018MS001583,  
1922 doi:10.1029/2018MS001583, 2019.

1923 Le Quéré, C., Raupach, M. R., Canadell, J. G., Marland, G., Bopp, L., Ciais, P., Conway, T. J.,  
1924 Doney, S. C., Feely, R. A., Foster, P., Friedlingstein, P., Gurney, K., Houghton, R. A., House, J.

1925 I., Huntingford, C., Levy, P. E., Lomas, M. R., Majkut, J., Metzl, N., Ometto, J. P., Peters, G.

1926 P., Prentice, I. C., Randerson, J. T., Running, S. W., Sarmiento, J. L., Schuster, U., Sitch, S.,

1927 Takahashi, T., Viovy, N., Van Der Werf, G. R. and Woodward, F. I.: Trends in the sources

1928 and sinks of carbon dioxide, *Nat. Geosci.*, 2(12), 831–836, doi:10.1038/ngeo689, 2009.

1929 Le Quéré, C., Andres, R. J., Boden, T., Conway, T., Houghton, R. A., House, J. I., Marland, G.,

1930 Peters, G. P., van der Werf, G. R., Ahlström, A., Andrew, R. M., Bopp, L., Canadell, J. G.,

1931 Ciais, P., Doney, S. C., Enright, C., Friedlingstein, P., Huntingford, C., Jain, A. K., Jourdain, C.,

1932 Kato, E., Keeling, R. F., Klein Goldewijk, K., Levis, S., Levy, P., Lomas, M., Poulter, B.,

1933 Raupach, M. R., Schwinger, J., Sitch, S., Stocker, B. D., Viovy, N., Zaehle, S. and Zeng, N.:

1934 The global carbon budget 1959–2011, *Earth Syst. Sci. Data*, 5(1), 165–185,

1935 doi:10.5194/essd-5-165-2013, 2013.

1936 Le Quéré, C., Peters, G. P., Andres, R. J., Andrew, R. M., Boden, T. a., Ciais, P., Friedlingstein, P.,

1937 Houghton, R. a., Marland, G., Moriarty, R., Sitch, S., Tans, P., Arneeth, A., Arvanitis, A.,

1938 Bakker, D. C. E., Bopp, L., Canadell, J. G., Chini, L. P., Doney, S. C., Harper, A., Harris, I.,

1939 House, J. I., Jain, a. K., Jones, S. D., Kato, E., Keeling, R. F., Klein Goldewijk, K., Körtzinger,

1940 A., Koven, C., Lefèvre, N., Maignan, F., Omar, A., Ono, T., Park, G.-H., Pfeil, B., Poulter, B.,

1941 Raupach, M. R., Regnier, P., Rödenbeck, C., Saito, S., Schwinger, J., Segschneider, J.,

1942 Stocker, B. D., Takahashi, T., Tilbrook, B., van Heuven, S., Viovy, N., Wanninkhof, R.,

1943 Wiltshire, A. and Zaehle, S.: Global carbon budget 2013, *Earth Syst. Sci. Data*, 6(1), 235–

1944 263, doi:10.5194/essd-6-235-2014, 2014.

1945 Le Quéré, C., Moriarty, R., Andrew, R. M., Peters, G. P., Ciais, P., Friedlingstein, P., Jones, S. D.,

1946 Sitch, S., Tans, P., Arneeth, A., Boden, T. A., Bopp, L., Bozec, Y., Canadell, J. G., Chini, L. P.,

1947 Chevallier, F., Cosca, C. E., Harris, I., Hoppema, M., Houghton, R. A., House, J. I., Jain, A. K.,

1948 Johannessen, T., Kato, E., Keeling, R. F., Kitidis, V., Klein Goldewijk, K., Koven, C., Landa, C.

1949 S., Landschützer, P., Lenton, A., Lima, I. D., Marland, G., Mathis, J. T., Metzl, N., Nojiri, Y.,  
1950 Olsen, A., Ono, T., Peng, S., Peters, W., Pfeil, B., Poulter, B., Raupach, M. R., Regnier, P.,  
1951 Rödenbeck, C., Saito, S., Salisbury, J. E., Schuster, U., Schwinger, J., Séférian, R.,  
1952 Segschneider, J., Steinhoff, T., Stocker, B. D., Sutton, A. J., Takahashi, T., Tilbrook, B., van  
1953 der Werf, G. R., Viovy, N., Wang, Y.-P., Wanninkhof, R., Wiltshire, A. and Zeng, N.: Global  
1954 carbon budget 2014, *Earth Syst. Sci. Data*, 7(1), 47–85, doi:10.5194/essd-7-47-2015, 2015a.

1955 Le Quéré, C., Moriarty, R., Andrew, R. M., Canadell, J. G., Sitch, S., Korsbakken, J. I.,  
1956 Friedlingstein, P., Peters, G. P., Andres, R. J., Boden, T. A., Houghton, R. A., House, J. I.,  
1957 Keeling, R. F., Tans, P., Arneeth, A., Bakker, D. C. E., Barbero, L., Bopp, L., Chang, J.,  
1958 Chevallier, F., Chini, L. P., Ciais, P., Fader, M., Feely, R. A., Gkritzalis, T., Harris, I., Hauck, J.,  
1959 Ilyina, T., Jain, A. K., Kato, E., Kitidis, V., Klein Goldewijk, K., Koven, C., Landschützer, P.,  
1960 Lauvset, S. K., Lefèvre, N., Lenton, A., Lima, I. D., Metzl, N., Millero, F., Munro, D. R.,  
1961 Murata, A., S. Nabel, J. E. M., Nakaoka, S., Nojiri, Y., O'Brien, K., Olsen, A., Ono, T., Pérez, F.  
1962 F., Pfeil, B., Pierrot, D., Poulter, B., Rehder, G., Rödenbeck, C., Saito, S., Schuster, U.,  
1963 Schwinger, J., Séférian, R., Steinhoff, T., Stocker, B. D., Sutton, A. J., Takahashi, T., Tilbrook,  
1964 B., Van Der Laan-Luijkx, I. T., Van Der Werf, G. R., Van Heuven, S., Vandemark, D., Viovy,  
1965 N., Wiltshire, A., Zaehle, S. and Zeng, N.: Global Carbon Budget 2015, *Earth Syst. Sci. Data*,  
1966 doi:10.5194/essd-7-349-2015, 2015b.

1967 Le Quéré, C., Andrew, R. M., Canadell, J. G., Sitch, S., Ivar Korsbakken, J., Peters, G. P., Manning,  
1968 A. C., Boden, T. A., Tans, P. P., Houghton, R. A., Keeling, R. F., Alin, S., Andrews, O. D.,  
1969 Anthoni, P., Barbero, L., Bopp, L., Chevallier, F., Chini, L. P., Ciais, P., Currie, K., Delire, C.,  
1970 Doney, S. C., Friedlingstein, P., Gkritzalis, T., Harris, I., Hauck, J., Haverd, V., Hoppema, M.,  
1971 Klein Goldewijk, K., Jain, A. K., Kato, E., Körtzinger, A., Landschützer, P., Lefèvre, N., Lenton,  
1972 A., Lienert, S., Lombardozi, D., Melton, J. R., Metzl, N., Millero, F., Monteiro, P. M. S.,

1973 Munro, D. R., Nabel, J. E. M. S., Nakaoka, S. I., O'Brien, K., Olsen, A., Omar, A. M., Ono, T.,

1974 Pierrot, D., Poulter, B., Rödenbeck, C., Salisbury, J., Schuster, U., Schwinger, J., Séférian, R.,

1975 Skjelvan, I., Stocker, B. D., Sutton, A. J., Takahashi, T., Tian, H., Tilbrook, B., Van Der Laan-

1976 Luijkx, I. T., Van Der Werf, G. R., Viovy, N., Walker, A. P., Wiltshire, A. J. and Zaehle, S.:

1977 Global Carbon Budget 2016, *Earth Syst. Sci. Data*, doi:10.5194/essd-8-605-2016, 2016.

1978 Le Quéré, C., Andrew, R. M., Friedlingstein, P., Sitch, S., Pongratz, J., Manning, A. C.,

1979 Korsbakken, J. I., Peters, G. P., Canadell, J. G., Jackson, R. B., Boden, T. A., Tans, P. P.,

1980 Andrews, O. D., Arora, V. K., Bakker, D. C. E., Barbero, L., Becker, M., Betts, R. A., Bopp, L.,

1981 Chevallier, F., Chini, L. P., Ciais, P., Cosca, C. E., Cross, J., Currie, K., Gasser, T., Harris, I.,

1982 Hauck, J., Haverd, V., Houghton, R. A., Hunt, C. W., Hurtt, G., Ilyina, T., Jain, A. K., Kato, E.,

1983 Kautz, M., Keeling, R. F., Klein Goldewijk, K., Körtzinger, A., Landschützer, P., Lefèvre, N.,

1984 Lenton, A., Lienert, S., Lima, I., Lombardozi, D., Metzl, N., Millero, F., Monteiro, P. M. S.,

1985 Munro, D. R., Nabel, J. E. M. S., Nakaoka, S., Nojiri, Y., Padin, X. A., Peregón, A., Pfeil, B.,

1986 Pierrot, D., Poulter, B., Rehder, G., Reimer, J., Rödenbeck, C., Schwinger, J., Séférian, R.,

1987 Skjelvan, I., Stocker, B. D., Tian, H., Tilbrook, B., Tubiello, F. N., van der Laan-Luijkx, I. T.,

1988 van der Werf, G. R., van Heuven, S., Viovy, N., Vuichard, N., Walker, A. P., Watson, A. J.,

1989 Wiltshire, A. J., Zaehle, S. and Zhu, D.: Global Carbon Budget 2017, *Earth Syst. Sci. Data*,

1990 10(1), 405–448, doi:10.5194/essd-10-405-2018, 2018a.

1991 Le Quéré, C., Andrew, R. M., Friedlingstein, P., Sitch, S., Hauck, J., Pongratz, J., Pickers, P. A.,

1992 Korsbakken, J. I., Peters, G. P., Canadell, J. G., Arneeth, A., Arora, V. K., Barbero, L., Bastos,

1993 A., Bopp, L., Chevallier, F., Chini, L. P., Ciais, P., Doney, S. C., Gkritzalis, T., Goll, D. S., Harris,

1994 I., Haverd, V., Hoffman, F. M., Hoppema, M., Houghton, R. A., Hurtt, G., Ilyina, T., Jain, A.

1995 K., Johannessen, T., Jones, C. D., Kato, E., Keeling, R. F., Goldewijk, K. K., Landschützer, P.,

1996 Lefèvre, N., Lienert, S., Liu, Z., Lombardozi, D., Metzl, N., Munro, D. R., Nabel, J. E. M. S.,

1997 Nakaoka, S., Neill, C., Olsen, A., Ono, T., Patra, P., Peregón, A., Peters, W., Peylin, P., Pfeil,

1998 B., Pierrot, D., Poulter, B., Rehder, G., Resplandy, L., Robertson, E., Rocher, M., Rödenbeck,

1999 C., Schuster, U., Schwinger, J., Séférian, R., Skjelvan, I., Steinhoff, T., Sutton, A., Tans, P. P.,

2000 Tian, H., Tilbrook, B., Tubiello, F. N., van der Laan-Luijkx, I. T., van der Werf, G. R., Viivy, N.,

2001 Walker, A. P., Wiltshire, A. J., Wright, R., Zaehle, S. and Zheng, B.: Global Carbon Budget

2002 2018, *Earth Syst. Sci. Data*, 10(4), 2141–2194, doi:10.5194/essd-10-2141-2018, 2018b.

2003 Le Quéré, C., Korsbakken, J. I., Wilson, C., Tosun, J., Andrew, R., Andres, R. J., Canadell, J. G.,

2004 Jordan, A., Peters, G. P. and van Vuuren, D. P.: Drivers of declining CO<sub>2</sub> emissions in 18

2005 developed economies, *Nat. Clim. Chang.*, 9(3), 213–217, doi:10.1038/s41558-019-0419-7,

2006 2019.

2007 Lee, T. J. and Pielke, R. A.: Estimating the Soil Surface Specific Humidity, *J. Appl. Meteorol.*,

2008 31(5), 480–484, doi:10.1175/1520-0450(1992)031<0480:ETSSSH>2.0.CO;2, 1992.

2009 Li, H. and Ilyina, T.: Current and Future Decadal Trends in the Oceanic Carbon Uptake Are

2010 Dominated by Internal Variability, *Geophys. Res. Lett.*, 45(2), 916–925,

2011 doi:10.1002/2017gl075370, 2018.

2012 Lienert, S. and Joos, F.: A Bayesian ensemble data assimilation to constrain model parameters

2013 and land-use carbon emissions, *Biogeosciences*, 15(9), 2909–2930, doi:10.5194/bg-15-

2014 2909-2018, 2018.

2015 Liu, Z., Guan, D., Wei, W., Davis, S. J., Ciais, P., Bai, J., Peng, S., Zhang, Q., Hubacek, K., Marland,

2016 G., Andres, R. J., Crawford-Brown, D., Lin, J., Zhao, H., Hong, C., Boden, T. A., Feng, K.,

2017 Peters, G. P., Xi, F., Liu, J., Li, Y., Zhao, Y., Zeng, N. and He, K.: Reduced carbon emission

2018 estimates from fossil fuel combustion and cement production in China, *Nature*,

2019 doi:10.1038/nature14677, 2015.

2020 Manning, A. C. and Keeling, R. F.: Global oceanic and land biotic carbon sinks from the scripps

2021 atmospheric oxygen flask sampling network, *Tellus, Ser. B Chem. Phys. Meteorol.*, 58(2),  
2022 95–116, doi:10.1111/j.1600-0889.2006.00175.x, 2006.

2023 Marland, G.: Uncertainties in Accounting for CO<sub>2</sub> From Fossil Fuels, *J. Ind. Ecol.*, 12(2), 136–  
2024 139, doi:10.1111/j.1530-9290.2008.00014.x, 2008.

2025 Marland, G. and Rotty, R. M.: Carbon-Dioxide Emissions from Fossil-Fuels - a Procedure for  
2026 Estimation and Results for 1950-1982, *Tellus Ser. B-Chemical Phys. Meteorol.*, 36(4), 232–  
2027 261, doi:DOI 10.1111/j.1600-0889.1984.tb00245.x, 1984.

2028 Marland, G., Hamal, K. and Jonas, M.: How Uncertain Are Estimates of CO<sub>2</sub> Emissions?, *J. Ind.*  
2029 *Ecol.*, 13(1), 4–7, doi:10.1111/j.1530-9290.2009.00108.x, 2009.

2030 Masarie, K. A. and Tans, P. P.: Extension and Integration of Atmospheric Carbon-Dioxide Data  
2031 into a Globally Consistent Measurement Record, *J. Geophys. Res.*, 100(D6), 11593–11610,  
2032 doi:Doi 10.1029/95jd00859, 1995.

2033 Mauritsen, T., Bader, J., Becker, T., Behrens, J., Bittner, M., Brokopf, R., Brovkin, V., Claussen,  
2034 M., Crueger, T., Esch, M., Fast, I., Fiedler, S., Fläschner, D., Gayler, V., Giorgetta, M., Goll, D.  
2035 S., Haak, H., Hagemann, S., Hedemann, C., Hohenegger, C., Ilyina, T., Jahns, T., Jimenéz-de-  
2036 la-Cuesta, D., Jungclaus, J., Kleinen, T., Kloster, S., Kracher, D., Kinne, S., Kleberg, D.,  
2037 Lasslop, G., Kornblueh, L., Marotzke, J., Matei, D., Meraner, K., Mikolajewicz, U., Modali,  
2038 K., Möbis, B., Müller, W. A., Nabel, J. E. M. S., Nam, C. C. W., Notz, D., Nyawira, S., Paulsen,  
2039 H., Peters, K., Pincus, R., Pohlmann, H., Pongratz, J., Popp, M., Raddatz, T. J., Rast, S.,  
2040 Redler, R., Reick, C. H., Rohrschneider, T., Schemann, V., Schmidt, H., Schnur, R.,  
2041 Schulzweida, U., Six, K. D., Stein, L., Stemmler, I., Stevens, B., Storch, J., Tian, F., Voigt, A.,  
2042 Vrese, P., Wieners, K., Wilkenskjeld, S., Winkler, A. and Roeckner, E.: Developments in the  
2043 MPI-M Earth System Model version 1.2 (MPI-ESM1.2) and Its Response to Increasing CO<sub>2</sub>,  
2044 *J. Adv. Model. Earth Syst.*, 11(4), 998–1038, doi:10.1029/2018MS001400, 2019.

2045 MCI: Ministry of Commerce and Industry: Foreign Trade Data Dissemination Portal, available at:  
2046 <http://14.98.253.4/>, last access: 3 November 2019., 2019.

2047 McKinley, G. A., Pilcher, D. J., Fay, A. R., Lindsay, K., Long, M. C. and Lovenduski, N. S.:  
2048 Timescales for detection of trends in the ocean carbon sink, *Nature*, 530(7591), 469–472,  
2049 doi:10.1038/nature16958, 2016.

2050 McNeil, B. I., Matear, R. J., Key, R. M., Bullister, J. L. and Sarmiento, J. L.: Anthropogenic CO<sub>2</sub>  
2051 uptake by the ocean based on the global chlorofluorocarbon data set, *Science* (80-. ),  
2052 299(5604), 235–239, doi:10.1126/science.1077429, 2003.

2053 Meiyappan, P., Jain, A. K. and House, J. I.: Increased influence of nitrogen limitation on CO<sub>2</sub>  
2054 emissions from future land use and land use change, *Global Biogeochem. Cycles*, 29(9),  
2055 1524–1548, doi:10.1002/2015gb005086, 2015.

2056 Melton, J. R. and Arora, V. K.: Competition between plant functional types in the Canadian  
2057 Terrestrial Ecosystem Model (CTEM) v. 2.0, *Geosci. Model Dev.*, 9(1), 323–361,  
2058 doi:10.5194/gmd-9-323-2016, 2016.

2059 Mercado, L. M., Bellouin, N., Sitch, S., Boucher, O., Huntingford, C., Wild, M. and Cox, P. M.:  
2060 Impact of changes in diffuse radiation on the global land carbon sink, *Nature*, 458(7241),  
2061 1014–1017, doi:10.1038/nature07949, 2009.

2062 Merlin, O., Al Bitar, A., Rivalland, V., Béziat, P., Ceschia, E. and Dedieu, G.: An Analytical Model  
2063 of Evaporation Efficiency for Unsaturated Soil Surfaces with an Arbitrary Thickness, *J. Appl.*  
2064 *Meteorol. Climatol.*, 50(2), 457–471, doi:10.1175/2010JAMC2418.1, 2011.

2065 Mikaloff Fletcher, S. E., Gruber, N., Jacobson, A. R., Doney, S. C., Dutkiewicz, S., Gerber, M.,  
2066 Follows, M., Joos, F., Lindsay, K., Menemenlis, D., Mouchet, A., Müller, S. A. and  
2067 Sarmiento, J. L.: Inverse estimates of anthropogenic CO<sub>2</sub> uptake, transport, and storage by  
2068 the ocean, *Global Biogeochem. Cycles*, 20(2), GB2002, doi:10.1029/2005GB002530, 2006.

2069 Millar, R. J., Fuglestvedt, J. S., Friedlingstein, P., Rogelj, J., Grubb, M. J., Matthews, H. D., Skeie,  
2070 R. B., Forster, P. M., Frame, D. J. and Allen, M. R.: Emission budgets and pathways  
2071 consistent with limiting warming to 1.5 °C, *Nat. Geosci.*, 10(10), 741–747,  
2072 doi:10.1038/ngeo3031, 2017.

2073 Ministry of Mines: Ministry of Mines: Mineral Production, available at:  
2074 <http://ibm.nic.in/index.php?c=pages&m=index&id=497>, last access: 18 September 2019.,  
2075 2019.

2076 Myhre, G., Alterskjær, K. and Lowe, D.: A fast method for updating global fossil fuel carbon  
2077 dioxide emissions, *Environ. Res. Lett.*, 4(3), 034012, doi:10.1088/1748-9326/4/3/034012,  
2078 2009.

2079 Myneni, R. B., Ramakrishna, R., Nemani, R. and Running, S. W.: Estimation of global leaf area  
2080 index and absorbed par using radiative transfer models, *IEEE Trans. Geosci. Remote Sens.*,  
2081 35(6), 1380–1393, doi:10.1109/36.649788, 1997.

2082 Narayanan, B., Aguiar, A. and McDougall, R.: Global Trade, Assistance, and Production: The  
2083 GTAP 9 Data Base, *Cent. Glob. Trade Anal. Purdue Univ.*, 2015(September) [online]  
2084 Available from: <https://www.gtap.agecon.purdue.edu/databases/v9/default.asp>, 2015.

2085 NBS: Energy supply growth is speeding up, and the share of clean energy is continuously  
2086 increasing. The department director interprets the half-yearly report.  
2087 [http://www.stats.gov.cn/tjsj/sjjd/201907/t20190717\\_1676924.html](http://www.stats.gov.cn/tjsj/sjjd/201907/t20190717_1676924.html). Last access 23  
2088 September 2019., National Bureau of Statistics., 2019a.

2089 NBS: National Bureau of Statistics, 2019. Statistical Communiqué of the People’s Republic of  
2090 China on the 2018 National Economic and Social Development, available at:  
2091 [http://www.stats.gov.cn/english/PressRelease/201902/t20190228\\_1651335.html](http://www.stats.gov.cn/english/PressRelease/201902/t20190228_1651335.html). Last  
2092 access: 23 S., 2019b.

2093 NBS: National Bureau of Statistics (NBS): National Data (online database).  
2094 <http://data.stats.gov.cn/>. Last access 1 November 2019., National Bureau of Statistics.,  
2095 2019c.

2096 NOAA/ESRL: NOAA Greenhouse Gas Marine Boundary Layer Reference, available at:  
2097 <https://www.esrl.noaa.gov/gmd/ccgg/mb/mb.html>, last access: 27 September 2019.,  
2098 2019.

2099 OEA: Index of Eight Core Industries, available at: <http://eaindustry.nic.in/home.asp>, last access:  
2100 5 November 2019., 2019.

2101 Paulsen, H., Ilyina, T., Six, K. D. and Stemmler, I.: Incorporating a prognostic representation of  
2102 marine nitrogen fixers into the global ocean biogeochemical model HAMOCC, *J. Adv.*  
2103 *Model. Earth Syst.*, 9(1), 438–464, doi:10.1002/2016MS000737, 2017.

2104 Peters, G. P., Andrew, R. and Lennox, J.: Constructing an environmentally-extended multi-  
2105 regional input-output table using the GTAP database, *Econ. Syst. Res.*, 23(2), 131–152,  
2106 doi:10.1080/09535314.2011.563234, 2011a.

2107 Peters, G. P., Minx, J. C., Weber, C. L. and Edenhofer, O.: Growth in emission transfers via  
2108 international trade from 1990 to 2008, *Proc. Natl. Acad. Sci.*, 108(21), 8903–8908,  
2109 doi:10.1073/pnas.1006388108, 2011b.

2110 Peters, G. P., Davis, S. J. and Andrew, R.: A synthesis of carbon in international trade,  
2111 *Biogeosciences*, 9(8), 3247–3276, doi:10.5194/bg-9-3247-2012, 2012a.

2112 Peters, G. P., Marland, G., Le Quéré, C., Boden, T., Canadell, J. G. and Raupach, M. R.: Rapid  
2113 growth in CO<sub>2</sub> emissions after the 2008–2009 global financial crisis, *Nat. Clim. Chang.*, 2(1),  
2114 2–4, doi:10.1038/nclimate1332, 2012b.

2115 Peters, G. P., Andrew, R. M., Boden, T., Canadell, J. G., Ciais, P., Le Quéré, C., Marland, G.,  
2116 Raupach, M. R. and Wilson, C.: The challenge to keep global warming below 2 °C, *Nat.*

2117 Clim. Chang., 3(1), 4–6, doi:10.1038/nclimate1783, 2013.

2118 Peters, G. P., Le Quéré, C., Andrew, R. M., Canadell, J. G., Friedlingstein, P., Ilyina, T., Jackson, R.  
2119 B., Joos, F., Korsbakken, J. I., McKinley, G. A., Sitch, S. and Tans, P.: Towards real-time  
2120 verification of CO<sub>2</sub> emissions, Nat. Clim. Chang., 7(12), 848–850, doi:10.1038/s41558-017-  
2121 0013-9, 2017.

2122 Peylin, P., Law, R. M., Gurney, K. R., Chevallier, F., Jacobson, A. R., Maki, T., Niwa, Y., Patra, P. K.,  
2123 Peters, W., Rayner, P. J., Rödenbeck, C., van der Laan-Luijkx, I. T. and Zhang, X.: Global  
2124 atmospheric carbon budget: results from an ensemble of atmospheric CO<sub>2</sub> inversions,  
2125 Biogeosciences, 10(10), 6699–6720, doi:10.5194/bg-10-6699-2013, 2013.

2126 Peylin, P. et al.: The new ORCHIDEE land surface model version V2.0 as used for the CMIP6  
2127 climate simulation intercomparison exercise, in preparation, 2019.

2128 Pfeil, B., Olsen, A., Bakker, D. C. E., Hankin, S., Koyuk, H., Kozyr, A., Malczyk, J., Manke, A., Metzl,  
2129 N., Sabine, C. L., Akl, J., Alin, S. R., Bates, N., Bellerby, R. G. J., Borges, A., Boutin, J., Brown,  
2130 P. J., Cai, W. J., Chavez, F. P., Chen, A., Cosca, C., Fassbender, A. J., Feely, R. A., Gonzalez-  
2131 Davila, M., Goyet, C., Hales, B., Hardman-Mountford, N., Heinze, C., Hood, M., Hoppema,  
2132 M., Hunt, C. W., Hydes, D., Ishii, M., Johannessen, T., Jones, S. D., Key, R. M., Kortzinger, A.,  
2133 Landschutzer, P., Lauvset, S. K., Lefevre, N., Lenton, A., Lourantou, A., Merlivat, L.,  
2134 Midorikawa, T., Mintrop, L., Miyazaki, C., Murata, A., Nakadate, A., Nakano, Y., Nakaoka,  
2135 S., Nojiri, Y., Omar, A. M., Padin, X. A., Park, G. H., Paterson, K., Perez, F. F., Pierrot, D.,  
2136 Poisson, A., Rios, A. F., Santana-Casiano, J. M., Salisbury, J., Sarma, V. V. S. S., Schlitzer, R.,  
2137 Schneider, B., Schuster, U., Sieger, R., Skjelvan, I., Steinhoff, T., Suzuki, T., Takahashi, T.,  
2138 Tedesco, K., Telszewski, M., Thomas, H., Tilbrook, B., Tjiputra, J., Vandemark, D., Veness,  
2139 T., Wanninkhof, R., Watson, A. J., Weiss, R., Wong, C. S. and Yoshikawa-Inoue, H.: A  
2140 uniform, quality controlled Surface Ocean CO<sub>2</sub> Atlas (SOCAT), Earth Syst. Sci. Data, 5(1),

2141 125–143, doi:10.5194/essd-5-125-2013, 2013.

2142 Piao, S., Huang, M., Liu, Z., Wang, X. H., Ciais, P., Canadell, J. G., Wang, K., Bastos, A.,  
2143 Friedlingstein, P., Houghton, R. A., Le Quéré, C., Liu, Y. W., Myneni, R. B., Peng, S. S.,  
2144 Pongratz, J., Sitch, S., Yan, T., Wang, Y. L., Zhu, Z. C., Wu, D. H. and Wang, T.: Lower land-  
2145 use emissions responsible for increased net land carbon sink during the slow warming  
2146 period, *Nat. Geosci.*, 11(10), 739–+, doi:10.1038/s41561-018-0204-7, 2018.

2147 Pongratz, J., Reick, C. H., Raddatz, T. and Claussen, M.: Effects of anthropogenic land cover  
2148 change on the carbon cycle of the last millennium, *Global Biogeochem. Cycles*,  
2149 doi:10.1029/2009GB003488, 2009.

2150 Pongratz, J., Reick, C. H., Houghton, R. A. and House, J. I.: Terminology as a key uncertainty in  
2151 net land use and land cover change carbon flux estimates, *Earth Syst. Dyn.*, 5(1), 177–195,  
2152 doi:10.5194/esd-5-177-2014, 2014.

2153 Poulter, B., Frank, D. C., Hodson, E. L. and Zimmermann, N. E.: Impacts of land cover and  
2154 climate data selection on understanding terrestrial carbon dynamics and the CO<sub>2</sub> airborne  
2155 fraction, *Biogeosciences*, 8(8), 2027–2036, doi:10.5194/bg-8-2027-2011, 2011.

2156 PPAC: Natural Gas. Petroleum Planning and Analysis Cell, Ministry of Petroleum and Natural  
2157 Gas, available at: <http://eaindstry.nic.in/home.asp>, last access: 5 November 2019.,  
2158 2019a.

2159 PPAC: Petroleum. Petroleum Planning and Analysis Cell, Ministry of Petroleum and Natural Gas,  
2160 available at: <http://eaindstry.nic.in/home.asp>, last access: 17 October 2019., 2019b.

2161 Prentice, I. C., Farquhar, G. D., Fasham, M. J. R., Goulden, M. L., Heimann, M., Jaramillo, V. J.,  
2162 Khesghi, H. S., Le Quéré, C., Scholes, R. J., Wallace, D. W. R. and Press, C. U.: The Carbon  
2163 Cycle and Atmospheric Carbon Dioxide, in *Climate Change 2001: The Scientific Basis*.  
2164 Contribution of Working Group I to the Third Assessment Report of the Intergovernmental

2165 Panel on Climate Change, edited by J. T. Houghton, Y. Ding, D. J. Griggs, M. Noguer, P. J.  
2166 van der Linden, X. Dai, K. Maskell, and C. A. Johnson, pp. 183–237, Cambridge University  
2167 Press, Cambridge, United Kingdom and New York, NY, USA., 2001.

2168 Price, J. T. and Warren, R.: Review of the Potential of “Blue Carbon” Activities to Reduce  
2169 Emissions; available at [http://avoid-net-uk.cc.ic.ac.uk/wp-content/uploads/delightful-](http://avoid-net-uk.cc.ic.ac.uk/wp-content/uploads/delightful-downloads/2016/03/Literature-review-of-the-potential-of-blue-carbon-activities-to-reduce-emissions-AVOID2-W.)  
2170 [downloads/2016/03/Literature-review-of-the-potential-of-blue-carbon-activities-to-](http://avoid-net-uk.cc.ic.ac.uk/wp-content/uploads/delightful-downloads/2016/03/Literature-review-of-the-potential-of-blue-carbon-activities-to-reduce-emissions-AVOID2-W.)  
2171 [reduce-emissions-AVOID2-W.](http://avoid-net-uk.cc.ic.ac.uk/wp-content/uploads/delightful-downloads/2016/03/Literature-review-of-the-potential-of-blue-carbon-activities-to-reduce-emissions-AVOID2-W.), 2016.

2172 Raupach, M. R., Marland, G., Ciais, P., Le Quéré, C., Canadell, J. G., Klepper, G. and Field, C. B.:  
2173 Global and regional drivers of accelerating CO<sub>2</sub> emissions, *Proc Natl Acad Sci U S A*,  
2174 104(24), 10288–10293, doi:10.1073/pnas.0700609104, 2007.

2175 Regnier, P., Friedlingstein, P., Ciais, P., Mackenzie, F. T., Gruber, N., Janssens, I. A., Laruelle, G.  
2176 G., Lauerwald, R., Luysaert, S., Andersson, A. J., Arndt, S., Arnosti, C., Borges, A. V., Dale,  
2177 A. W., Gallego-Sala, A., Goddérís, Y., Goossens, N., Hartmann, J., Heinze, C., Ilyina, T., Joos,  
2178 F., LaRowe, D. E., Leifeld, J., Meysman, F. J. R., Munhoven, G., Raymond, P. A., Spahni, R.,  
2179 Suntharalingam, P. and Thullner, M.: Anthropogenic perturbation of the carbon fluxes  
2180 from land to ocean, *Nat. Geosci.*, 6(8), 597–607, doi:10.1038/ngeo1830, 2013.

2181 Remaud, M., Chevallier, F., Cozic, A., Lin, X. and Bousquet, P.: On the impact of recent  
2182 developments of the LMDz atmospheric general circulation model on the simulation of  
2183 CO<sub>2</sub> transport, *Geosci. Model Dev.*, 11(11), 4489–4513, doi:10.5194/gmd-11-4489-2018,  
2184 2018.

2185 Resplandy, L., Keeling, R. F., Rödenbeck, C., Stephens, B. B., Khatiwala, S., Rodgers, K. B., Long,  
2186 M. C., Bopp, L. and Tans, P. P.: Revision of global carbon fluxes based on a reassessment of  
2187 oceanic and riverine carbon transport, *Nat. Geosci.*, 11(7), 504–+, doi:10.1038/s41561-018-  
2188 0151-3, 2018.

2189 Rhein, M., Rintoul, S. R., Aoki, S., Campos, E., Chambers, D., Feely, R. A., Gulev, S., Johnson, G.  
2190 C., Josey, S. A., Kostianoy, A., Mauritzen, C., Roemmich, D., Talley, L. D., Wang, F., Stocker,  
2191 T., Qin, D. and Platner, G.-K.: Chapter 3: Observations: Ocean, in Climate Change 2013 The  
2192 Physical Science Basis, Cambridge University Press., 2013.

2193 Rödenbeck, C.: Estimating CO<sub>2</sub> sources and sinks from atmospheric mixing ratio measurements  
2194 using a global inversion of atmospheric transport, Technical Report 6, available at:  
2195 [http://www.bgc-jena.mpg.de/CarboScope/s/tech\\_report6.pdf](http://www.bgc-jena.mpg.de/CarboScope/s/tech_report6.pdf), Max Planck Institute for  
2196 Biogeochemistry, Jena., 2005.

2197 Rödenbeck, C., Houweling, S., Gloor, M. and Heimann, M.: CO<sub>2</sub> flux history 1982–2001  
2198 inferred from atmospheric data using a global inversion of atmospheric transport, Atmos.  
2199 Chem. Phys. Discuss., 3(3), 2575–2659, doi:10.5194/acpd-3-2575-2003, 2003.

2200 Rödenbeck, C., Keeling, R. F., Bakker, D. C. E., Metzl, N., Olsen, A., Sabine, C. and Heimann, M.:  
2201 Global surface-ocean  
2202  $\text{CO}_2$  and sea–air  
2203  $\text{CO}_2$  flux variability from an observation-driven ocean mixed-layer  
2204 scheme, Ocean Sci., 9(2), 193–216, doi:10.5194/os-9-193-2013, 2013.

2205 Rödenbeck, C., Bakker, D. C. E., Metzl, N., Olsen, A., Sabine, C., Cassar, N., Reum, F., Keeling, R.  
2206 F. and Heimann, M.: Interannual sea–air  $\text{CO}_2$  flux variability from  
2207 an observation-driven ocean mixed-layer scheme, Biogeosciences, 11(17), 4599–4613,  
2208 doi:10.5194/bg-11-4599-2014, 2014.

2209 Rödenbeck, C., Bakker, D. C. E., Gruber, N., Iida, Y., Jacobson, A. R., Jones, S., Landschützer, P.,  
2210 Metzl, N., Nakaoka, S., Olsen, A., Park, G.-H., Peylin, P., Rodgers, K. B., Sasse, T. P.,  
2211 Schuster, U., Shutler, J. D., Valsala, V., Wanninkhof, R. and Zeng, J.: Data-based estimates  
2212 of the ocean carbon sink variability – first results of the Surface Ocean pCO<sub>2</sub> Mapping

2213 intercomparison (SOCOM), *Biogeosciences*, 12(23), 7251–7278, doi:10.5194/bg-12-7251-  
2214 2015, 2015.

2215 Rödenbeck, C., Zaehle, S., Keeling, R. and Heimann, M.: How does the terrestrial carbon  
2216 exchange respond to inter-annual climatic variations? A quantification based on  
2217 atmospheric CO<sub>2</sub> data, *Biogeosciences*, 15(8), 2481–2498, doi:10.5194/bg-15-2481-2018,  
2218 2018.

2219 Rogelj, J., Schaeffer, M., Friedlingstein, P., Gillett, N. P., van Vuuren, D. P., Riahi, K., Allen, M.  
2220 and Knutti, R.: Differences between carbon budget estimates unravelled, *Nat. Clim.*  
2221 *Chang.*, 6(3), 245–252, doi:10.1038/Nclimate2868, 2016.

2222 Rogelj, J., Forster, P. M., Kriegler, E., Smith, C. J. and Séférian, R.: Estimating and tracking the  
2223 remaining carbon budget for stringent climate targets, *Nature*, 571(7765), 335–342,  
2224 doi:10.1038/s41586-019-1368-z, 2019.

2225 Rypdal, K., Paciomik, N., Eggleston, S., Goodwin, J., Irving, W., Penman, J. and Woodfield, M.:  
2226 Chapter 1 Introduction to the 2006 Guidelines, in 2006 IPCC Guidelines for National  
2227 Greenhouse Gas Inventories, edited by S. Eggleston, L. Buendia, K. Miwa, T. Ngara, and K.  
2228 Tanabe, Institute for Global Environmental Strategies (IGES), Hayama, Kanagawa, Japan.,  
2229 2006.

2230 Saatchi, S. S., Harris, N. L., Brown, S., Lefsky, M., Mitchard, E. T. A., Salas, W., Zutta, B. R.,  
2231 Buermann, W., Lewis, S. L., Hagen, S., Petrova, S., White, L., Silman, M. and Morel, A.:  
2232 Benchmark map of forest carbon stocks in tropical regions across three continents, *Proc.*  
2233 *Natl. Acad. Sci.*, 108(24), 9899–9904, doi:10.1073/pnas.1019576108, 2011.

2234 Saunio, M., Bousquet, P., Poulter, B., Peregon, A., Ciais, P., Canadell, J. G., Dlugokencky, E. J.,  
2235 Etiope, G., Bastviken, D., Houweling, S., Janssens-Maenhout, G., Tubiello, F. N., Castaldi, S.,  
2236 Jackson, R. B., Alexe, M., Arora, V. K., Beerling, D. J., Bergamaschi, P., Blake, D. R.,

2237 Brailsford, G., Brovkin, V., Bruhwiler, L., Crevoisier, C., Crill, P., Covey, K., Curry, C.,  
2238 Frankenberg, C., Gedney, N., Höglund-Isaksson, L., Ishizawa, M., Ito, A., Joos, F., Kim, H. S.,  
2239 Kleinen, T., Krummel, P., Lamarque, J. F., Langenfelds, R., Locatelli, R., Machida, T.,  
2240 Maksyutov, S., McDonald, K. C., Marshall, J., Melton, J. R., Morino, I., Naik, V., O'Doherty,  
2241 S., Parmentier, F. J. W., Patra, P. K., Peng, C., Peng, S., Peters, G. P., Pison, I., Prigent, C.,  
2242 Prinn, R., Ramonet, M., Riley, W. J., Saito, M., Santini, M., Schroeder, R., Simpson, I. J.,  
2243 Spahni, R., Steele, P., Takizawa, A., Thornton, B. F., Tian, H., Tohjima, Y., Viovy, N.,  
2244 Voulgarakis, A., Van Weele, M., Van Der Werf, G. R., Weiss, R., Wiedinmyer, C., Wilton, D.  
2245 J., Wiltshire, A., Worthy, D., Wunch, D., Xu, X., Yoshida, Y., Zhang, B., Zhang, Z. and Zhu, Q.:  
2246 The global methane budget 2000-2012, *Earth Syst. Sci. Data*, 8(2), 697–751,  
2247 doi:10.5194/essd-8-697-2016, 2016.

2248 SCCL: Singareni Collieries Company Limited (SCCL): Provisional Production and Dispatches  
2249 Performance. Singareni Collieries Company Limited, available at:  
2250 [https://scclmines.com/scclnew/performance\\_production.asp](https://scclmines.com/scclnew/performance_production.asp), last access: 3 September  
2251 2019., 2019.

2252 Schimel, D., Alves, D., Enting, I., Heimann, M., Joos, F., Raynaud, D., Wigley, T., Prater, M.,  
2253 Derwent, R., Ehhalt, D., Fraser, P., Sanhueza, E., Zhou, X., Jonas, P., Charlson, R., Rodhe, H.,  
2254 Sadasivan, S., Shine, K. P., Fouquart, Y., Ramaswamy, V., Solomon, S., Srinivasan, J.,  
2255 Albritton, D., Derwent, R., Isaksen, I., Lal, M., Wuebbles, D. and Press, C. U.: Radiative  
2256 Forcing of Climate Change, in *Climate Change 1995 The Science of Climate Change*.  
2257 Contribution of Working Group I to the Second Assessment Report of the  
2258 Intergovernmental Panel on Climate Change, edited by J. T. Houghton, L. G. Meira Rillo, B.  
2259 A. Callander, N. Harris, A. Kattenberg, and K. Maskell, Cambridge University Press,  
2260 Cambridge, United Kingdom and New York, NY, USA., 1995.

2261 Schimel, D., Stephens, B. B. and Fisher, J. B.: Effect of increasing CO<sub>2</sub> on the terrestrial carbon  
2262 cycle, *Proc Natl Acad Sci U S A*, 112(2), 436–441, doi:10.1073/pnas.1407302112, 2015.

2263 Schwietzke, S., Sherwood, O. A., Bruhwiler, L. M., Miller, J. B., Etiope, G., Dlugokencky, E. J.,  
2264 Michel, S. E., Arling, V. A., Vaughn, B. H., White, J. W. and Tans, P. P.: Upward revision of  
2265 global fossil fuel methane emissions based on isotope database, *Nature*, 538(7623), 88–91,  
2266 doi:10.1038/nature19797, 2016.

2267 Schwinger, J., Goris, N., Tjiputra, J. F., Kriest, I., Bentsen, M., Bethke, I., Ilicak, M., Assmann, K.  
2268 M. and Heinze, C.: Evaluation of NorESM-OC (versions 1 and 1.2), the ocean carbon-cycle  
2269 stand-alone configuration of the Norwegian Earth System Model (NorESM1), *Geosci.*  
2270 *Model Dev.*, 9(8), 2589–2622, doi:10.5194/gmd-9-2589-2016, 2016.

2271 Séférian, R., Delire, C., Decharme, B., Voldoire, A., Salas y Melia, D., Chevallier, M., Saint-Martin,  
2272 D., Aumont, O., Calvet, J.-C., Carrer, D., Douville, H., Franchistéguy, L., Joetzjer, E. and  
2273 Sénési, S.: Development and evaluation of CNRM Earth system model – CNRM-ESM1,  
2274 *Geosci. Model Dev.*, 9(4), 1423–1453, doi:10.5194/gmd-9-1423-2016, 2016.

2275 Sellar, A. A., Jones, C. G., Mulcahy, J., Tang, Y., Yool, A., Wiltshire, A., O’Connor, F. M., Stringer,  
2276 M., Hill, R., Palmieri, J., Woodward, S., Mora, L., Kuhlbrodt, T., Rumbold, S., Kelley, D. I.,  
2277 Ellis, R., Johnson, C. E., Walton, J., Abraham, N. L., Andrews, M. B., Andrews, T., Archibald,  
2278 A. T., Berthou, S., Burke, E., Blockley, E., Carslaw, K., Dalvi, M., Edwards, J., Folberth, G. A.,  
2279 Gedney, N., Griffiths, P. T., Harper, A. B., Hendry, M. A., Hewitt, A. J., Johnson, B., Jones, A.,  
2280 Jones, C. D., Keeble, J., Liddicoat, S., Morgenstern, O., Parker, R. J., Predoi, V., Robertson,  
2281 E., Siahahan, A., Smith, R. S., Swaminathan, R., Woodhouse, M. T., Zeng, G. and Zerroukat,  
2282 M.: UKESM1: Description and evaluation of the UK Earth System Model, *J. Adv. Model.*  
2283 *Earth Syst.*, 2019MS001739, doi:10.1029/2019MS001739, 2019.

2284 Shangguan, W., Hengl, T., Mendes de Jesus, J., Yuan, H. and Dai, Y.: Mapping the global depth to

2285 bedrock for land surface modeling, *J. Adv. Model. Earth Syst.*, 9(1), 65–88,  
2286 doi:10.1002/2016MS000686, 2017.

2287 Shevliakova, E., Pacala, S. W., Malyshev, S., Hurtt, G. C., Milly, P. C. D., Caspersen, J. P.,  
2288 Sentman, L. T., Fisk, J. P., Wirth, C. and Crevoisier, C.: Carbon cycling under 300 years of  
2289 land use change: Importance of the secondary vegetation sink, *Global Biogeochem. Cycles*,  
2290 23(2), doi:10.1029/2007GB003176, 2009.

2291 Sitch, S., Huntingford, C., Gedney, N., Levy, P. E., Lomas, M., Piao, S. L., Betts, R., Ciais, P., Cox,  
2292 P., Friedlingstein, P., Jones, C. D., Prentice, I. C. and Woodward, F. I.: Evaluation of the  
2293 terrestrial carbon cycle, future plant geography and climate-carbon cycle feedbacks using  
2294 five Dynamic Global Vegetation Models (DGVMs), *Glob. Chang. Biol.*, 14(9), 2015–2039,  
2295 doi:10.1111/j.1365-2486.2008.01626.x, 2008.

2296 Smith, B., Warlind, D., Arneth, A., Hickler, T., Leadley, P., Siltberg, J. and Zaehle, S.: Implications  
2297 of incorporating N cycling and N limitations on primary production in an individual-based  
2298 dynamic vegetation model, *Biogeosciences*, 11(7), 2027–2054, doi:10.5194/bg-11-2027-  
2299 2014, 2014.

2300 Stephens, B. B., Gurney, K. R., Tans, P. P., Sweeney, C., Peters, W., Bruhwiler, L., Ciais, P.,  
2301 Ramonet, M., Bousquet, P., Nakazawa, T., Aoki, S., Machida, T., Inoue, G., Vinnichenko, N.,  
2302 Lloyd, J., Jordan, A., Heimann, M., Shibistova, O., Langenfelds, R. L., Steele, L. P., Francey,  
2303 R. J. and Denning, A. S.: Weak northern and strong tropical land carbon uptake from  
2304 vertical profiles of atmospheric CO<sub>2</sub>, *Science* (80-. ), 316(5832), 1732–1735,  
2305 doi:10.1126/science.1137004, 2007.

2306 Stocker, T., Qin, D. and Plattner, G.-K.: *Climate Change 2013 The Physical Science Basis*,  
2307 Cambridge University Press., 2013.

2308 Swart, N. C., Fyfe, J. C., Saenko, O. A. and Eby, M.: Wind-driven changes in the ocean carbon

2309 sink, *Biogeosciences*, 11(21), 6107–6117, doi:10.5194/bg-11-6107-2014, 2014.

2310 Tian, H., Xu, X., Lu, C., Liu, M., Ren, W., Chen, G., Melillo, J. and Liu, J.: Net exchanges of CO<sub>2</sub>,  
2311 CH<sub>4</sub>, and N<sub>2</sub>O between China’s terrestrial ecosystems and the atmosphere and their  
2312 contributions to global climate warming, *J. Geophys. Res.*, 116(G2),  
2313 doi:10.1029/2010jg001393, 2011.

2314 Tian, H., Chen, G., Lu, C., Xu, X., Hayes, D. J., Ren, W., Pan, S., Huntzinger, D. N. and Wofsy, S. C.:  
2315 North American terrestrial CO<sub>2</sub> uptake largely offset by CH<sub>4</sub> and N<sub>2</sub>O emissions: toward a  
2316 full accounting of the greenhouse gas budget, *Clim Chang.*, 129(3–4), 413–426,  
2317 doi:10.1007/s10584-014-1072-9, 2015.

2318 Todd-Brown, K. E. O., Randerson, J. T., Post, W. M., Hoffman, F. M., Tarnocai, C., Schuur, E. A. G.  
2319 and Allison, S. D.: Causes of variation in soil carbon simulations from CMIP5 Earth system  
2320 models and comparison with observations, *Biogeosciences*, 10(3), 1717–1736,  
2321 doi:10.5194/bg-10-1717-2013, 2013.

2322 UN: United Nations Statistics Division: National Accounts Main Aggregates Database, available  
2323 at: <http://unstats.un.org/unsd/snaama/Introduction.asp>, last access: 2 January 2018.,  
2324 2017.

2325 UN: United Nations Statistics Division: Energy Statistics, available at:  
2326 <http://unstats.un.org/unsd/energy/>, last access: 27 September 2019., 2018.

2327 UNFCCC: National Inventory Submissions, available at: [https://unfccc.int/process-and-](https://unfccc.int/process-and-meetings/transparency-and-reporting/reporting-and-review-under-the-convention/greenhouse-gas-inventories-annex-i-parties/national-inventory-submissions-2019)  
2328 [meetings/transparency-and-reporting/reporting-and-review-under-the-](https://unfccc.int/process-and-meetings/transparency-and-reporting/reporting-and-review-under-the-convention/greenhouse-gas-inventories-annex-i-parties/national-inventory-submissions-2019)  
2329 [convention/greenhouse-gas-inventories-annex-i-parties/national-inventory-submissions-](https://unfccc.int/process-and-meetings/transparency-and-reporting/reporting-and-review-under-the-convention/greenhouse-gas-inventories-annex-i-parties/national-inventory-submissions-2019)  
2330 [2019](https://unfccc.int/process-and-meetings/transparency-and-reporting/reporting-and-review-under-the-convention/greenhouse-gas-inventories-annex-i-parties/national-inventory-submissions-2019), last access: June 20., 2019.

2331 Varadhan, S.: Coal India expects to resume a third of output at flooded Dipka mine within 10  
2332 days. Reuters. Available at: <https://www.reuters.com/article/coal-india-mine-floods/refile->

2333 update-1-coal-india-expects-to-resume-a-third-of-output-at-flooded-dipka-mine-within-,  
2334 2019.

2335 Van Der Laan-Luijkx, I. T., Van Der Velde, I. R., Van Der Veen, E., Tsuruta, A., Stanislawska, K.,  
2336 Babenhausheide, A., Fang Zhang, H., Liu, Y., He, W., Chen, H., Masarie, K. A., Krol, M. C.  
2337 and Peters, W.: The CarbonTracker Data Assimilation Shell (CTDAS) v1.0: Implementation  
2338 and global carbon balance 2001-2015, *Geosci. Model Dev.*, 10(7), 2785–2800,  
2339 doi:10.5194/gmd-10-2785-2017, 2017.

2340 van der Velde, I. R., Miller, J. B., Schaefer, K., van der Werf, G. R., Krol, M. C. and Peters, W.:  
2341 Terrestrial cycling of CO<sub>2</sub>; by photosynthesis, respiration, and biomass burning in SiBCASA,  
2342 *Biogeosciences*, 11(23), 6553–6571, doi:10.5194/bg-11-6553-2014, 2014.

2343 van der Werf, G. R., Randerson, J. T., Giglio, L., Collatz, G. J., Mu, M., Kasibhatla, P. S., Morton,  
2344 D. C., DeFries, R. S., Jin, Y. and van Leeuwen, T. T.: Global fire emissions and the  
2345 contribution of deforestation, savanna, forest, agricultural, and peat fires (1997–2009),  
2346 *Atmos. Chem. Phys.*, 10(23), 11707–11735, doi:10.5194/acp-10-11707-2010, 2010.

2347 van der Werf, G. R., Randerson, J. T., Giglio, L., van Leeuwen, T. T., Chen, Y., Rogers, B. M., Mu,  
2348 M., van Marle, M. J. E., Morton, D. C., Collatz, G. J., Yokelson, R. J. and Kasibhatla, P. S.:  
2349 Global fire emissions estimates during 1997–2016, *Earth Syst. Sci. Data*, 9(2), 697–720,  
2350 doi:10.5194/essd-9-697-2017, 2017.

2351 Van Minnen, J. G., Klein Goldewijk, K., Stehfest, E., Eickhout, B., van Drecht, G. and Leemans, R.:  
2352 The importance of three centuries of land-use change for the global and regional  
2353 terrestrial carbon cycle, *Clim. Change*, 97(1–2), 123–144, doi:10.1007/s10584-009-9596-0,  
2354 2009.

2355 Viovy, N.: CRUNCEP data set, available at:  
2356 [ftp://nacp.ornl.gov/synthesis/2009/frescati/temp/land\\_use\\_change/original/readme.htm](ftp://nacp.ornl.gov/synthesis/2009/frescati/temp/land_use_change/original/readme.htm),

2357 last access: June 2016., 2016.

2358 Walker, A. P., Quaife, T., van Bodegom, P. M., De Kauwe, M. G., Keenan, T. F., Joiner, J., Lomas,  
2359 M. R., MacBean, N., Xu, C. G., Yang, X. J. and Woodward, F. I.: The impact of alternative  
2360 trait-scaling hypotheses for the maximum photosynthetic carboxylation rate ( $V_{cmax}$ ) on  
2361 global gross primary production, *New Phytol.*, 215(4), 1370–1386, doi:10.1111/nph.14623,  
2362 2017.

2363 Wanninkhof, R., Park, G. H., Takahashi, T., Sweeney, C., Feely, R., Nojiri, Y., Gruber, N., Doney, S.  
2364 C., McKinley, G. A., Lenton, A., Le Quéré, C., Heinze, C., Schwinger, J., Graven, H. and  
2365 Khatiwala, S.: Global ocean carbon uptake: magnitude, variability and trends,  
2366 *Biogeosciences*, 10(3), 1983–2000, doi:10.5194/bg-10-1983-2013, 2013.

2367 Watson, R. T., Rodhe, H., Oeschger, H., Siegenthaler, U. and Press, C. U.: Greenhouse Gases and  
2368 Aerosols, in *Climate Change: The IPCC Scientific Assessment*. Intergovernmental Panel on  
2369 Climate Change (IPCC), edited by J. T. Houghton, G. J. Jenkins, and J. J. Ephraums, pp. 1–40,  
2370 Cambridge University Press, Cambridge., 1990.

2371 Wenzel, S., Cox, P. M., Eyring, V. and Friedlingstein, P.: Projected land photosynthesis  
2372 constrained by changes in the seasonal cycle of atmospheric  $CO_2$ , *Nature*, 538(7626), 499–  
2373 501, doi:10.1038/nature19772, 2016.

2374 Wilkenskjaeld, S., Kloster, S., Pongratz, J., Raddatz, T. and Reick, C. H.: Comparing the influence  
2375 of net and gross anthropogenic land-use and land-cover changes on the carbon cycle in the  
2376 MPI-ESM, *Biogeosciences*, 11(17), 4817–4828, doi:10.5194/bg-11-4817-2014, 2014.

2377 Woodward, F. I. and Lomas, M. R.: Vegetation dynamics – simulating responses to climatic  
2378 change, *Biol. Rev.*, 79(3), 643–670, doi:10.1017/S1464793103006419, 2004.

2379 Xi, F., Davis, S. J., Ciais, P., Crawford-Brown, D., Guan, D., Pade, C., Shi, T., Syddall, M., Lv, J., Ji,  
2380 L., Bing, L., Wang, J., Wei, W., Yang, K.-H., Lagerblad, B., Galan, I., Andrade, C., Zhang, Y.

2381 and Liu, Z.: Substantial global carbon uptake by cement carbonation, *Nat. Geosci.*, 9(12),  
2382 880–883, doi:10.1038/ngeo2840, 2016.

2383 Yin, X. W.: Responses of leaf nitrogen concentration and specific leaf area to atmospheric CO<sub>2</sub>  
2384 enrichment: a retrospective synthesis across 62 species, *Glob. Chang. Biol.*, 8(7), 631–642,  
2385 doi:DOI 10.1046/j.1365-2486.2002.00497.x, 2002.

2386 Zaehle, S. and Friend, A. D.: Carbon and nitrogen cycle dynamics in the O-CN land surface  
2387 model: 1. Model description, site-scale evaluation, and sensitivity to parameter estimates,  
2388 *Global Biogeochem. Cycles*, 24(1), n/a-n/a, doi:10.1029/2009GB003521, 2010.

2389 Zaehle, S., Ciais, P., Friend, A. D. and Prieur, V.: Carbon benefits of anthropogenic reactive  
2390 nitrogen offset by nitrous oxide emissions, *Nat. Geosci.*, 4(9), 601–605,  
2391 doi:10.1038/ngeo1207, 2011.

2392 Zheng, B., Chevallier, F., Yin, Y., Ciais, P., Fortems-Cheiney, A., Deeter, M. N., Parker, R. J., Wang,  
2393 Y., Worden, H. M. and Zhao, Y.: Global atmospheric carbon monoxide budget 2000–2017  
2394 inferred from multi-species atmospheric inversions, *Earth Syst. Sci. Data*, 11(3), 1411–  
2395 1436, doi:10.5194/essd-11-1411-2019, 2019.

2396 Zscheischler, J., Mahecha, M. D., Avitabile, V., Calle, L., Carvalhais, N., Ciais, P., Gans, F., Gruber,  
2397 N., Hartmann, J., Herold, M., Ichii, K., Jung, M., Landschutzer, P., Laruelle, G. G., Lauerwald,  
2398 R., Papale, D., Peylin, P., Poulter, B., Ray, D., Regnier, P., Rödenbeck, C., Roman-Cuesta, R.  
2399 M., Schwalm, C., Tramontana, G., Tyukavina, A., Valentini, R., van der Werf, G., West, T. O.,  
2400 Wolf, J. E. and Reichstein, M.: Reviews and syntheses: An empirical spatiotemporal  
2401 description of the global surface-atmosphere carbon fluxes: opportunities and data  
2402 limitations, *Biogeosciences*, 14(15), 3685–3703, doi:10.5194/bg-14-3685-2017, 2017.

2403

2404

2405 **Tables**

2406  
2407

**Table 1.** Factors used to convert carbon in various units (by convention, Unit 1 = Unit 2 × conversion).

Unit 1	Unit 2	Conversion	Source
GtC (gigatonnes of carbon)	ppm (parts per million) <sup>a</sup>	2.124 <sup>b</sup>	Ballantyne et al. (2012)
GtC (gigatonnes of carbon)	PgC (petagrams of carbon)	1	SI unit conversion
GtCO <sub>2</sub> (gigatonnes of carbon dioxide)	GtC (gigatonnes of carbon)	3.664	44.01/12.011 in mass equivalent
GtC (gigatonnes of carbon)	MtC (megatonnes of carbon)	1000	SI unit conversion

<sup>a</sup> Measurements of atmospheric CO<sub>2</sub> concentration have units of dry-air mole fraction. ‘ppm’ is an abbreviation for micromole/mol, dry air.

<sup>b</sup>The use of a factor of 2.124 assumes that all the atmosphere is well mixed within one year. In reality, only the troposphere is well mixed and the growth rate of CO<sub>2</sub> concentration in the less well-mixed stratosphere is not measured by sites from the NOAA network. Using a factor of 2.124 makes the approximation that the growth rate of CO<sub>2</sub> concentration in the stratosphere equals that of the troposphere on a yearly basis.

2408  
2409

**Table 2.** How to cite the individual components of the global carbon budget presented here.

<b>Component</b>	<b>Primary reference</b>
Global fossil CO <sub>2</sub> emissions (E <sub>FF</sub> ), total and by fuel type	Gilfillan et al. (2019)
National territorial fossil CO <sub>2</sub> emissions (E <sub>FF</sub> )	CDIAC source: Gilfillan et al. (2019) UNFCCC (2019)
National consumption-based fossil CO <sub>2</sub> emissions (E <sub>FF</sub> ) by country (consumption)	Peters et al. (2011b) updated as described in this paper
Land-use change emissions (E <sub>LUC</sub> )	Average from Houghton and Nassikas (2017) and Hansis et al., (2015), both updated as described in this paper
Growth rate in atmospheric CO <sub>2</sub> concentration (G <sub>ATM</sub> )	Dlugokencky and Tans (2019)
Ocean and land CO <sub>2</sub> sinks (S <sub>OCEAN</sub> and S <sub>LAND</sub> )	This paper for S <sub>OCEAN</sub> and S <sub>LAND</sub> and references in Table 4 for individual models.

2410

**Table 3.** Main methodological changes in the global carbon budget since 2015. Methodological changes introduced in one year are kept for the following years unless noted. Empty cells mean there were no methodological changes introduced that year. Table A7 lists methodological changes from the first global carbon budget publication up to 2014.

Publication year	Fossil fuel emissions			LUC emissions	Reservoirs		Uncertainty & other changes	
	Global	Country (territorial)	Country (consumption)		Atmosphere	Ocean		Land
2015								
Le Quéré et al. (2015a)	Projection for current year based Jan-Aug data	National emissions from UNFCCC extended to 2014 also provided	Detailed estimates introduced for 2011 based on GTAP9					
Jackson et al. (2016)					Based on eight models	Based on ten models with assessment of minimum realism	The decadal uncertainty for the DGVM ensemble mean now uses $\pm 1\sigma$ of the decadal spread across models	
2016								
Le Quéré et al. (2016)	Two years of BP data	Added three small countries; China's (RMA) emissions from 1990 from BP data (this release only)		Preliminary $E_{LUC}$ using FRA-2015 shown for comparison; use of five DGVMs		Based on seven models	Based on fourteen models	Discussion of projection for full budget for current year
2017								
Le Quéré et al. (2018a) GCB2017	Projection includes India-specific data			Average of two bookkeeping models; use of twelve DGVMs		Based on eight models that match the observed sink for the 1990s; no longer normalised	Based on fifteen models that meet observation-based criteria (see Sect. 2.5)	Land multi-model average now used in main carbon budget, with the carbon imbalance presented separately; new table of key uncertainties

2018	Revision in cement emissions; Projection includes EU-specific data	Aggregation of overseas territories into governing nations for total of 213 countries a	Use of sixteen DGVMs	Use of four atmospheric inversions	Based on seven models	Based on sixteen models; revised atmospheric forcing from CRUNCEP to CRU-JRA-55	Introduction of metrics for evaluation of individual models using observations
2019	Global emissions calculated as sum of all countries plus bunkers, rather than taken directly from CDIAC.		Use of fifteen DGVMs (a)	Use of three atmospheric inversions	Based on nine models	Based on sixteen models	

(a) E<sub>LUC</sub> is still estimated based on bookkeeping models, as in 2018 (Le Quéré et al., 2018b), but the number of DGVMs used to characterise the uncertainty has changed.

**Table 4.** References for the process models, pCO<sub>2</sub>-based ocean flux products, and atmospheric inversions included in Figs. 6-8. All models and products are updated with new data to end of year 2018, and the atmospheric forcing for the DGVMs has been updated as described in Section 2.2.2.

Model/data name	Reference	Change from Global Carbon Budget 2018 (Le Quéré et al., 2018b)
<i>Bookkeeping models for land-use change emissions</i>		
BLUE	Hansis et al. (2015)	No change.
H&N2017	Houghton and Nassikas (2017)	No change.
<i>Dynamic global vegetation models</i>		
CABLE-POP	Haverd et al. (2018)	Thermal acclimation of photosynthesis; Residual stomatal conductance (g <sub>0</sub> ) now non-zero; stomatal conductance set to maximum of g <sub>0</sub> and vapour-pressure-deficit-dependent term
CLASS-CTEM	Melton and Arora (2016)	20 soil layers used. Soil depth is prescribed following Shangguan et al. (2017). - The bare soil evaporation efficiency was previously that of Lee and Pielke (1992). This has been replaced by that of Merlin et al. (2011). - Plant roots can no longer grow into soil layers that are perennially frozen (permafrost). - The V <sub>cmax</sub> value of C3 grass changes from 75 umol CO <sub>2</sub> /m <sup>2</sup> /s to 55 umol CO <sub>2</sub> /m <sup>2</sup> /s which is more in line with observations (Alton 2017) - Land use change product pools are now tracked separately (rather than thrown into litter and soil C pools). They behave the same as previously but now it is easier to distinguish the C in those pools from other soil/litter C.
CLM5.0	Lawrence et al. (2019)	Added representation of shifting cultivation, fixed a bug in the fire model, used updated & higher resolution lightning strike dataset
DLEM	Tian et al. (2015) (a)	No Change.
ISAM	Meiyappan et al. (2015)	No Change.
ISBA-CTRIP	Decharme et al. (2019) (b)	Updated spinup protocol + model name updated (SURFEXv8 in GCB2017)
JSBACH	Mauritsen et al. (2019)	No Change.
JULES-ES	Sellar et al., (2019) (c)	Major update. Model configuration is now JULES-ES v1.0, the land surface and vegetation component of the UK Earth System Model (UKESM1). Includes interactive Nitrogen scheme, extended number of plant functional types represented, trait based physiology and crop harvest.
LPJ-GUESS	Smith et al. (2014) (d)	Using daily climate forcing instead of monthly forcing. Using nitrogen inputs from NMIP. Adjustment in the spinup procedure. Growth suppression mortality parameter of PFT IBS changed to 0.12.
LPJ	Poulter et al. (2011) (e)	No Change.
LPX-Bern	Lienert and Joos (2018)	Using Nitrogen input from NMIP.

OCN	Zaehle and Friend (2010) (f)	No change (uses r294).
ORCHIDEE-CNP	Goll et al. (2017) (g)	Refinement of parameterization (r6176); change in N forcing (different N deposition, no (N & P) manure)
ORCHIDEE-Trunk	Krinner et al. (2005), Peylin et al. (in prep) (h)	No major changes, except some small bug corrections linked to the implementation of land cover changes
SDGVM	Walker et al. (2017) (i)	1) Changed the multiplicative scale parameters of these diagnostic output variables from: evapotranspft, evapo, transpft 2.257e6->2.257e6/(30*24*3600) swepft NA->0.001 2) The autotrophic respiration diagnostic output variable is now properly initialized to zero for bare ground. 3) A very minor change that prevents the soil water limitation scalar (often called beta) being applied to g0 in the stomatal conductance (gs) equation. Previously it was applied to both g0 and g1 in the gs equation. Now beta is applied only to g1 in the gs equation. 4) The climate driving data and land cover data are in 0.5degree resolution.
VISIT	Kato et al. (2013) (j)	No change.
<i>Global ocean biogeochemistry models</i>		
NEMO-PlankTOM5	Buitenhuis et al. (2013)	No change
MICOM-HAMOCC (NorESM-OC)	Schwinger et al. (2016)	Flux calculation improved to take into account correct land-sea mask after interpolation
MPIOM-HAMOCC6	Paulsen et al. (2017)	No change
NEMO3.6-PISCESv2-gas (CNRM)	Berthet et al. (2019)	No change
CSIRO	Law et al (2017)	No change
MITgcm-REcoM2	Hauck et al. (2018)	No change
MOM6-COBALT (Princeton)	Adcroft et al. (2019)	New this year
CESM-ETHZ	Doney et al. (2009)	New this year
NEMO-PISCES (IPSL)	Aumont et al. (2015)	updated spin-up procedure
<i>pCO<sub>2</sub>-based flux ocean products</i>		
Landschützer (MPI-SOMFFN)	Landschützer et al. (2016)	update to SOCATv2019 measurements
Rödenbeck (Jena-MLS)	Rödenbeck et al. (2014)	update to SOCATv2019 measurements. Interannual NEE variability estimated through a regression to air temperature anomalies. Using 89 atmospheric stations. Fossil fuel emissions taken from Jones et al (in prep) consistent with country totals of this study.

CMEMS	Denvil-Sommer et al. (2019)	New this year
<i>Atmospheric inversions</i>		
CAMS	Chevallier et al. (2005) (k)	Updated version of atmospheric transport model LMDz
CarbonTracker Europe (CTE)	van der Laan-Luijkx et al. (2017)	No change.
Jena CarboScope	Rödenbeck et al. (2003, 2018)	Temperature-NEE relations additionally estimated

a See also Tian et al. (2011)

b See also Joetzjer et al., (2015), Séférian et al. (2016) and Delire et al. (in review)

c JULES-ES is the Earth System configuration of the Joint UK Land Environment Simulator. See also Best et al. (2011) and Clarke et al. (2011).

d To account for the differences between the derivation of shortwave radiation from CRU cloudiness and DSWRF from CRUJRA, the photosynthesis scaling parameter  $\alpha$  was modified (-15%) to yield similar results.

e Compared to published version, decreased LPJ wood harvest efficiency so that 50 % of biomass was removed off-site compared to 85 % used in the 2012 budget. Residue management of managed grasslands increased so that 100 % of harvested grass enters the litter pool.

f See also Zaehle et al. (2011).

g see also Goll et al (2018).

h Compared to published version: revised parameters values for photosynthetic capacity for boreal forests (following assimilation of FLUXNET data), updated parameter values for stem allocation, maintenance respiration and biomass export for tropical forests (based on literature), and CO<sub>2</sub> down-regulation process added to photosynthesis. Hydrology model updated to a multi-layer scheme (11 layers). See also Peylin et al. (in prep)

i See also Woodward and Lomas (2004)

j See also Ito and Inatomi (2012).

k see also Remaud et al. (2018)

**Table 5.** Comparison of results from the bookkeeping method and budget residuals with results from the DGVMs and inverse estimates for different periods, the last decade, and the last year available. All values are in  $\text{GtCyr}^{-1}$ . The DGVM uncertainties represent  $\pm 1\sigma$  of the decadal or annual (for 2018 only) estimates from the individual DGVMs: for the inverse models the range of available results is given. All values are rounded to the nearest 0.1 GtC and therefore columns do not necessarily add to zero.

	Mean ( $\text{GtC yr}^{-1}$ )						
	1960-1969	1970-1979	1980-1989	1990-1999	2000-2009	2009-2018	2018
<i>Land-use change emissions (<math>E_{LUC}</math>)</i>							
Bookkeeping methods (1a)	$1.4 \pm 0.7$	$1.2 \pm 0.7$	$1.2 \pm 0.7$	$1.3 \pm 0.7$	$1.4 \pm 0.7$	$1.5 \pm 0.7$	$1.5 \pm 0.7$
DGVMs (1b)	$1.3 \pm 0.5$	$1.3 \pm 0.5$	$1.4 \pm 0.5$	$1.2 \pm 0.4$	$1.5 \pm 0.4$	$2.0 \pm 0.5$	$2.3 \pm 0.6$
<i>Terrestrial sink (<math>S_{LAND}</math>)</i>							
Residual sink from global budget ( $E_{FF} + E_{LUC} - G_{ATM} - S_{OCEAN}$ ) (2a)	$1.7 \pm 0.9$	$1.8 \pm 0.9$	$1.6 \pm 0.9$	$2.6 \pm 0.9$	$3.0 \pm 0.9$	$3.6 \pm 1.0$	$3.7 \pm 1.0$
DGVMs (2b)	$1.3 \pm 0.4$	$2.0 \pm 0.3$	$1.8 \pm 0.5$	$2.4 \pm 0.4$	$2.7 \pm 0.6$	$3.2 \pm 0.6$	$3.5 \pm 0.7$
<i>Total land fluxes (<math>S_{LAND} - E_{LUC}</math>)</i>							
GCB2019 Budget (2b - 1a)	$-0.2 \pm 0.8$	$0.9 \pm 0.8$	$0.6 \pm 0.9$	$1.0 \pm 0.8$	$1.3 \pm 0.9$	$1.7 \pm 0.9$	$2.0 \pm 1.0$
Budget constraint (2a - 1a)	$0.3 \pm 0.5$	$0.6 \pm 0.5$	$0.4 \pm 0.6$	$1.3 \pm 0.6$	$1.6 \pm 0.6$	$2.1 \pm 0.7$	$2.2 \pm 0.7$
DGVMs (2b - 1b)	$-0.1 \pm 0.5$	$0.7 \pm 0.6$	$0.4 \pm 0.6$	$1.2 \pm 0.6$	$1.1 \pm 0.6$	$1.0 \pm 0.8$	$1.0 \pm 0.8$
Inversions*	—	—	-0.1–0.1	0.5–1.1	0.7–1.5	1.1–2.2	0.9–2.7

\*Estimates are adjusted for the pre-industrial influence of river fluxes and adjusted to common  $E_{FF}$  (Sect. 2.7.2). The ranges given include 2 inversions from 1980-1999 and 3 inversions from 2001 onwards (Table A3).

**Table 6.** Decadal mean in the five components of the anthropogenic CO<sub>2</sub> budget for different periods, and last year available. All values are in GtC yr<sup>-1</sup>, and uncertainties are reported as ±1σ. The table also shows the budget imbalance (B<sub>IM</sub>), which provides a measure of the discrepancies among the nearly independent estimates and has an uncertainty exceeding ± 1 GtC yr<sup>-1</sup>. A positive imbalance means the emissions are overestimated and/or the sinks are too small. All values are rounded to the nearest 0.1 GtC and therefore columns do not necessarily add to zero.

	Mean (GtC yr <sup>-1</sup> )						2018
	1960-1969	1970-1979	1980-1989	1990-1999	2000-2009	2009-2018	
<i>Total emissions (E<sub>FF</sub>+E<sub>LUC</sub>)</i>							
Fossil CO <sub>2</sub> emissions (E <sub>FF</sub> )	3.0 ± 0.2	4.7 ± 0.2	5.5 ± 0.3	6.4 ± 0.3	7.8 ± 0.4	9.5 ± 0.5	10.0 ± 0.5
Land-use change emissions (E <sub>LUC</sub> )	1.4 ± 0.7	1.2 ± 0.7	1.2 ± 0.7	1.3 ± 0.7	1.4 ± 0.7	1.5 ± 0.7	1.5 ± 0.7
Total emissions	4.5 ± 0.7	5.8 ± 0.7	6.7 ± 0.8	7.7 ± 0.8	9.2 ± 0.8	11.0 ± 0.8	11.5 ± 0.9
<i>Partitioning</i>							
Growth rate in atmospheric CO <sub>2</sub> concentration (G <sub>ATM</sub> )	1.8 ± 0.07	2.8 ± 0.07	3.4 ± 0.02	3.1 ± 0.02	4.0 ± 0.02	4.9 ± 0.02	5.1 ± 0.2
Ocean sink (S <sub>OCEAN</sub> )	1.0 ± 0.6	1.3 ± 0.6	1.7 ± 0.6	2.0 ± 0.6	2.2 ± 0.6	2.5 ± 0.6	2.6 ± 0.6
Terrestrial sink (S <sub>LAND</sub> )	1.3 ± 0.4	2.0 ± 0.3	1.8 ± 0.5	2.4 ± 0.4	2.7 ± 0.6	3.2 ± 0.6	3.5 ± 0.7
<i>Budget imbalance</i>							
B <sub>IM</sub> = E <sub>FF</sub> +E <sub>LUC</sub> - (G <sub>ATM</sub> +S <sub>OCEAN</sub> +S <sub>LAND</sub> )	0.5	-0.2	-0.2	0.3	0.3	0.4	0.3

**Table 7.** Comparison of the projection with realised fossil CO<sub>2</sub> emissions ( $E_{FF}$ ). The ‘Actual’ values are first estimate available using actual data, and the ‘Projected’ values refers to estimate made before the end of the year for each publication. Projections based on a different method from that described here during 2008-2014 are available in Le Quéré et al., (2016). All values are adjusted for leap years.

	World		China		USA		EU28		India		Rest of World	
	Projected	Actual	Projected	Actual	Projected	Actual	Projected	Actual	Projected	Actual	Projected	Actual
2015 (a)	-0.6% (-1.6 to 0.5)	0.06%	-3.9% (-4.6 to -1.1)	-0.7%	-1.5% (-5.5 to 0.3)	-2.5%	-	-	-	-	1.2% (-0.2 to 2.6)	1.20%
2016 (b)	-0.2% (-1.0 to +1.8)	0.20%	-0.5% (-3.8 to +1.3)	-0.3%	-1.7% (-4.0 to +0.6)	-2.1%	-	-	-	-	1.0% (-0.4 to +2.5)	1.30%
2017 (c)	2.0% (+0.8 to +3.0)	1.60%	3.5% (+0.7 to +5.4)	1.50%	-0.4% (-2.7 to +1.0)	-0.5%	-	-	2.00% (+0.2 to +3.8)	3.90%	1.6% (0.0 to +3.2)	1.90%
2018 (d)	2.7% (+1.8 to +3.7)	2.13%	4.7% (+2.0 to +7.4)	2.30%	2.5% (+0.5 to +4.5)	2.76%	-0.7% (-2.6 to +1.3)	-2.08%	6.3% (+4.3 to +8.3)	8.02%	1.8% (+0.5 to +3.0)	1.69%
2019 (e)	0.5% (-0.3 to +1.4)	-	2.6% (+0.7 to +4.4)	-	-2.4% (-4.7 to -0.1)	-	-1.7% (-5.1% to +1.8%)	-	1.8% (-0.7 to +3.7)	-	0.5% (-0.8 to +1.8)	-

(a) Jackson et al. (2016) and Le Quéré et al. (2015a). (b) Le Quéré et al. (2016). (c) Le Quéré et al. (2018a). (d) Le Quéré et al. (2018b). (e) This study.

**Table 8.** Cumulative CO<sub>2</sub> for different time periods in gigatonnes of carbon (GtC). All uncertainties are reported as  $\pm 1\sigma$ . The budget imbalance provides a measure of the discrepancies among the nearly independent estimates. Its uncertainty exceeds  $\pm 60$  GtC. The method used here does not capture the loss of additional sink capacity from reduced forest cover, which is about 20 GtC for the years 1850-2018 and would exacerbate the budget imbalance (see Sect. 2.8.4). All values are rounded to the nearest 5 GtC and therefore columns do not necessarily add to zero.

Units of GtC	1750-2018	1850-2014	1959-2018	1850-2018	1850-2019 (a)
<i>Emissions</i>					
Fossil CO <sub>2</sub> emissions (E <sub>FF</sub> )	440 ± 20	400 ± 20	365 ± 20	440 ± 20	450 ± 20
Land-use change CO <sub>2</sub> emissions (E <sub>LUC</sub> )	235 ± 75 (b)	195 ± 60 (c)	80 ± 40 (d)	205 ± 60 (c)	205 ± 60
<b>Total emissions</b>	<b>675 ± 80</b>	<b>600 ± 65</b>	<b>445 ± 30</b>	<b>645 ± 65</b>	<b>655 ± 65</b>
<i>Partitioning</i>					
Growth rate in atmospheric CO <sub>2</sub> concentration (G <sub>ATM</sub> )	275 ± 5	235 ± 5	200 ± 5	255 ± 5	260 ± 5
Ocean sink (S <sub>OCEAN</sub> ) (e)	170 ± 20	150 ± 20	105 ± 20	160 ± 20	160 ± 20
Terrestrial sink (S <sub>LAND</sub> )	220 ± 50	185 ± 40	130 ± 25	195 ± 40	200 ± 40
<i>Budget imbalance</i>					
B <sub>IM</sub> = E <sub>FF</sub> +E <sub>LUC</sub> - (G <sub>ATM</sub> +S <sub>OCEAN</sub> +S <sub>LAND</sub> )	10	30	10	30	30

(a) Using projections for year 2019 (Sect. 3.4). Uncertainties are the same as 1850-2018 period

(b) Cumulative E<sub>LUC</sub> 1750-1849 of 30 GtC based on multi-model mean of Pongratz et al. (2009), Shevliakova et al. (2009), Zaehle et al. (2011), Van Minnen et al. (2009). 1850-2018 from mean of H&N (Houghton and Nassikas, 2017) and BLUE (Hansis et al., 2015). 1750-2018 uncertainty is estimated from standard deviation of DGVMs over 1850-2018 scaled by 1750-2018 emissions.

(c) Cumulative E<sub>LUC</sub> based on H&N and BLUE. Uncertainty is estimated from the standard deviation of DGVM estimates

(d) Cumulative E<sub>LUC</sub> based on H&N and BLUE. Uncertainty is formed from the uncertainty in annual E<sub>LUC</sub> over 1959-2018, which is 0.7 GtC/yr multiplied by length of the time series

e Ocean sink uncertainty from IPCC (Denman et al., 2007)

**Table 9.** Major known sources of uncertainties in each component of the Global Carbon Budget, defined as input data or processes that have a demonstrated effect of at least  $\pm 0.3 \text{ GtC yr}^{-1}$ .

Source of uncertainty	Time scale (years)	Location	Status	Evidence
<b>Fossil CO<sub>2</sub> emissions (E<sub>FF</sub>; section 2.1)</b>				
energy statistics	annual to decadal	Global, but mainly China & major developing countries	see Sect. 2.1	(Korsbakken et al., 2016)
carbon content of coal	annual to decadal	Global, but mainly China & major developing countries	see Sect. 2.1	(Liu et al., 2015)
System boundary	annual to decadal	All countries	see Sect. 2.1	
<b>Emissions from land-use change (E<sub>LUC</sub>; section 2.2)</b>				
land-cover and land-use change statistics	continuous	global; in particular tropics	see Sect. 2.2	(Houghton et al., 2012)
sub-grid-scale transitions	annual to decadal	global	see Table A1	(Wilkenskjeld et al., 2014)
vegetation biomass	annual to decadal	global; in particular tropics	see Table A1	(Houghton et al., 2012)
wood and crop harvest	annual to decadal	global; SE Asia	see Table A1	(Arneth et al., 2017)
peat burning (a)	multi-decadal trend	global	see Table A1	(van der Werf et al., 2010)
loss of additional sink capacity	multi-decadal trend	global	not included; Section 2.7.4	(Gitz and Ciais, 2003)
<b>Atmospheric growth rate (G<sub>ATM</sub>) no demonstrated uncertainties larger than <math>\pm 0.3 \text{ GtC yr}^{-1}</math> (b)</b>				
<b>Ocean sink (S<sub>OCEAN</sub>)</b>				
variability in oceanic circulation (c)	semi-decadal to decadal	global	see Sect. 2.4	(DeVries et al., 2017, 2019)
Internal variability	annual to decadal	high latitudes; Equatorial Pacific	no ensembles/ coarse resolution	(McKinley et al., 2016)
anthropogenic changes in nutrient supply	multi-decadal trend	global	not included	(Duce et al., 2008)
<b>Land sink (S<sub>LAND</sub>)</b>				
strength of CO <sub>2</sub> fertilisation	multi-decadal trend	global	see Sect. 2.5	(Wenzel et al., 2016)

response to variability in temperature and rainfall	annual to decadal	global; in particular tropics	see Sect. 2.5	(Cox et al., 2013)
nutrient limitation and supply	multi-decadal trend	global	see Sect. 2.5	(Zaehle et al., 2011)
response to diffuse radiation	annual	global	see Sect. 2.5	(Mercado et al., 2009)

---

a As result of interactions between land-use and climate

b The uncertainties in  $G_{ATM}$  have been estimated as  $\pm 0.2 \text{ GtC yr}^{-1}$ , although the conversion of the growth rate into a global annual flux assuming instantaneous mixing throughout the atmosphere introduces additional errors that have not yet been quantified.

c Could in part be due to uncertainties in atmospheric forcing (Swart et al., 2014)

## Appendix A. Supplementary tables.

**Table A1.** Comparison of the processes included in the bookkeeping method and DGVMs in their estimates of  $E_{LUC}$  and  $S_{LAND}$ . See Table 4 for model references. All models include deforestation and forest regrowth after abandonment of agriculture (or from afforestation activities on agricultural land). Processes relevant for  $E_{LUC}$  are only described for the DGVMs used with land-cover change in this study (Fig. 6 top panel).

	Bookkeeping Models		DGVMs															
	H&N	BLUE	CABLE-POP	CLASS-CTEM	CLM5.0	DLEM	ISAM	ISBA-CT RIP(h)	JSBACH	JULES-ES	LPJ-GUESS	LPJ	LPX-Bern	OCN	ORCHIDEE-CNP	ORCHIDEE-Trunk	SDGVM	VISIT
<b>Processes relevant for <math>E_{LUC}</math></b>																		
Wood harvest and forest degradation (a)	yes	yes	yes	no	yes	yes	yes	no	yes	no	yes	yes	no (d)	yes	no	yes	no	
Shifting cultivation / Subgrid scale transitions	no (b)	yes	yes	no	yes	no	no	no	yes	no	yes	yes	no (d)	no	no	no	no	
Cropland harvest (removed, r, or added to litter, l)	yes (r) (j)	yes (r) (j)	yes (r)	yes (added to litter)	yes (r)	yes	yes	no	yes (r+l)	no	yes (r)	yes (l)	yes (r)	yes (r+l)	yes (r)	yes	yes (r)	
Peat fires	yes	yes	no	no	yes	no	no	no	no	no	no	no	no	no	no	no	no	
fire as a management tool	yes (j)	yes (j)	no	no	no	no	no	no	no	no	no	no	no	no	no	no	no	
N fertilization	yes (j)	yes (j)	no	no	yes	yes	yes	no	no	no	yes	no	yes	yes	yes	no	no	
tillage	yes (j)	yes (j)	yes	yes (g)	no	no	no	no	no	no	yes	no	no	no	no	yes	no	
irrigation	yes (j)	yes (j)	no	no	yes	yes	yes	no	no	no	yes	no	no	no	no	no	no	
wetland drainage	yes (j)	yes (j)	no	no	no	no	no	no	no	no	no	no	no	no	no	no	no	
erosion	yes (j)	yes (j)	no	no	no	no	no	no	no	no	no	no	no	no	no	no	no	
South East Asia peat drainage	yes	yes	no	no	no	no	no	no	no	no	no	no	no	no	no	no	no	
Grazing and mowing Harvest (removed, r, or added to litter, l)	yes (r) (j)	yes (r) (j)	yes (r)	no	no	no	yes (l)	no	yes (l)	no	yes (r)	yes (l)	no	yes (r+l)	no	no	no	
<b>Processes also relevant for <math>S_{LAND}</math></b>																		

Fire simulation and/or suppression	for US only	no	no	yes	yes	yes	no	yes	yes	no	yes	yes	yes	no	no	no	yes	yes
Climate and variability	no	no	yes	yes	yes	yes	yes	yes	yes	yes	yes	yes	yes	yes	yes	yes	yes	yes
CO <sub>2</sub> fertilisation	no (i)	no (i)	yes	yes	yes	yes	yes	yes	yes	yes	yes	yes	yes	yes	yes	yes	yes	yes
Carbon-nitrogen interactions, including N deposition	no (j)	no (j)	yes	no (f)	yes	yes	yes	no (e)	yes	no	yes	no	yes	yes	yes	no	yes (c)	no

(a) Refers to the routine harvest of established managed forests rather than pools of harvested products.

(b) No back- and forth-transitions between vegetation types at the country-level, but if forest loss based on FRA exceeded agricultural expansion based on FAO, then this amount of area was cleared for cropland and the same amount of area of old croplands abandoned.

(c) Limited. Nitrogen uptake is simulated as a function of soil C, and Vcmax is an empirical function of canopy N. Does not consider N deposition.

(d) Available but not active.

(e) Simple parameterization of nitrogen limitation based on Yin (2002; assessed on FACE experiments)

(f) Although C-N cycle interactions are not represented, the model includes a parameterization of down-regulation of photosynthesis as CO<sub>2</sub> increases to emulate nutrient constraints (Arora et al., 2009)

(g) Tillage is represented over croplands by increased soil carbon decomposition rate and reduced humification of litter to soil carbon.

(h) ISBA-CTRIP corresponds to SURFEXv8 in GCB2018

(i) Bookkeeping models include effect of CO<sub>2</sub>-fertilization as captured by observed carbon densities, but not as an effect transient in time.

(j) Process captured implicitly by use of observed carbon densities.

**Table A2.** Comparison of the processes and model set up for the Global Ocean Biogeochemistry Models for their estimates of  $S_{OCEAN}$ . See Table 4 for model references.

	NEMO-PlankTOM5	MICOM-HAMOCC (NorESM-OC)	MPIOM-HAMOCC6	NEMO3.6-PISCESv2-gas (CNRM)	CSIRO	MITgcm-REcoM2	MOM6-COBALT (Princeton)	CESM-ETHZ	NEMO-PISCES (IPSL)
Atmospheric forcing for simulation A	NCEP	CORE-I (spin-up) / NCEP-R1 with CORE-II corrections	NCEP / NCEP+ERA-20C (spin-up)	NCEP with CORE-II corrections	JRA55	JRA-55, <a href="https://doi.org/10.5065/D6HH6H41">https://doi.org/10.5065/D6HH6H41</a>	JRA-55 version 1.4	JRA-55 version 1.3	JRA-55
Atmospheric forcing for simulation B (constant climate and CO <sub>2</sub> )	NCEP 1980	CORE-I	spin-up initial restart file (278) with cyclic 1957 NCEP; run 1957-2017 with 278	NCEP with CORE-II corrections cycling over 1948-1957	JRA55 1958	JRA climatology	JRA-55 version 1.4 year 1959	normal year forcing created from JRA-55 version 1.3, NYF = climatology with anomalies from the year 2001	interannual forcing JRA-55
Initialisation of carbon chemistry	GLODAPv1 corrected for anthropogenic carbon from Sabine et al (2004) to 1920	GLODAP v1 preindustrial + spin-up 1000 years	initialization from previous model simulations	GLODAPv2	GLODAPv1 preindustrial	GLODAPv1 preindustrial	GLODAPv2, DIC is corrected to 1959 level for the historical simulation and to pre-industrial level for the control simulation using Khatiwala et al 2009, 2013.	GLODAPv2 preindustrial	GLODAPv2 preindustrial
Spin-up procedure	Spin-up 39 years: 28 years (1920-1947) NCEP1980, followed by interannual forcing (in simulations A and D) from 1948	Initialisation from WOA/GLODAPv1 and 1000 years spin-up simulation using CORE-I (normal-year) forcing	spin-up with ERA20C	300 years online cycling over 1948-1957	Spin-up 300+ years BGC and 800 years for physics, historical carbon 1850-1957 (constant climate)	Spin-up 116 years (2 cycles JRA55), either with constant (278 ppm, RunB) or increasing (RunA) atm CO <sub>2</sub>	Spin-up 81 years using JRA-55 year 1959	Spin-up from initial conditions for 180 years, using CORE forcing and preindustrial atm. CO <sub>2</sub> and N cycle, switch to JRA forcing, additional 14 years spin-up with JRA forcing. Production run: starting from preindustrial spin-up, 3x cycling through JRA with historical forcing (simulation A) including time-varying N inputs, or normal year forcing, constant atm. CO <sub>2</sub> (simulation B).	Spin-up starting in 1836 with 3 loops of JRA forcing.
Physical ocean model	NEMOv2.3-ORCA2	MICOM (NorESM-OCv1.2)	MPIOM	NEMOv3.6-GELATOV6-eORCA1L75	MOM5	MITgcm (checkpoit 66k)	MOM6-SIS2	CESMv1.4 (ocean model based on POP2)	NEMO-v3.6
Biogeochemistry model	PlankTOM5.3	HAMOCC (NorESM-OCv1.2)	HAMOCC6	PISCESv2-gas	WOMBAT	REcoM-2	COBALTv2	BEC (modified & extended)	PISCESv2
Horizontal resolution	2o lon, 0.3 to 1.5o lat	1° lon, 0.17 to 0.25 lat	1.5°	1° lon, 0.3 to 1° lat	1° x1° with enhanced resolution at	2° lon, 0.38-2° lat,	0.5° lon, 0.25 to 0.5° lat	Lon: 1.125°, Lat varying from 0.53° in the	2° long, 0.3 to 1.5° lat

					the tropics and in the high lat Southern Ocean			extratropics to 0.27° near the equator	
Vertical resolution	31 levels	51 isopycnic layers + 2 layers representing a bulk mixed layer	40 levels, layer thickness increase with depth	75 levels, 1m at surface	50 levels, 20 in the upper 200m	30 levels (9 in the upper 200 m)	75 levels hybrid coordinates, 2 m at surface	60 levels (z-coordinates)	31 levels
Total ocean area on native grid (km <sup>2</sup> )	357200000	360060000	365980000	362700000	357640000	352050000	362000000	359260000	362700000

**Table A3.** Comparison of the inversion set up and input fields for the atmospheric inversions. Atmospheric inversions see the full CO<sub>2</sub> fluxes, including the anthropogenic and pre-industrial fluxes. Hence they need to be adjusted for the pre-industrial flux of CO<sub>2</sub> from the land to the ocean that is part of the natural carbon cycle before they can be compared with S<sub>OCEAN</sub> and S<sub>LAND</sub> from process models. See Table 4 for references.

	<b>CarbonTracker Europe (CTE)</b>	<b>Jena CarboScope</b>	<b>CAMS</b>
<b>Version number</b>	<b>CTE2019-FT</b>	<b>sEXTocNEET_v4.3</b>	<b>v18r2</b>
<b>Observations</b>			
Atmospheric observations	Hourly resolution (well-mixed conditions) obspack GLOBALVIEWplus v4.2 and NRT_v4.4 (a)	Flasks and hourly (outliers removed by 2-sigma criterion)	Daily averages of well-mixed conditions - OBSPACK GLOBALVIEWplus v4.2a& NRT v4.4, WDCGG, RAMCES and ICOS ATC
<b>Prior fluxes</b>			
Biosphere and fires	SIBCASA-GFED4s (b)	No prior	ORCHIDEE (climatological), GFEDv4.1 & GFAS
Ocean	Ocean inversion by Jacobson et al. (2007)	oc_v1.7 updates: from 1993, interannual variability from PlankTOM5 (Buitenhuis et al) GOBM; before 1985, linear transition over the years in between (update of Rödenbeck et al., 2014)	Landschützer et al. (2018)
Fossil fuels	EDGAR+IER, scaled to GCP2018 and GCP2019	Jones et al. (in prep.) - EDGAR scaled nationally and by fuel type to GCP2019	EDGAR scaled to GCP2019
<b>Transport and optimization</b>			
Transport model	TM5	TM3	LMDZ v6A
Weather forcing	ECMWF	NCEP	ECMWF
Resolution (degrees)	Global: 3° x 2°, Europe: 1° x 1°, North America: 1° x 1°	Global: 4° x 5°	Global: 3.75° x 1.875°
Optimization	Ensemble Kalman filter	Conjugate gradient (re-ortho-normalization) (c)	Variational

a (GLOBALVIEW, 2018; Carbontracker Team, 2017)

b (van der Velde et al., 2014)

c ocean prior not optimised

**Table A4.** Attribution of fCO<sub>2</sub> measurements for the year 2018 included in SOCATv2019 (Bakker et al., 2016) to inform ocean pCO<sub>2</sub>-based flux products.

Platform	Regions	No. of samples	Principal Investigators	No. of data sets	Platform Type
AkzoNobel	North Atlantic; Southern Ocean	553	Tanhua, T.; Gutekunst, S.	1	Ship
Allure of the Seas	Tropical Atlantic	118652	Wanninkhof, R.; Pierrot, D.	50	Ship
Aurora Australis	Southern Ocean	59586	Tilbrook, B.	3	Ship
Bjarni Saemundsson	North Atlantic	7938	Benoit-Cattin-Breton, A.; Ólafsdóttir, S.R.	1	Ship
Cap Blanche	Southern Ocean; Tropical Pacific	28554	Cosca, C.; Alin, S.; Feely, R.; Herndon, J.; Collins A.	5	Ship
Cap San Lorenzo	Tropical Atlantic	16071	Lefèvre, N.	4	Ship
Colibri	North Atlantic; Tropical Atlantic	6541	Lefèvre, N.	1	Ship
Equinox	Tropical Atlantic	119384	Wanninkhof, R.; Pierrot, D.	48	Ship
F.G. Walton Smith	North Atlantic	2830	Millero, F.; Wanninkhof, R.	2	Ship
Finnmaid	North Atlantic	135597	Rehder, G.; Glockzin, M.	9	Ship
G.O. Sars	North Atlantic	105172	Skjelvan, I.	11	Ship
Gordon Gunter	North Atlantic	73634	Wanninkhof, R.; Pierrot, D.	12	Ship
Henry B. Bigelow	North Atlantic	64935	Wanninkhof, R.; Pierrot, D.	14	Ship
Heron Island	Tropical Pacific	3631	Tilbrook, B.	2	Mooring
Investigator	Southern Ocean	88217	Tilbrook, B.	6	Ship
Isabu	North Pacific	2350	Park, G.-H.	1	Ship
Kangaroo Island	Southern Ocean	4016	Tilbrook, B.	2	Mooring
Laurence M. Gould	Southern Ocean	28666	Sweeney, C.; Takahashi, T.; Newberger, T.; Sutherland, S.C.; Munro, D.R.	5	Ship
Maria Island	Southern Ocean	4015	Tilbrook, B.	2	Mooring
Marion Dufresne	Southern Ocean; Indian	6796	Lo Monaco, C.; Metzl, N.	1	Ship
New Century 2	North Pacific; Tropical Pacific; North Atlantic	33316	Nakaoka, S.-I.	14	Ship
Nuka Arctica	North Atlantic	143430	Becker, M.; Olsen, A.	23	Ship
Ronald H. Brown	North Atlantic; Tropical Pacific	28239	Wanninkhof, R.; Pierrot, D.	5	Ship
Simon Stevin	North Atlantic	33760	Gkritzalis, T.	8	Ship
Soyo Maru	North Pacific	91491	Ono, T.	5	Ship
Station M	North Atlantic	1313	Skjelvan, I.; Lauvset, S. K.	1	Mooring
Tangaroa	Southern Ocean	136893	Currie, K.I.	8	Ship
Trans Carrier	North Atlantic	12966	Omar, A. M.; Johannessen, T.	1	Ship
Trans Future 5	North Pacific; Tropical Pacific; Southern Ocean	27856	Nakaoka, S.-I.; Nojiri, Y.	19	Ship
Turn the Tide on Plastic	North Atlantic; Tropical Atlantic; Southern Ocean; Tropical Pacific	13043	Gutekunst, S.	1	Ship
Wakmatha	Tropical Pacific	25457	Tilbrook, B.	8	Ship

**Table A5.** Funding supporting the production of the various components of the global carbon budget in addition to the authors' supporting institutions (see also acknowledgements).

<b>Funder and grant number (where relevant)</b>	<b>Author Initials</b>
Australia, Integrated Marine Observing System (IMOS)	BT, CN
Australian Government as part of the Antarctic Science Collaboration Initiative program	AL
Australian Government National Environment Science Program (NESP)	JGC, VH
Belgium Research Foundation – Flanders (FWO) (grant number UA C130206-18)	TG
BNP Paribas Foundation through Climate & Biodiversity initiative, philanthropic grant for developments of the Global Carbon Atlas	PC, AP
BONUS INTEGRAL	GR
EC Copernicus Atmosphere Monitoring Service implemented by ECMWF	FC
EC Copernicus Marine Environment Monitoring Service implemented by Mercator Ocean	MG
EC H2020 (AtlantOS: grant no 633211)	SV, MG
EC H2020 (CCiCC; grant no 821003)	PF, RMA, SS, GPP, MOS, JIK, SL, NG, PL
EC H2020 (CHE; grant no 776186)	MWJ
EC H2020 (CRESCENDO: grant no. 641816)	RS, EJ
EC H2020 European Research Council (ERC) Synergy grant (IMBALANCE-P; grant no. ERC-2013-SyG-610028)	DSG
EC H2020 ERC (QUINCY; grant no. 647204)	SZ
EC H2020 (RINGO: grant no. 730944)	DB
EC H2020 project (VERIFY: grant no. 776810)	CLQ, GPP, JIK, RMA, MWJ, PC
European Space Agency Climate Change Initiative ESA-CCI RECCAP2 project 655 (ESRIN/4000123002/18/I-NB)	PF, PC, SS, MOS
French Institut National des Sciences de l'Univers (INSU) and Institut Pau- Emile Victor (IPEV), Sorbonne Universités (OSU Ecce-Terra)	NM
French Institut de Recherche pour le Développement (IRD)	NL
French Integrated Carbon Observation System (ICOS) France Océan;	NL
German Integrated Carbon Observation System (ICOS), Federal Ministry for Education and Research (BMBF);	GR
German Future Ocean (grant number CP1756)	SG
German Helmholtz Association in its ATMO programme	PA
German Helmholtz Association Innovation and Network Fund (VH-NG-1301)	JH
German Research Foundation's Emmy Noether Programme (grant no. PO1751/1-1)	JP
Japan Ministry of the Environment (grant number E1432)	TO
Japan Global Environmental Research Coordination System, Ministry of the Environment (grant number E1751)	SN
Netherlands Organization for Scientific Research (NWO; Ruisdael Infrastructure)	NS
Norwegian Research Council (grant no. 270061)	JS
Norwegian ICOS Norway and OTC Research Infrastructure Project, Research Council of Norway (grant number 245927)	SV, MB, AO
New Zealand, NIWA SSIF Funding	KC
Swiss National Science Foundation (grant no. 200020_172476)	SL
UK Natural Environment Research Council (SONATA: grant no. NE/P021417/1)	ETB
UK Newton Fund, Met Office Climate Science for Service Partnership Brazil (CSSP Brazil)	AW, ER
UK Royal Society (grant no RP\R1\191063)	CLQ
USA Department of Agriculture, National Institute of Food and Agriculture (grants no. 2015-67003-23489 and 2015-67003-23485)	DLL

USA Department of Commerce, NOAA/OAR's Global Observations and Monitoring of the Oceans Program	RF
USA Department of Commerce, NOAA/OAR's Ocean Observations and Monitoring Division (grant number 100007298);	LB, DP
USA Department of Commerce, NOAA/OAR's Ocean Acidification Program	DP, LB
USA Department of Energy, Office of Science and BER prg. (grant no. DE-SC000 0016323)	ATJ
USA Department of Energy, SciDac award number is DESC0012972; IDS grant award number is 80NSSC17K0348	LC, GH
USA CIMAS, a Cooperative Institute of the University of Miami and the National Oceanic and Atmospheric Administration (cooperative agreement NA10OAR4320143)	DP, LB
USA NASA Interdisciplinary Research in Earth Science Program.	BP
US National Science Foundation (grant number 1461590)	JOK
US National Science Foundation (grant number 1903722)	HT
US National Science Foundation (grant number PLR-1543457)	DM
USA Princeton University Environmental Institute and the NASA OCO2 science team, grant number 80NSSC18K0893.	LR
<b>Computing resources</b>	
Norway UNINETT Sigma2, National Infrastructure for High Performance Computing and Data Storage in Norway (NN2980K/NS2980K)	JS
Japan National Institute for Environmental Studies computational resources	EK
TGCC under allocation 2018-A0050102201" made by GENCI	FC
UK Centre for Environmental Data Analysis (CEDA) JASMIN Super-data-cluster	PCM
Supercomputing time was provided by the Météo-France/DSI supercomputing center.	RS, EJ
CarbonTracker Europe was supported by the Netherlands Organization for Scientific Research (NWO; grant no. SH-312, 17616)	WP, NS
Deutsches Klimarechenzentrum (allocation bm0891)	JEMSN, JP
PRACE for awarding access to JOLIOT CURIE at GENCI@CEA, France	LB
<b>Support for aircraft measurements in Obspack</b>	
L. V. Gatti, M. Gloor, J.B. Miller: AMAZONICA consortium project was funded by NERC (NE/F005806/1), FAPESP (08/58120-3), GEOCARBON project (283080)	
The CESM project is supported primarily by the National Science Foundation (NSF). This material is based upon work supported by the National Center for Atmospheric Research, which is a major facility sponsored by the NSF under Cooperative Agreement No. 1852977. Computing and data storage resources, including the Cheyenne supercomputer (doi:10.5065/D6RX99HX), were provided by the Computational and Information Systems Laboratory (CISL) at NCAR. We thank all the scientists, software engineers, and administrators who contributed to the development of CESM2.	DLL

**Table A6.** Aircraft measurement programs archived by Cooperative Global Atmospheric Data Integration Project (CGADIP, 2019) that contribute to the evaluation of the atmospheric inversions (Figure B3).

Measurement program name in Obspack	Specific doi	Data providers
Alta Floresta		Gatti, L.V.; Gloor, E.; Miller, J.B.;
Aircraft Observation of Atmospheric trace gases by JMA		ghg_obs@met.kishou.go.jp
Beaver Crossing, Nebraska		Sweeney, C.; Dlugokencky, E.J.
Bradgate, Iowa		Sweeney, C.; Dlugokencky, E.J.
Briggsdale, Colorado		Sweeney, C.; Dlugokencky, E.J.
Cape May, New Jersey		Sweeney, C.; Dlugokencky, E.J.
CONTRAIL (Comprehensive Observation Network for TRace gases by AirLiner)	<a href="http://dx.doi.org/10.17595/20180208.001">http://dx.doi.org/10.17595/20180208.001</a>	Machida, T.; Matsueda, H.; Sawa, Y. Niwa, Y.
Carbon in Arctic Reservoirs Vulnerability Experiment (CARVE)		Sweeney, C.; Karion, A.; Miller, J.B.; Miller, C.E.; Dlugokencky, E.J.
Dahlen, North Dakota		Sweeney, C.; Dlugokencky, E.J.
Estevan Point, British Columbia		Sweeney, C.; Dlugokencky, E.J.
East Trout Lake, Saskatchewan		Sweeney, C.; Dlugokencky, E.J.
Fairchild, Wisconsin		Sweeney, C.; Dlugokencky, E.J.
Molokai Island, Hawaii		Sweeney, C.; Dlugokencky, E.J.
Homer, Illinois		Sweeney, C.; Dlugokencky, E.J.
HIPPO (HIAPER Pole-to-Pole Observations)	<a href="https://doi.org/10.3334/CDIAC/HIPPO_010">https://doi.org/10.3334/CDIAC/HIPPO_010</a>	Wofsy, S.C.; Stephens, B.B.; Elkins, J.W.; Hints, E.J.; Moore, F.
INFLUX (Indianapolis Flux Experiment)		Sweeney, C.; Dlugokencky, E.J.; Shepson, P.B.; Turnbull, J.
NASA Goddard Space Flight Center Aircraft Campaign		Kawa, S.R.; Abshire, J.B.; Riris, H.
Park Falls, Wisconsin		Sweeney, C.; Dlugokencky, E.J.
Offshore Corpus Christi, Texas		Sweeney, C.; Dlugokencky, E.J.
Offshore Portsmouth, New Hampshire (Isles of Shoals)		Sweeney, C.; Dlugokencky, E.J.
Oglesby, Illinois		Sweeney, C.; Dlugokencky, E.J.
Poker Flat, Alaska		Sweeney, C.; Dlugokencky, E.J.
Rio Branco		Gatti, L.V.; Gloor, E.; Miller, J.B.
Rarotonga		Sweeney, C.; Dlugokencky, E.J.
Santarem		Sweeney, C.; Dlugokencky, E.J.
Charleston, South Carolina		Sweeney, C.; Dlugokencky, E.J.
Southern Great Plains, Oklahoma		Sweeney, C.; Dlugokencky, E.J.; Biraud, S.
Harvard University Aircraft Campaign		Wofsy, S.C.
Tabatinga		Gatti, L.V.; Gloor, E.; Miller, J.B.
Trinidad Head, California		Sweeney, C.; Dlugokencky, E.J.
West Branch, Iowa		Sweeney, C.; Dlugokencky, E.J.

**Table A7.** Main methodological changes in the global carbon budget from first publication until 2014. Post-2014 methodological changes are presented in Table 3. Methodological changes introduced in one year are kept for the following years unless noted. Empty cells mean there were no methodological changes introduced that year.

Publication year	Fossil fuel emissions			LUC emissions	Reservoirs		Uncertainty & other changes
	Global	Country (territorial)	Country (consumption)		Atmosphere	Ocean	
2006 (a)		Split in regions					
2007 (b)				$E_{LUC}$ based on FAO-FRA 2005; constant $E_{LUC}$ for 2006	1959-1979 data from Mauna Loa; data after 1980 from global average	Based on one ocean model tuned to reproduced observed 1990s sink	$\pm 1\sigma$ provided for all components
2008 (c)				Constant $E_{LUC}$ for 2007			
2009 (d)		Split between Annex B and non-Annex B	Results from an independent study discussed	Fire-based emission anomalies used for 2006-2008		Based on four ocean models normalised to observations with constant delta	First use of five DGVMs to compare with budget residual
2010 (e)	Projection for current year based on GDP	Emissions for top emitters		$E_{LUC}$ updated with FAO-FRA 2010			
2011 (f)			Split between Annex B and non-Annex B				
2012 (g)		129 countries from 1959	129 countries and regions from 1990-2010 based on GTAP8.0	$E_{LUC}$ for 1997-2011 includes interannual anomalies from fire-based emissions	All years from global average	Based on 5 ocean models normalised to observations with ratio	Ten DGVMs available for $S_{LAND}$ ; First use of four models to compare with $E_{LUC}$
2013 (h)		250 countries	134 countries and regions 1990-2011 based on GTAP8.1, with detailed estimates for years 1997, 2001, 2004, and 2007	$E_{LUC}$ for 2012 estimated from 2001-2010 average		Based on six models compared with two data-products to year 2011	Coordinated DGVM experiments for $S_{LAND}$ and $E_{LUC}$
2014 (i)	Three years of BP data	Three years of BP data	Extended to 2012 with updated GDP data	$E_{LUC}$ for 1997-2013 includes		Based on seven models	Based on ten models
							Confidence levels; cumulative emissions; budget from 1750
							Inclusion of breakdown of

---

interannual  
anomalies from  
fire-based  
emissions

the sinks in three  
latitude bands  
and comparison  
with three  
atmospheric  
inversions

---

a Raupach et al. (2007)

b Canadell et al. (2007)

c Online

d Le Quéré et al. (2009)

e Friedlingstein et al. (2010)

f Peters et al. (2012b)

g Le Quéré et al. (2013), Peters et al. (2013)

h Le Quéré et al. (2014)

i Le Quéré et al. (2015b)

## Figure Captions

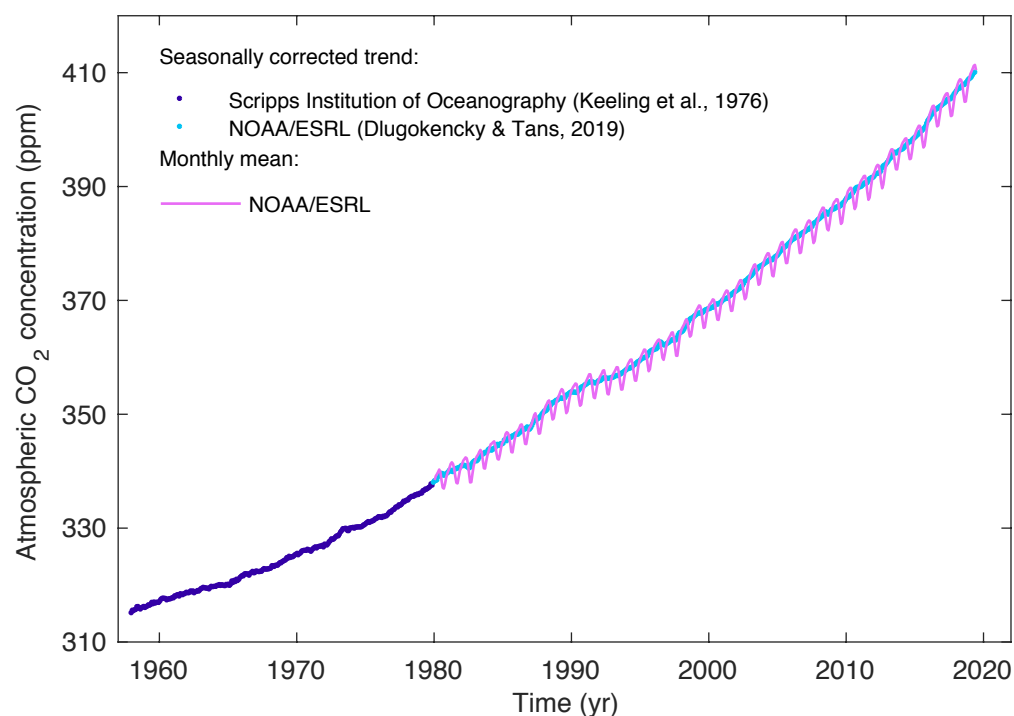


**Figure 1.** Surface average atmospheric CO<sub>2</sub> concentration (ppm). The 1980-2018 monthly data are from NOAA/ESRL (Dlugokencky and Tans, 2019) and are based on an average of direct atmospheric CO<sub>2</sub> measurements from multiple stations in the marine boundary layer (Masarie and Tans, 1995). The 1958-1979 monthly data are from the Scripps Institution of Oceanography, based on an average of direct atmospheric CO<sub>2</sub> measurements from the Mauna Loa and South Pole stations (Keeling et al., 1976). To take into account the difference of mean CO<sub>2</sub> and seasonality between the NOAA/ESRL and the Scripps station networks used here, the Scripps surface average (from two stations) was deseasonalised and harmonised to match the NOAA/ESRL surface average (from multiple stations) by adding the mean difference of 0.542 ppm, calculated here from overlapping data during 1980-2012.

# The global carbon cycle

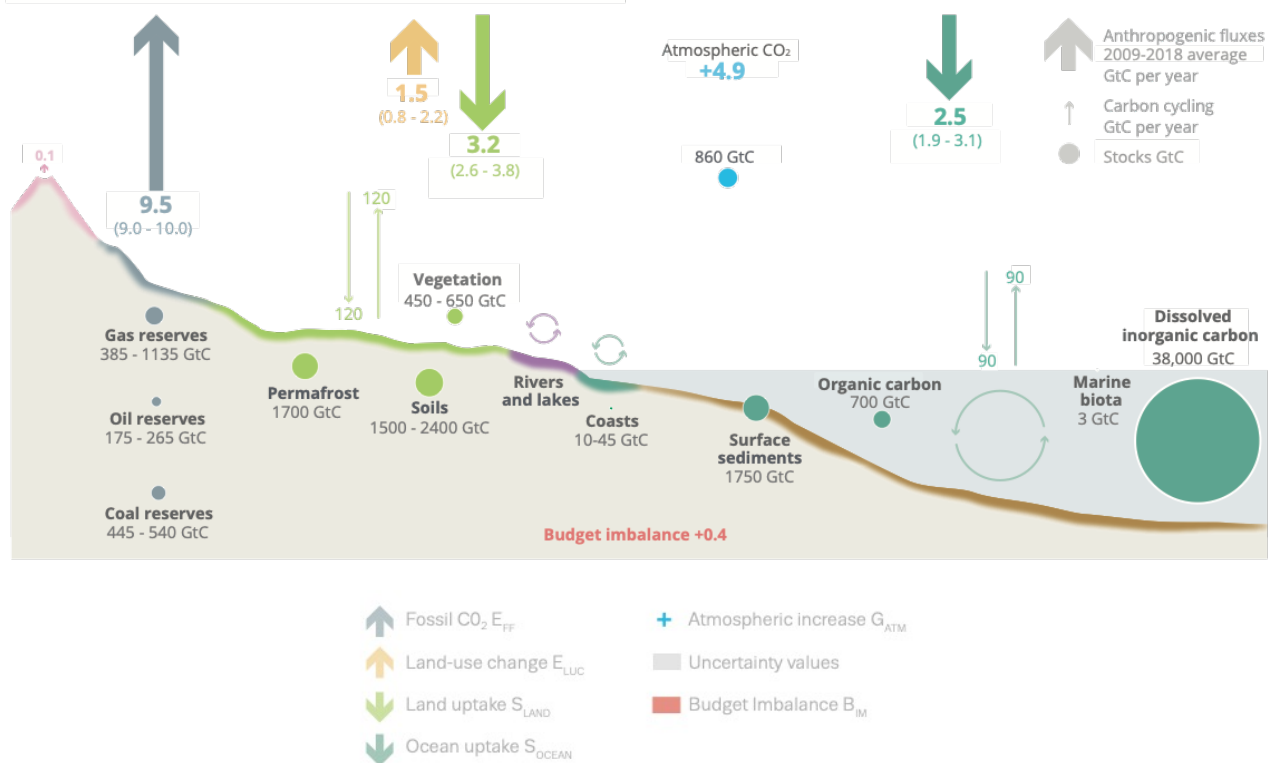


**Figure 2.** Schematic representation of the overall perturbation of the global carbon cycle caused by anthropogenic activities, averaged globally for the decade 2009-2018. See legends for the corresponding arrows and units. The uncertainty in the atmospheric CO<sub>2</sub> growth rate is very small ( $\pm 0.02$  Gt C yr<sup>-1</sup>) and is neglected for the figure. The anthropogenic perturbation occurs on top of an active carbon cycle, with fluxes and stocks represented in the background and taken from Ciais et al. (2013) for all numbers, with the ocean gross fluxes updated to 90 GtC yr<sup>-1</sup> to account for the increase in atmospheric CO<sub>2</sub> since publication, and except for the carbon stocks in coasts which is from a literature review of coastal marine sediments (Price and Warren, 2016).

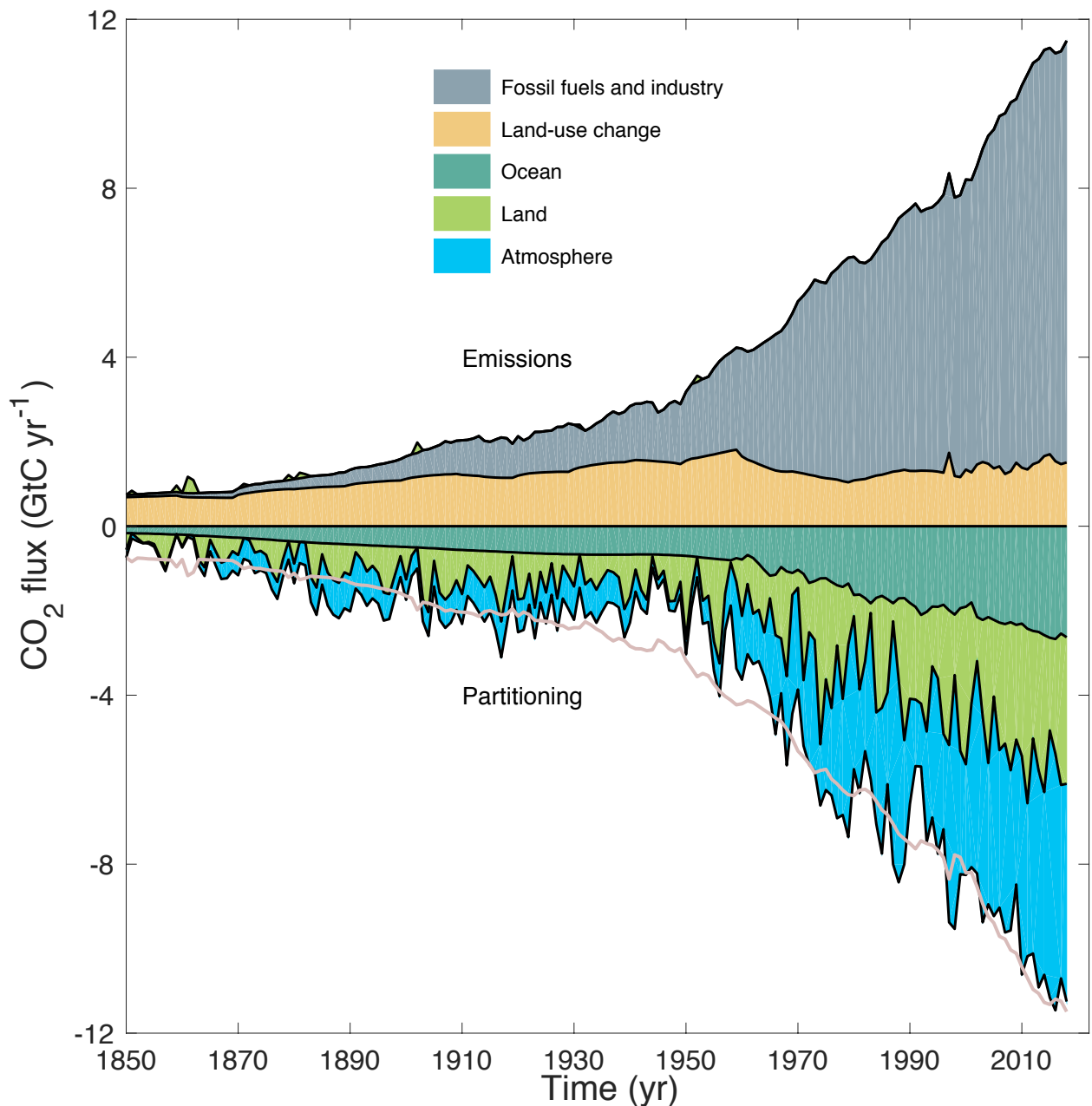


**Figure 3.** Combined components of the global carbon budget illustrated in Fig. 2 as a function of time, for fossil CO<sub>2</sub> emissions ( $E_{FF}$ ; grey) and emissions from land-use change ( $E_{LUC}$ ; brown), as well as their partitioning among the atmosphere ( $G_{ATM}$ ; blue), ocean ( $S_{OCEAN}$ ; turquoise), and land ( $S_{LAND}$ ; green). The partitioning is based on nearly independent estimates from observations (for  $G_{ATM}$ ) and from process model ensembles constrained by data (for  $S_{OCEAN}$  and  $S_{LAND}$ ), and does not exactly add up to the sum of the emissions, resulting in a budget imbalance which is represented by the difference between the bottom pink line (reflecting total emissions) and the sum of the ocean, land and atmosphere. All time series are in GtC yr<sup>-1</sup>.  $G_{ATM}$  and  $S_{OCEAN}$  prior to 1959 are based on different methods.  $E_{FF}$  are primarily from (Gilfillan et al.

2019), with uncertainty of about  $\pm 5\%$  ( $\pm 1\sigma$ );  $E_{LUC}$  are from two bookkeeping models (Table 2) with uncertainties of about  $\pm 50\%$ ;  $G_{ATM}$  prior to 1959 is from Joos and Spahni (2008) with uncertainties equivalent to about  $\pm 0.1-0.15 \text{ GtC yr}^{-1}$ , and from Dlugokencky and Tans (2019) from 1959 with uncertainties of about  $\pm 0.2 \text{ GtC yr}^{-1}$ ;  $S_{OCEAN}$  prior to 1959 is averaged from Khatiwala et al. (2013) and DeVries (2014) with uncertainty of about  $\pm 30\%$ , and from a multi-model mean (Table 4) from 1959 with uncertainties of about  $\pm 0.5 \text{ GtC yr}^{-1}$ ;  $S_{LAND}$  is a multi-model mean (Table 4) with uncertainties of about  $\pm 0.9 \text{ GtC yr}^{-1}$ . See the text for more details of each component and their uncertainties.

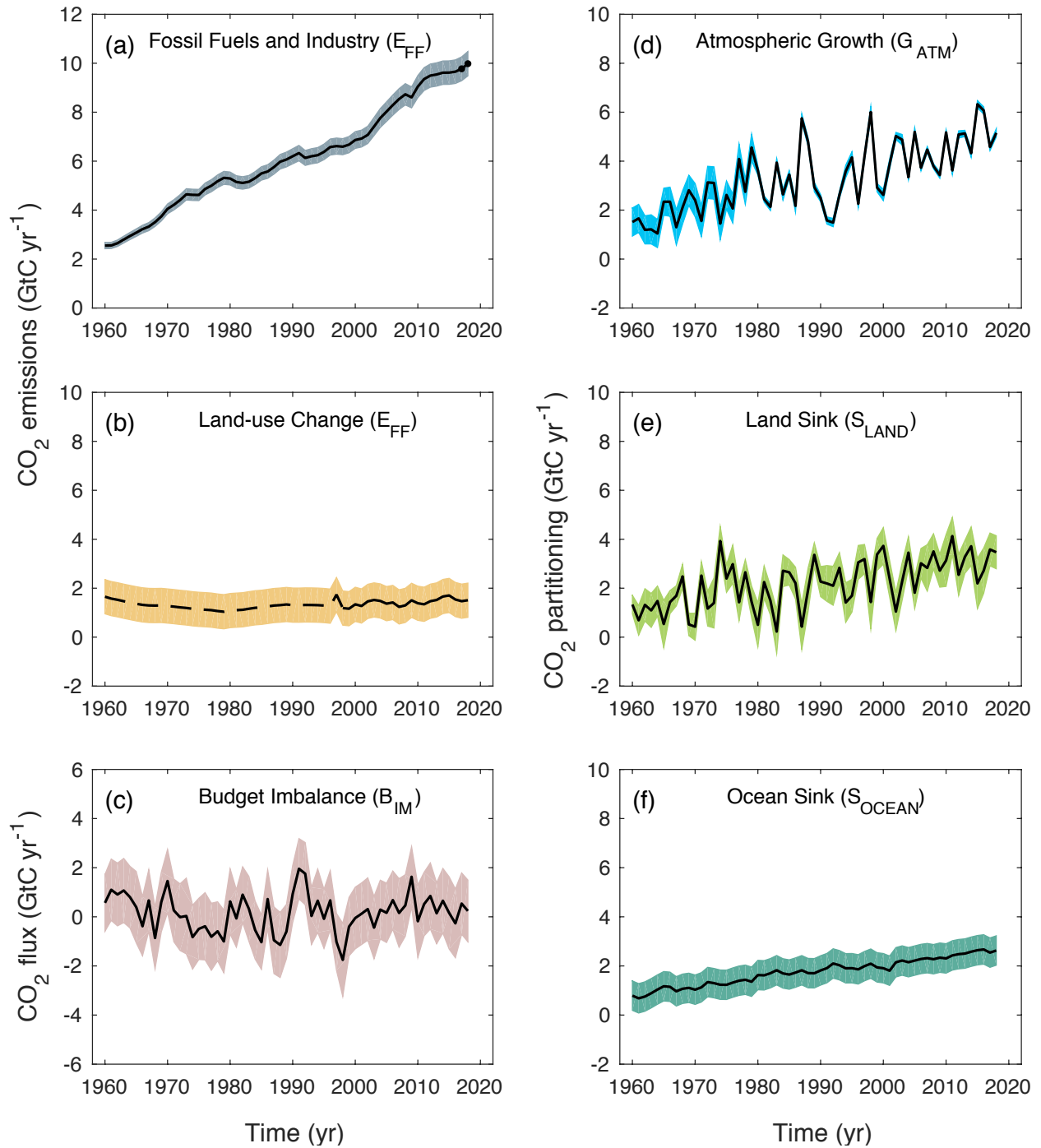


**Figure 4.** Components of the global carbon budget and their uncertainties as a function of time, presented individually for **(a)** fossil CO<sub>2</sub> emissions ( $E_{FF}$ ), **(b)** emissions from land-use change ( $E_{LUC}$ ), **(c)** the budget imbalance that is not accounted for by the other terms, **(d)** growth rate in atmospheric CO<sub>2</sub> concentration ( $G_{ATM}$ ), and **(e)** the land CO<sub>2</sub> sink ( $S_{LAND}$ , positive indicates a flux from the atmosphere to the land), **(f)** the ocean CO<sub>2</sub> sink ( $S_{OCEAN}$ , positive indicates a flux from the atmosphere to the ocean). All time series are in GtC yr<sup>-1</sup> with the uncertainty bounds representing  $\pm 1\sigma$  in shaded colour. Data sources are as in Fig. 3. The black dots in **(a)** show

values for 2017-2018 that originate from a different data set to the remainder of the data (see text). The dashed line in **(b)** identifies the pre-satellite period before the inclusion of emissions from peatland burning.

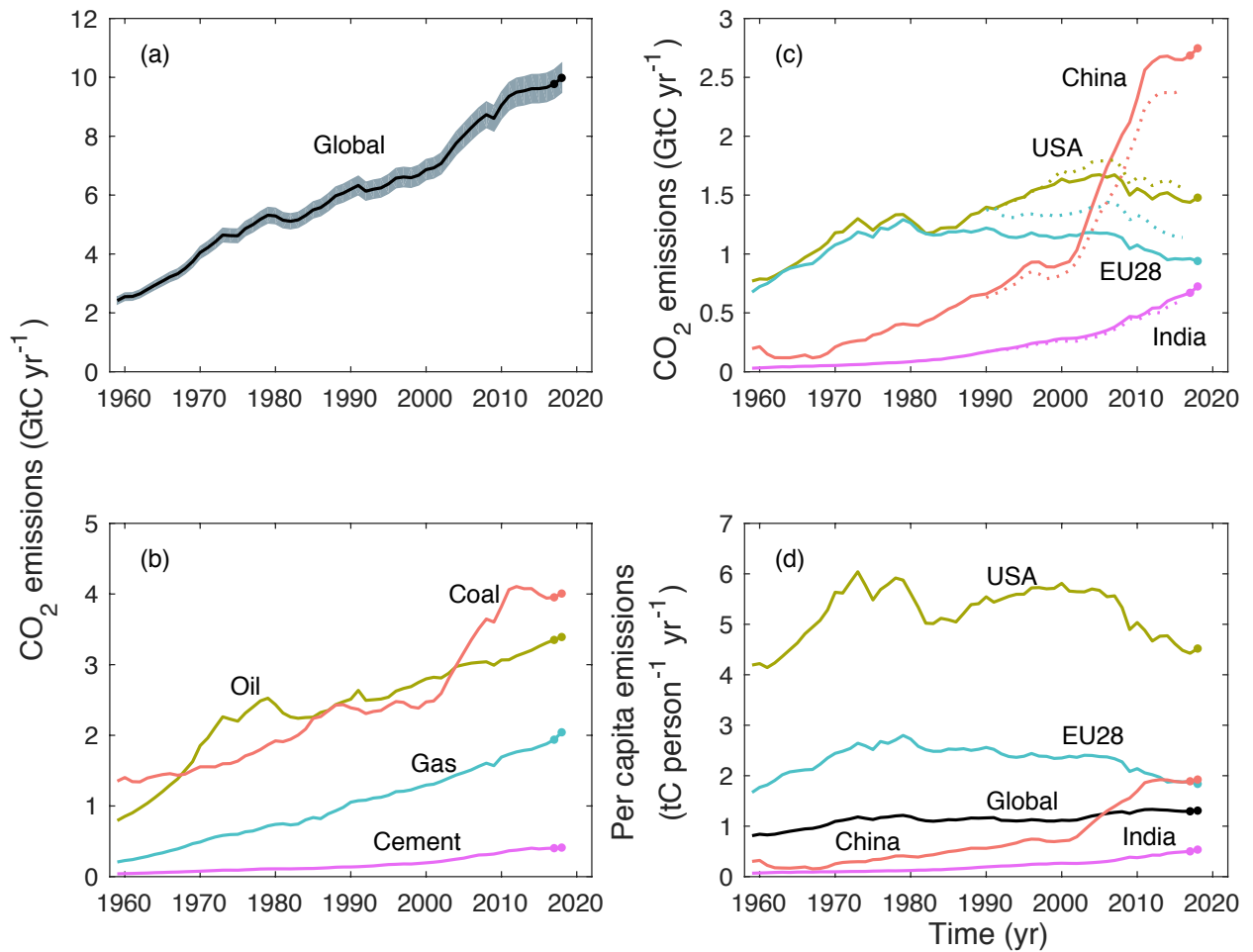


**Figure 5.** Fossil CO<sub>2</sub> emissions for **(a)** the globe, including an uncertainty of  $\pm 5\%$  (grey shading), and the emissions extrapolated using BP energy statistics (black dots), **(b)** global emissions by fuel type, including coal (salmon), oil (olive), gas (turquoise), and cement (purple), and excluding gas flaring which is small (0.6% in 2013), **(c)** territorial (solid lines) and consumption (dashed lines) emissions for the top three country emitters (USA - olive; China - salmon; India - purple) and for the European Union (EU; turquoise for the 28 member states of the EU as of 2012), and **(d)** per-capita emissions for the top three country emitters and the EU (all colours as in panel **(c)**) and the world (black). In **(b-c)**, the dots show the data that were extrapolated from BP energy statistics for 2017-2018. All time series are in GtC yr<sup>-1</sup> except the per-capita emissions **(d)**, which are in tonnes of carbon per person per year (tC person<sup>-1</sup> yr<sup>-1</sup>). Territorial emissions are primarily from Gilfillan et al. (2019) except national data for the USA and EU28 (the 28 member states of the EU) for 1990-2017, which are reported by the countries to the UNFCCC as detailed in the text; consumption-based emissions are updated from Peters et al. (2011a). See Section 2.1.1 for details of the calculations and data sources.

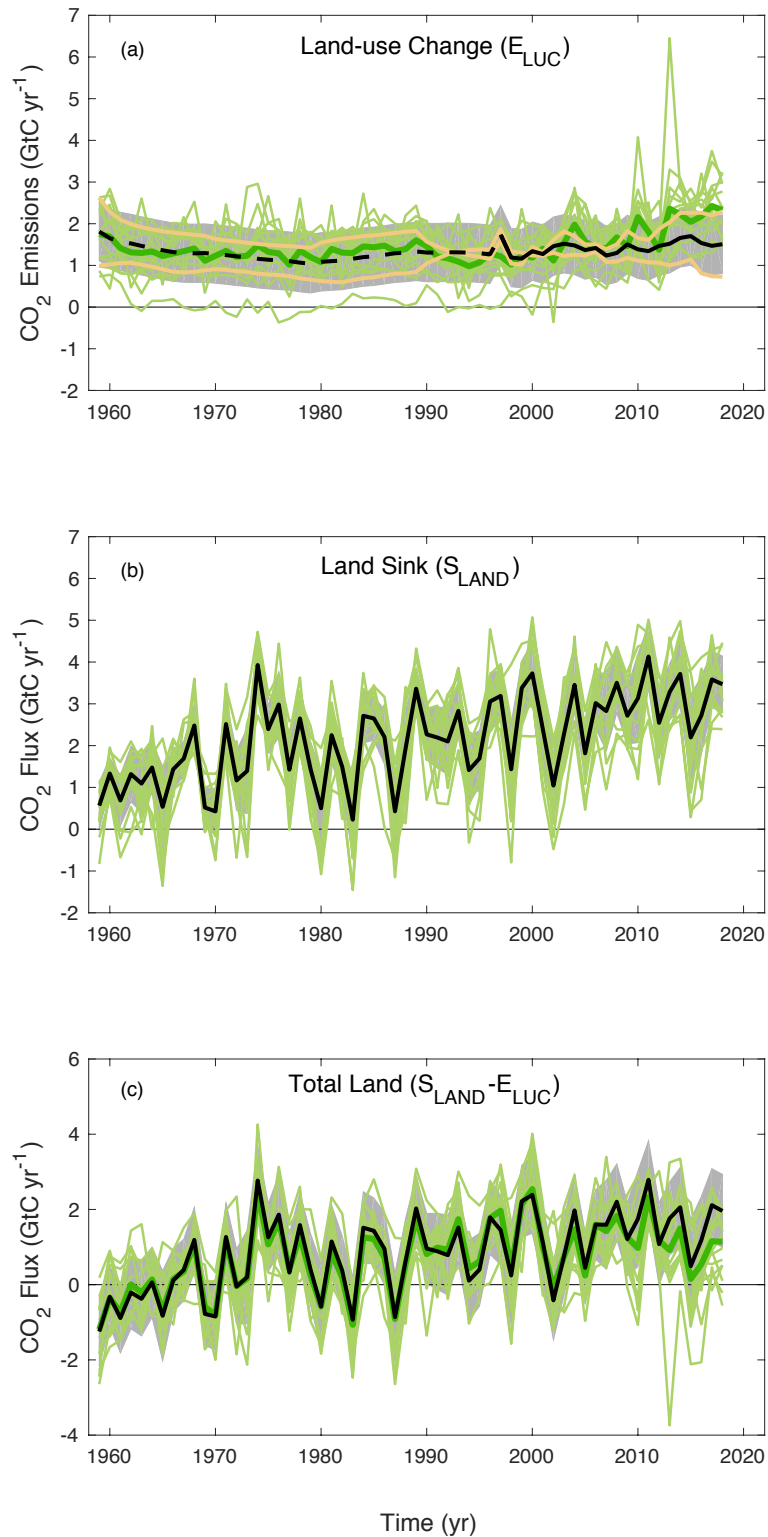


**Figure 6.** CO<sub>2</sub> exchanges between the atmosphere and the terrestrial biosphere as used in the global carbon budget (black with  $\pm 1\sigma$  uncertainty in grey shading), for **(a)** CO<sub>2</sub> emissions from land-use change ( $E_{LUC}$ ), showing also individually the two bookkeeping models (two brown lines) and the DGVM model results (green) and their multi-model mean (dark green). The dashed line identifies the pre-satellite period before the inclusion of peatland burning; **(b)** Land

CO<sub>2</sub> sink ( $S_{\text{LAND}}$ ) with individual DGVMs (green); **(c)** Total land CO<sub>2</sub> fluxes (**b minus a**) with individual DGVMs (green) and their multi-model mean (dark green).

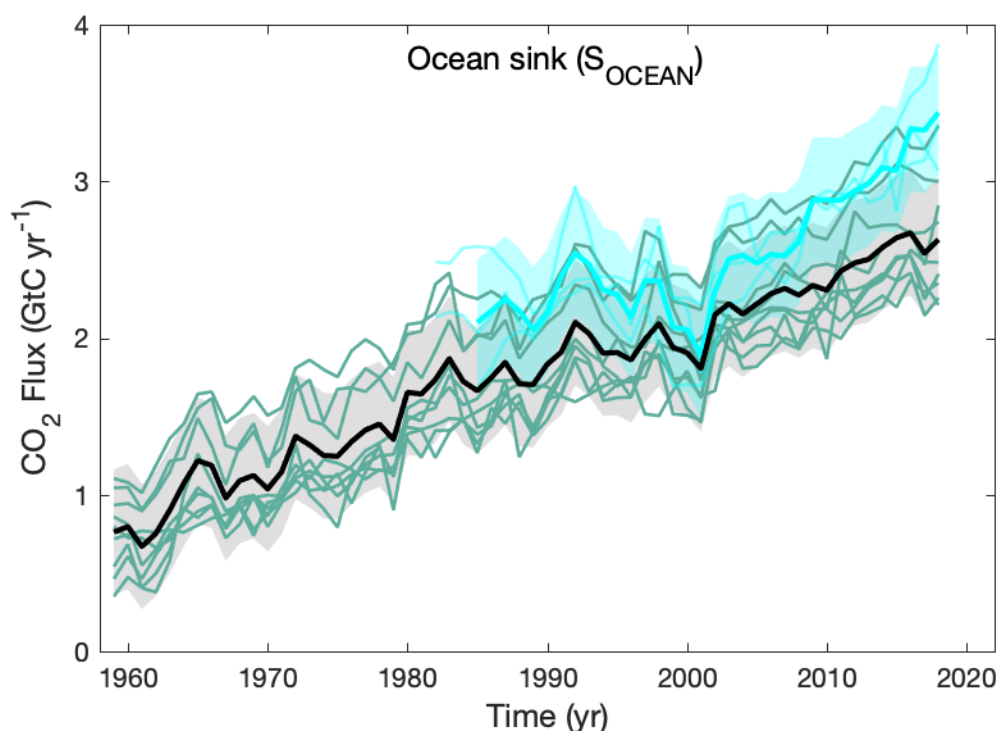


**Figure 7.** Comparison of the anthropogenic atmosphere-ocean CO<sub>2</sub> flux showing the budget values of  $S_{\text{OCEAN}}$  (black; with  $\pm 1\sigma$  uncertainty in grey shading), individual ocean models (teal), and the three ocean pCO<sub>2</sub>-based flux products (light blue; with  $\pm 1\sigma$  uncertainty in light blue shading see Table 4). The pCO<sub>2</sub>-based flux products were adjusted for the pre-industrial ocean source of CO<sub>2</sub> from river input to the ocean, which is not present in the ocean models, by adding a sink of 0.78 GtC yr<sup>-1</sup> (Resplandy et al., 2018), to make them comparable to  $S_{\text{OCEAN}}$ . This adjustment does not take into account the anthropogenic contribution to river fluxes (see Section 2.7.3)

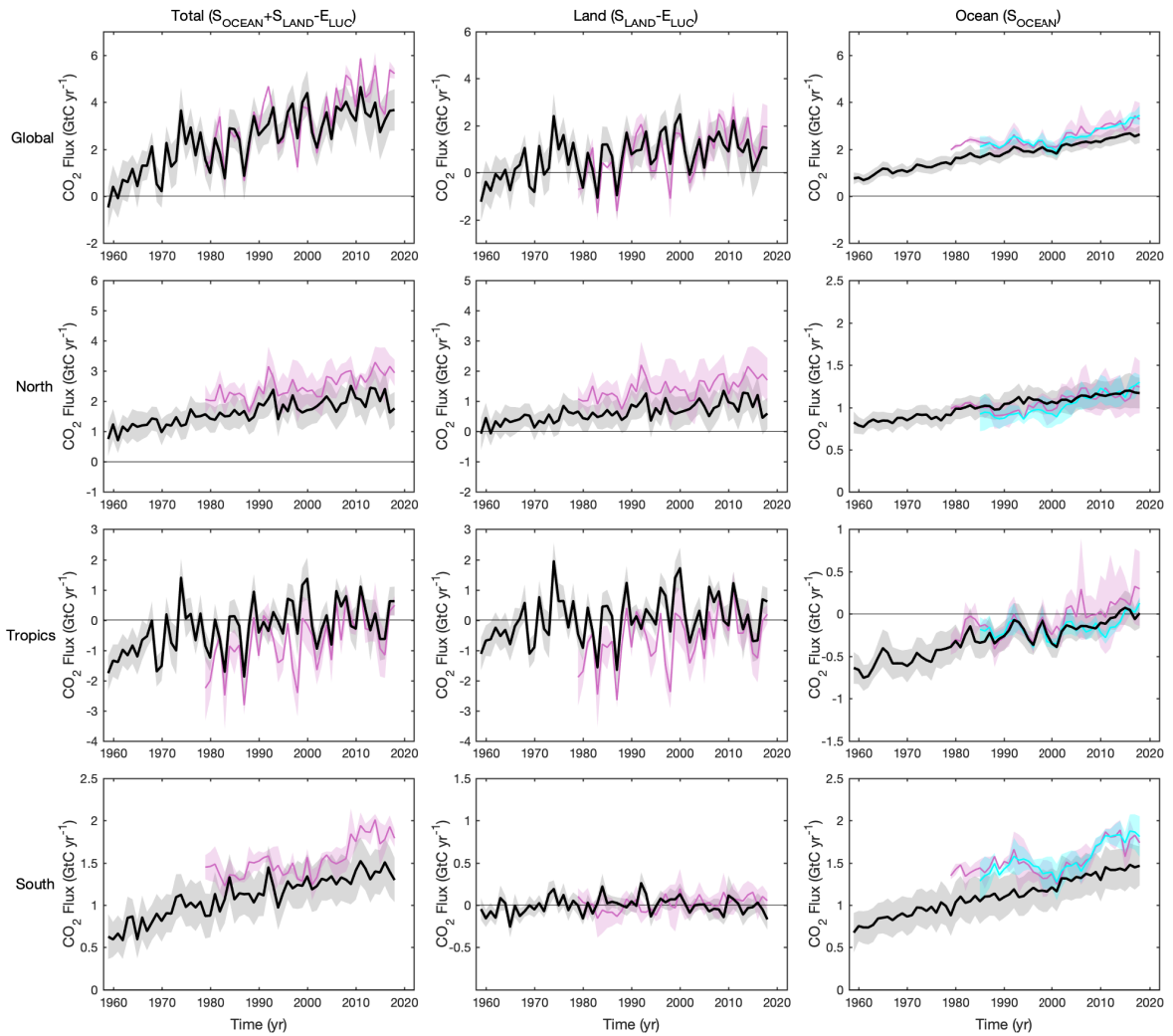


**Figure 8.** CO<sub>2</sub> fluxes between the atmosphere and the surface,  $S_{\text{OCEAN}}$  and  $(S_{\text{LAND}} - E_{\text{LUC}})$  by latitude bands for the (top) globe, (2<sup>nd</sup> row) north (north of 30°N), (3<sup>rd</sup> row) tropics (30°S-30°N), and (bottom) south (south of 30°S), and over (left) total ( $S_{\text{OCEAN}} + S_{\text{LAND}} - E_{\text{LUC}}$ ), (middle) land only ( $S_{\text{LAND}} - E_{\text{LUC}}$ ) and (right) ocean only ( $S_{\text{OCEAN}}$ ). Positive values indicate a flux from the atmosphere to the land and/or ocean. Mean estimates from the combination of the process models for the land and oceans are shown (black line) with  $\pm 1\sigma$  of the model ensemble (grey shading). For total uncertainty, the land and ocean uncertainties are summed in quadrature. Mean estimates from the atmospheric inversions are shown (pink lines) with their  $\pm 1\sigma$  spread (pink shading). Mean estimates from the pCO<sub>2</sub>-based flux products are shown for the ocean domain (cyan lines) with their  $\pm 1\sigma$  spread (cyan shading). The global  $S_{\text{OCEAN}}$  (upper right) and the

sum of  $S_{\text{OCEAN}}$  in all three regions represents the anthropogenic atmosphere-to-ocean flux based on the assumption that the preindustrial ocean sink was  $0 \text{ GtC yr}^{-1}$  when riverine fluxes are not considered. This assumption does not hold on the regional level, where preindustrial fluxes can be significantly different from zero. Hence, the regional panels for  $S_{\text{OCEAN}}$  represent a combination of natural and anthropogenic fluxes. Bias-correction and area-weighting were only applied to global  $S_{\text{OCEAN}}$ , hence the sum of the regions is slightly different from the global estimate ( $<0.05 \text{ GtC yr}^{-1}$ ).

# Anthropogenic carbon flows

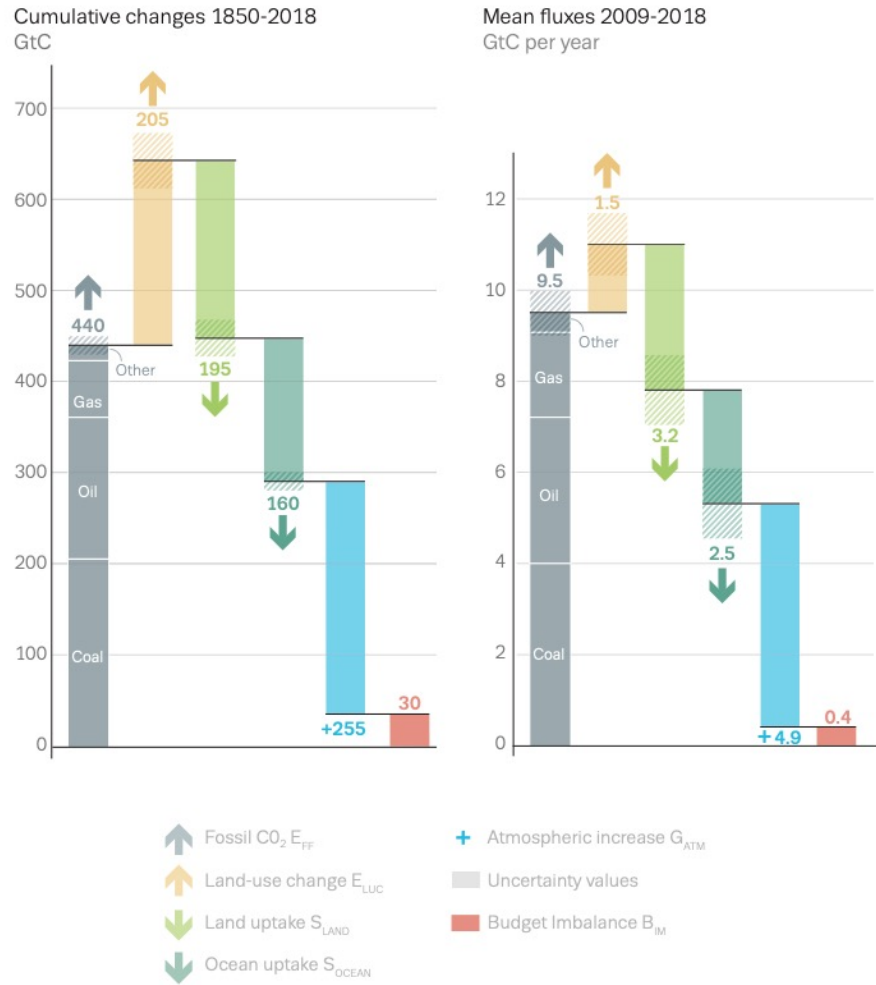


**Figure 9.** Cumulative changes during 1850-2018 and mean fluxes during 2009-2018 for the anthropogenic perturbation as defined in the legend.

## Appendix B. Supplementary figures.

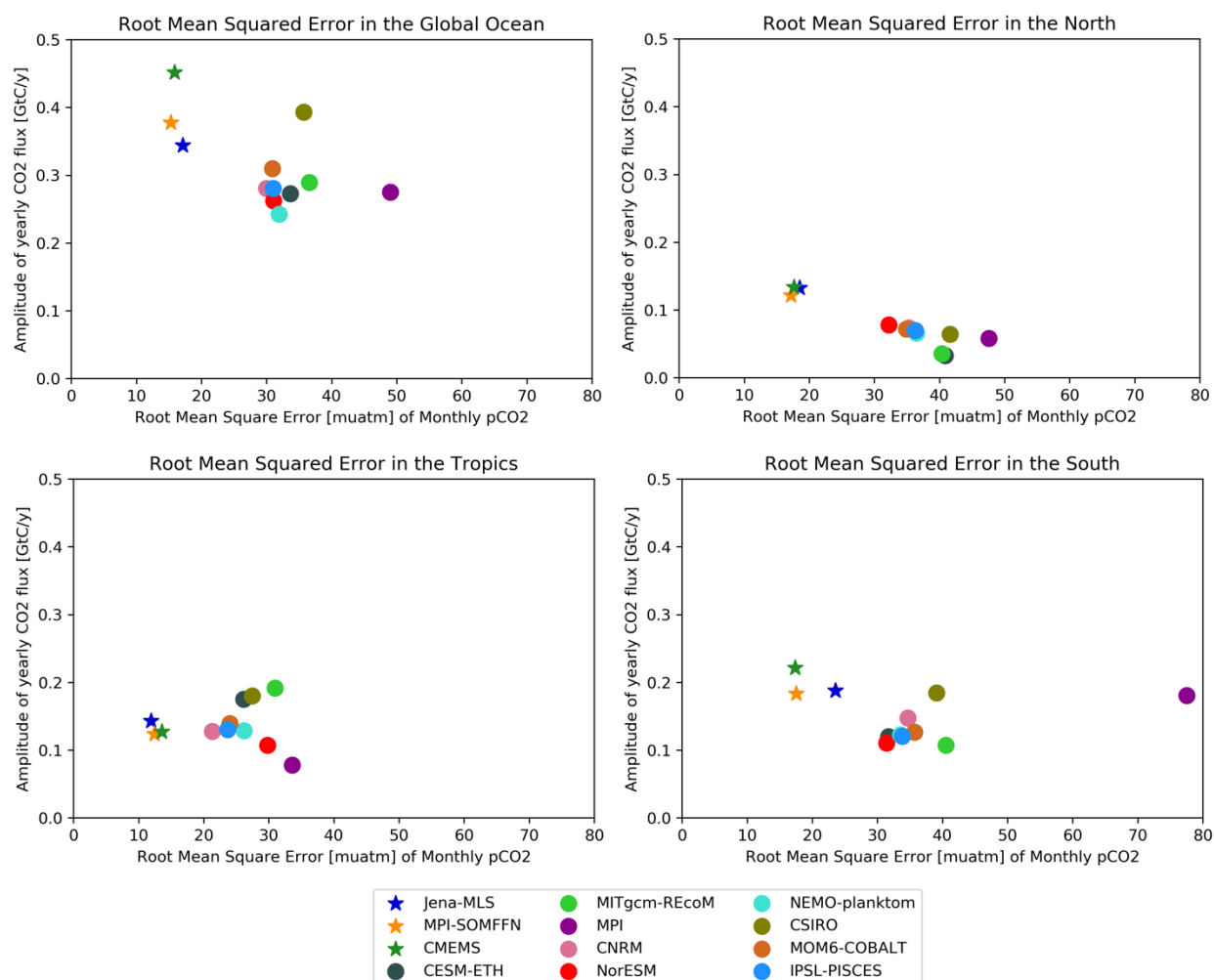


**Figure B1.** Evaluation of the GOBMs and flux products using the root mean squared error (RMSE) for the period 1985 to 2018, between the individual surface ocean pCO<sub>2</sub> estimates and the SOCAT v2019 database. The y-axis shows the amplitude of the interannual variability (A-IAV, taken as the standard deviation of a 12-months running mean over the monthly flux time-series, Rödenbeck et al., 2015). Results are presented for the globe, north (>30°N), tropics (30°S-30°N), and south (<30°S) for the GOBMs (circles) and for the pCO<sub>2</sub>-based flux products (star symbols). The three pCO<sub>2</sub>-based flux products use the SOCAT database and therefore are not fully independent from the data (see section 2.4.1).

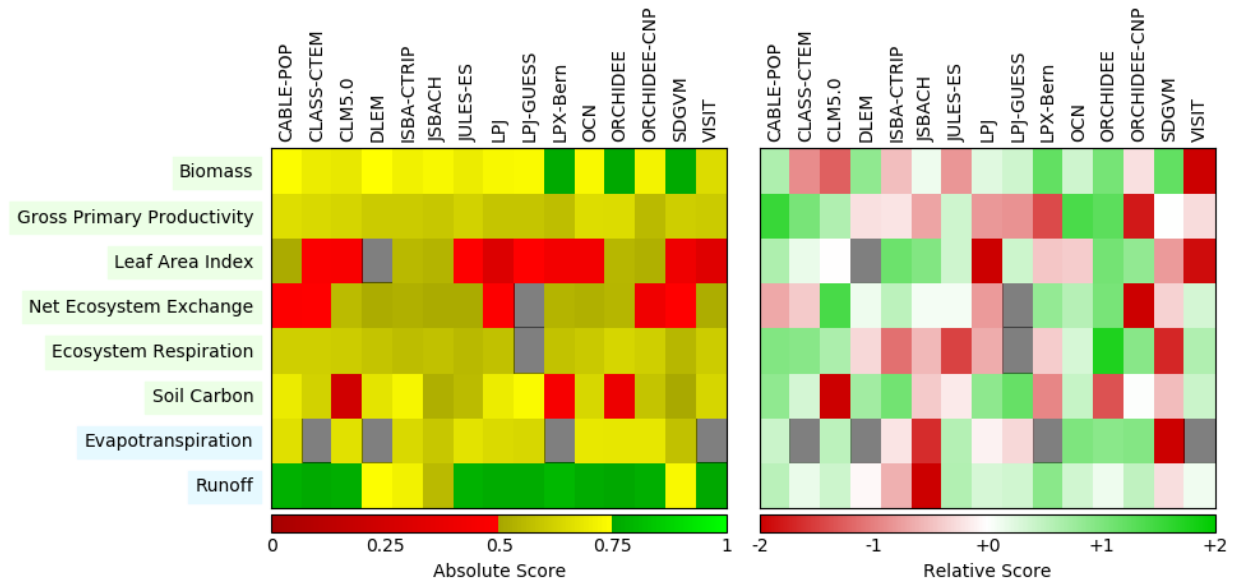


**Figure B2.** Evaluation of the DGVM using the International Land Model Benchmarking system (ILAMB; Collier et al., 2018) (left) absolute skill scores and (right) skill scores relative to other models. The benchmarking is done with observations for vegetation biomass (Saatchi et al., 2011; and GlobalCarbon unpublished data; Avitabile et al., 2016), GPP (Jung et al., 2010; Lasslop et al., 2010), leaf area index (De Kauwe et al., 2011; Myneni et al., 1997), net ecosystem exchange (Jung et al., 2010; Lasslop et al., 2010), ecosystem respiration (Jung et al., 2010; Lasslop et al., 2010), soil carbon (Hugelius et al., 2013; Todd-Brown et al., 2013), evapotranspiration (De Kauwe et al., 2011), and runoff (Dai and Trenberth, 2002). For each model-observation comparison a series of error metrics are calculated, scores are then calculated as an exponential function of each error metric, finally for each variable the multiple scores from different metrics and observational data sets are combined to give the overall variable scores shown in the left panel. Overall variable scores increase from 0 to 1 with improvements in model performance. The set of error metrics vary with data set and can include metrics based on the period mean, bias, root mean squared error, spatial distribution, interannual variability and seasonal cycle. The relative skill score shown in the right panel is a Z-score, which indicates in units of standard deviation the model scores relative to the multi-model mean score for a given variable. Grey boxes represent missing model data.

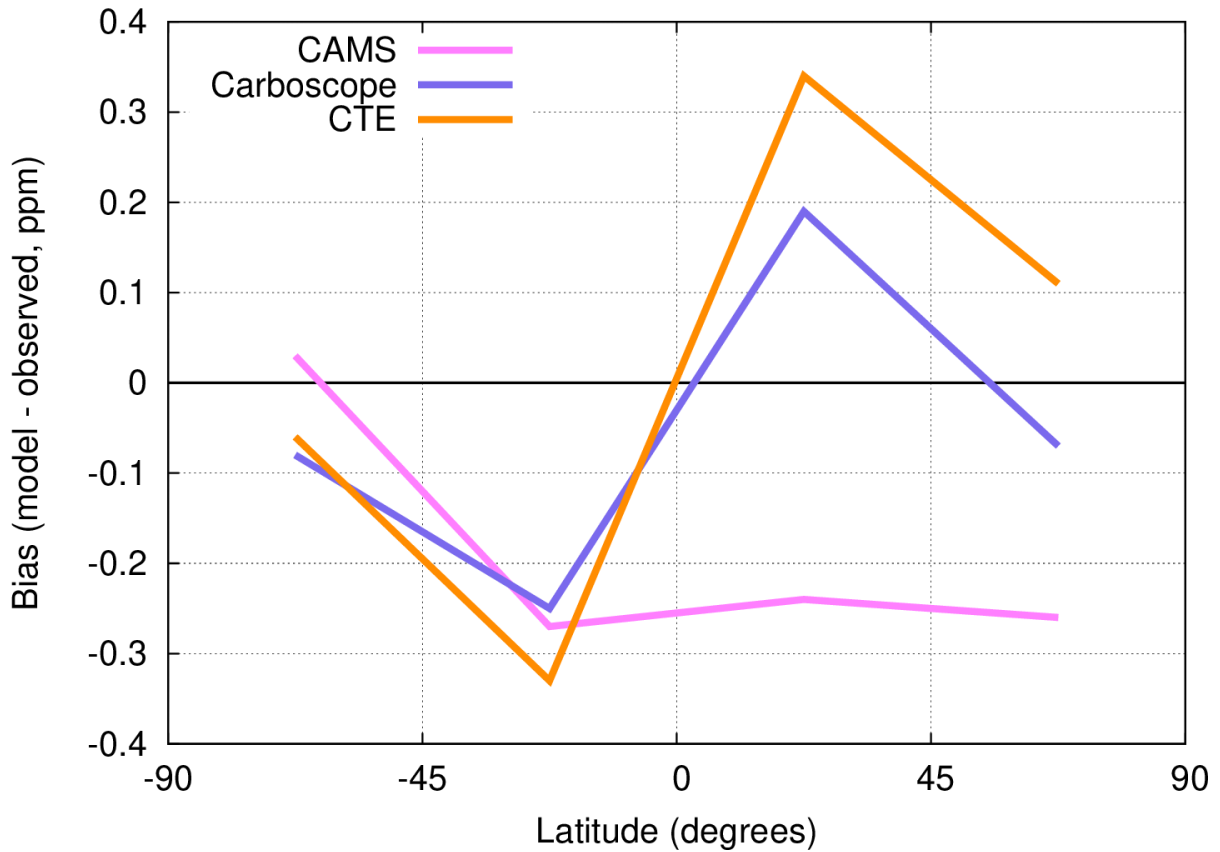


**Figure B3.** Evaluation of the atmospheric inversion products. The mean of the model minus observations is shown for four latitude bands. The four models are compared to independent CO<sub>2</sub> measurements made onboard aircraft over many places of the world between 2 and 7 km above sea level. Aircraft measurements archived in the Cooperative Global Atmospheric Data Integration Project (CGADIP, 2019) from sites, campaigns or programs that cover at least 9 months between 2001 and 2017 and that have not been assimilated, have been used to compute the biases of the differences in four 45° latitude bins. Land and ocean data are used without distinction. The number of data for each latitude band is 5000 (90–45°S), 124000 (45°S–0), 1042000 (0–45°N), and 139000 (45–90°N), rounded off to the nearest thousand.

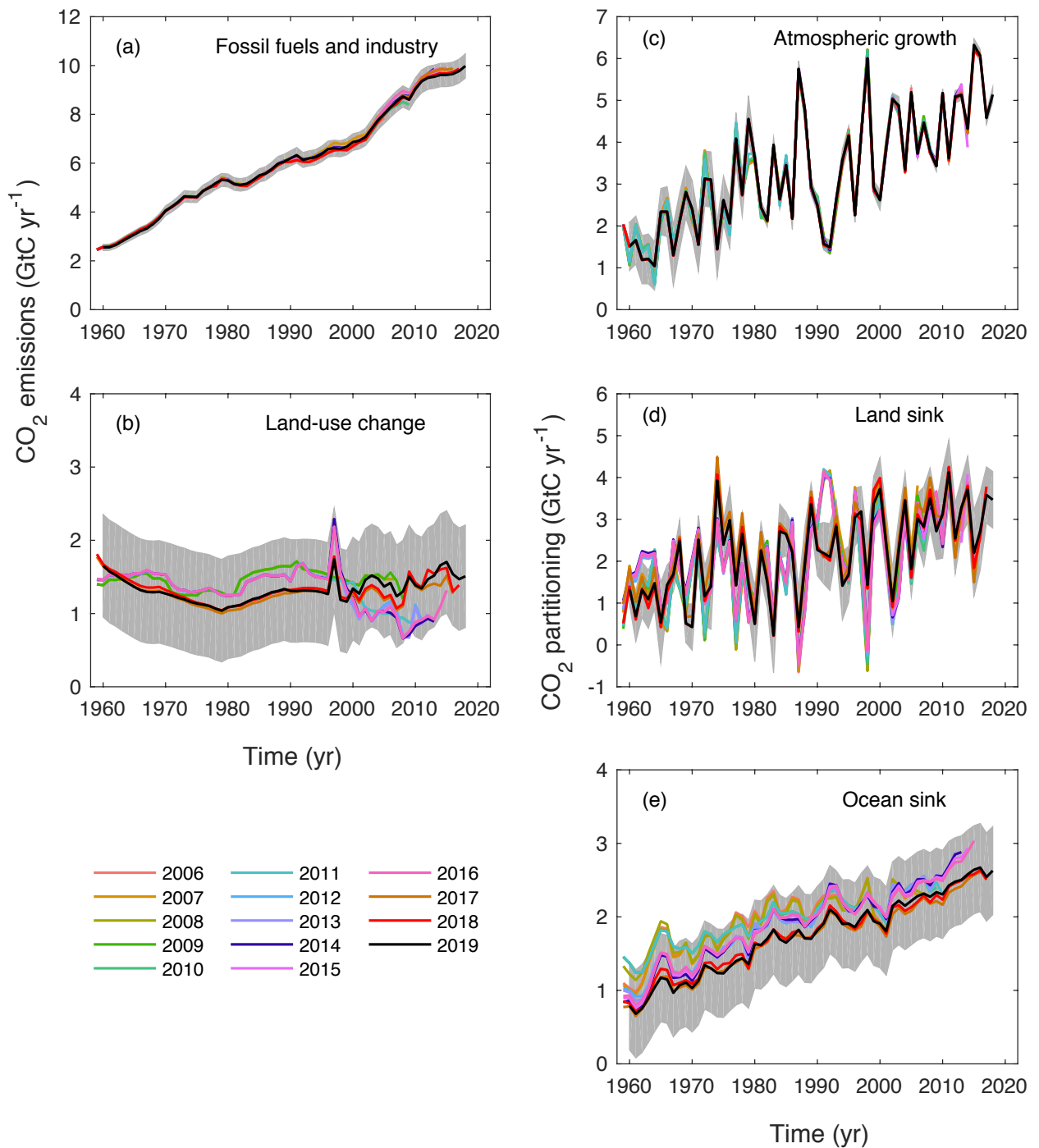


**Figure B4.** Comparison of global carbon budget components released annually by GCP since 2006. CO<sub>2</sub> emissions from **(a)** fossil CO<sub>2</sub> emissions ( $E_{FF}$ ), and **(b)** land-use change ( $E_{LUC}$ ), as well as their partitioning among **(c)** the atmosphere ( $G_{ATM}$ ), **(d)** the land ( $S_{LAND}$ ), and **(e)** the ocean ( $S_{OCEAN}$ ). See legend for the corresponding years, and Tables 3 and A7 for references. The budget year corresponds to the year when the budget was first released. All values are in GtC yr<sup>-1</sup>. Grey shading shows the uncertainty bounds representing  $\pm 1\sigma$  of the current global carbon budget.